

Stochasticity and Fluctuations in Non-equilibrium Transport Models



Justin Whitehouse

Doctor of Philosophy
University of Edinburgh
2015

Lay Summary

In this thesis I present the research I have done during my PhD on the subject of models of the transportation of mass. Mass transport processes are seen in a variety of contexts and at a variety of scales, from the movement of people and vehicles to the biochemical processes occurring in cells, and beyond.

In these kinds of process, there is a net flow of mass, such as cars or proteins, from one place to another. In theoretical physics, no one has yet been able to develop a general mathematical framework for studying systems with this simple property, and so current research focuses on building specific and somewhat abstract models for specific types on mass transport, with the hope of learning how certain properties and behaviours could be responsible for phenomena observed in nature.

In this spirit, this thesis examines the properties of three different models of specific transport processes using a combination of mathematics and computer simulations, with the aim of understanding the influence of specific features on the observed results.

The first model I study is of a search process. It consists of a particle that searches for a target by undergoing diffusion along a line and randomly going back to the start. This type of model is particularly relevant for modelling the action of proteins that search strands of DNA for specific binding sites. In particular, I study how an imperfection in the recognition of the target influences the mean time taken to locate it. I find that the imperfection increases the searching time in an intuitive way.

The second model I study is a model of units of mass jumping between sites, like stepping stones. When moving between sites, either every unit of mass on the departure site except for one move to the next, or if there is only one unit of mass on the site then just this mass moves to the next site. The aim is to see

how a moving cluster was formed and what kinds of properties it has. Moving clusters of mass are seen in many places, such as in the formation of raindrops and in traffic jams in road networks. In this model I find that a certain kind of jump rate between sites leads to the aggregation of a cluster of mass that travels together with a very short tail of trailing mass, which helps to keep it moving.

Finally, the third model in this thesis describes an interface growing against a membrane which itself is diffusing, movingly randomly towards and away from the interface. This model is inspired by the growth of a mesh of filaments of a protein called actin, which is found in motile cells. The mesh of filaments grows towards the membrane, ratcheting it in a certain direction and allowing the whole cell to move that way. I find that when the motion of the membrane is strongly biased towards the interface it inhibits its growth and makes it smooth and flat. Interestingly, I also find that with the right amount of bias in the membrane away from the interface there is a maximum speed with which the interface pushes the membrane, which is greater than the speed the membrane would travel at on its own.

Abstract

The transportation of mass is an inherently ‘non-equilibrium’ process, relying on a current of mass between two or more locations. Life exists by necessity out of equilibrium and non-equilibrium transport processes are seen at all levels in living organisms, from DNA replication up to animal foraging. As such, biological processes are ideal candidates for modelling using non-equilibrium stochastic processes, but, unlike with equilibrium processes, there is as of yet no general framework for their analysis. In the absence of such a framework we must study specific models to learn more about the behaviours and bulk properties of systems that are out of equilibrium.

In this work I present the analysis of three distinct models of non-equilibrium mass transport processes. Each transport process is conceptually distinct but all share close connections with each other through a set of fundamental non-equilibrium models, which are outlined in Chapter 2. In this thesis I endeavour to understand at a more fundamental level the role of stochasticity and fluctuations in non-equilibrium transport processes.

In Chapter 3 I present a model of a diffusive search process with stochastic resetting of the searcher’s position, and discuss the effects of an imperfection in the interaction between the searcher and its target. Diffusive search process are particularly relevant to the behaviour of searching proteins on strands of DNA, as well as more diverse applications such as animal foraging and computational search algorithms. The focus of this study was to calculate analytically the effects of the imperfection on the survival probability and the mean time to absorption at the target of the diffusive searcher. I find that the survival probability of the searcher decreases exponentially with time, with a decay constant which increases as the imperfection in the interaction decreases. This study also revealed the importance of the ratio of two length scales to the search process: the

characteristic displacement of the searcher due to diffusion between reset events, and an effective attenuation depth related to the imperfection of the target.

The second model, presented in Chapter 4, is a spatially discrete mass transport model of the same type as the well-known Zero-Range Process (ZRP). This model predicts a phase transition into a state where there is a macroscopically occupied ‘condensate’ site. This condensate is static in the system, maintained by the balance of current of mass into and out of it. However in many physical contexts, such as traffic jams, gravitational clustering and droplet formation, the condensate is seen to be mobile rather than static. In this study I present a zero-range model which exhibits a moving condensate phase and analyse its mechanism of formation. I find that, for certain parameter values in the mass ‘hopping’ rate effectively all of the mass forms a single site condensate which propagates through the system followed closely by a short tail of small masses. This short tail is found to be crucial for maintaining the condensate, preventing it from falling apart.

Finally, in Chapter 5, I present a model of an interface growing against an opposing, diffusive membrane. In lamellipodia in cells, the ratcheting effect of a growing interface of actin filaments against a membrane, which undergoes some thermal motion, allows the cell to extrude protrusions and move along a surface. The interface grows by way of polymerisation of actin monomers onto actin filaments which make up the structure that supports the interface. I model the growth of this interface by the stochastic polymerisation of monomers using a Kardar-Parisi-Zhang (KPZ) class interface against an obstructing wall that also performs a random walk. I find three phases in the dynamics of the membrane and interface as the bias in the membrane diffusion is varied from towards the interface to away from the interface. In the smooth phase, the interface is tightly bound to the wall and pushes it along at a velocity dependent on the membrane bias. In the rough phase the interface reaches its maximal growth velocity and pushes the membrane at this speed, independently of the membrane bias. The interface is rough, bound to the membrane at a subextensive number of contact points. Finally, in the unbound phase the membrane travels fast enough away from the interface for the two to become uncoupled, and the interface grows as a free KPZ interface.

In all of these models stochasticity and fluctuations in the properties of the

systems studied play important roles in the behaviours observed. We see modified search times, strong condensation and a dramatic change in interfacial properties, all of which are the consequence of just small modifications to the processes involved.

Declaration

Except where otherwise stated, the research undertaken in this thesis was the unaided work of the author. Where the work was done in collaboration with others, a significant contribution was made by the author. This research has not been submitted for any other degree or qualification except as specified

J. Whitehouse
October 2015

Acknowledgements

I would like to record my thanks to all those who have helped me in the course of this thesis. In particular, the following:

My supervisors, Martin Evans and Richard Blythe, for their support and guidance.

Jane Patterson, without whose administrative support this period of study would not have passed by so smoothly.

The CM-CDT¹ for funding my studies, as well as providing extra training, courses and professional support. I would like to thank Christine Edwards and Julie Massey, who have made the support that CM-CDT has provided so valuable to me. I would also like to thank the EPSRC² who have funded me through the CM-DTC, and SUPA³, who have also provided training during this period.

Tim Bush, my office-mate from start to finish, who has kept me entertained and informed.

Rachel Forshaw, for getting me through the process of writing this thesis.

The computing support staff of the School of Physics and Astronomy, for their patience and support.

¹The Scottish Doctoral Training Centre in Condensed Matter Physics

²Engineering and Physical Sciences Research Council

³The Scottish Universities Physics Alliance

Contents

Lay Summary	i
Abstract	iii
Declaration	vii
Acknowledgements	ix
Contents	xi
List of figures	xv
List of tables	xxiii
1 Introduction	1
2 Concepts, Methods and Models	7
2.1 Introduction	7
2.2 Concepts and Methods	8
2.2.1 Master Equations	8
2.2.2 Phase Transitions and Universality	9
2.2.3 Mean-Field Theories	11
2.3 Random Walks and Diffusion	17
2.3.1 Random Walks	17
2.3.2 Diffusion	18
2.3.3 First-Passage Properties	19
2.4 The Asymmetric Simple Exclusion Process (ASEP)	23
2.4.1 Periodic Boundary Conditions	24
2.4.2 Open Boundary Conditions	25
2.5 The Zero-Range Process (ZRP)	29
2.5.1 Condensation	30
2.6 Interfacial Growth	34
2.6.1 The Edwards-Wilkinson (EW) Equation	38
2.6.2 The Kardar-Parisi-Zhang (KPZ) Equation	41

2.6.3	Connection to the ASEP	44
3	Partial Absorption in a Diffusive Search Process	47
3.1	Introduction	47
3.1.1	Background and Motivation	48
3.2	Model	49
3.2.1	Total Absorption	49
3.2.2	Partial Absorption	52
3.2.3	Absorption and Boundary Conditions	54
3.2.4	Significant Dimensionless Quantities	55
3.3	Survival Probability Calculation	56
3.3.1	Inverting the Laplace Transform	58
3.4	Mean Time to Absorption	61
3.4.1	Minimisation of the MTA with respect to resetting rate r .	65
3.5	Many Independent Searchers	67
3.5.1	Average Survival Probability of the Target	68
3.5.2	Typical Survival Probability	70
3.6	Discussion and Conclusions	75
4	A Moving Condensate in a Zero-Range Chipping Model	77
4.1	Introduction	77
4.1.1	Background and Motivation	78
4.2	Model	80
4.3	Numerical Analysis	82
4.3.1	Identifying Phases	83
4.3.2	Strong Condensate Phase	84
4.3.3	Standard Condensate Phase	87
4.4	Mean-Field Theory	88
4.4.1	Master Equations	88
4.4.2	Failure of the Generating Function Technique	89
4.4.3	Prediction of a Condensation Transition at $\rho_c = 1$	90
4.4.4	Special Case: $b = 0$	93
4.5	Condensate Frame Mean Current Analysis	96
4.5.1	Generalisation to any Real, Positive α	100
4.6	Classification of the Strong Condensate Phase Transition	104
4.6.1	Connection to the Driven Asymmetric Contact Process (DACP)	108
4.6.2	Divergence in the approximate theory	109
4.7	Discussion and Conclusions	111
5	A Membrane-Interface Model for Lamellipodia Growth	115
5.1	Introduction	115
5.2	Membrane-Interface (MI) Model	121

5.3	Numerical Methods	122
5.3.1	Quantities of Interest	123
5.4	Numerical Results and Discussion	125
5.4.1	Smooth Phase	126
5.4.2	Rough Phase	129
5.4.3	Transition Between the Smooth and Rough Phases	131
5.4.4	Unbound Phase	134
5.5	Simple Mean-Field Theory	135
5.5.1	Master Equation and Generating Function	135
5.5.2	Predictions of Critical Values	137
5.5.3	Prediction for the Scaling of the Width	138
5.6	The Importance of Jammed Regions of the Interface	142
5.6.1	A Simple Two-Random-Walker Model	144
5.6.2	Prediction of Phases in the Mean Length \bar{l}	145
5.7	Discussion and Conclusions	149
6	Conclusions	155
A	Concepts, Methods and Models	161
A.1	Relationship Between the Occupancy Distribution and the First-Passage Probability	161
A.2	Bose-Einstein Condensation	162
B	Partial Absorption in a Diffusive Search Process	165
B.1	Equivalence of the Radiation Boundary Condition and the Sink term.	165
B.2	MTA with a resetting position distribution $\mathcal{P}(x)$	167
C	Membrane-Interface Model	171
C.1	Width Scaling	171
	Bibliography	177
	Publications	191

CONTENTS

List of Figures

2.1	(Reproduced from [42]) Directed Percolation (DP) along bonds on a rotated square lattice. A cluster is defined as a set of points and bonds originating from a single source (shown in red). In what is known as “1+1 dimensions”, the vertical direction can be thought of as time instead of space.	13
2.2	(Reproduced from [42]) Schematic diagram of the contact process. Active sites, those containing a particle, become inactive with rate 1, or make an adjacent inactive site active with rate $\lambda/2$	14
2.3	A schematic diagram of the ASEP with periodic boundaries. Particles hop forwards with rate p , but cannot hop onto a site that is already occupied.	24
2.4	A schematic diagram of the ASEP with open boundaries. Particles enter at the left with rate α , hop to adjacent sites with rate p , and leave at the right with rate β	25
2.5	(Reproduced from [22]) The iterative density mapping in the mean-field theory for the ASEP. Profiles A and B quickly iterate close to the high-density fixed point ρ_+ . Profiles C and D begin infinitesimally close to the low-density fixed point until close to the right boundary, where they iterate away.	26
2.6	(Reproduced from [22]) The phase diagram for the ASEP predicted by the mean-field theory. The discontinuous-transition line between the high-density (HD) and low-density phases (LD) is indicated by the bold line. The transition between HD/LD and the maximal current (MC) phase is continuous.	28
2.7	Schematic diagram of the ZRP. One particle from a site containing n hops to the next site with rate $u(n)$	29
2.8	Illustration of the correspondence between the ZRP, ASEP, and KPZ interface.	33
2.9	Schematic diagram of Ballistic Deposition (BD). New particles dropped onto the surface stick to the first particle they come into contact with. (Inspired by figure in Ref [12].)	36

2.10 Schematic diagram showing the geometric relationship between growth in the direction of the local normal of the surface normal and the associated increase in height. (Inspired by illustration in Ref [12].)	42
3.1 Schematic diagram of the system studied. The particle starts at z and diffuses (diffusion constant D) along the x axis. With rate r it stochastically resets to x_0 , and when it reaches the target location x_T (in this case 0) it is absorbed at a rate proportional to a	52
3.2 Sketch of the singularities of the function (3.3.17) in the complex s plane.	59
3.3 Plot of the value of θ that minimises the MTA for a given ϕ_0 . The value of θ at $\phi_0 = 0$, found numerically to be $\theta^* = 1.5936$, is indicated.	65
3.4 The minimised MTA, T^* , as a function of ϕ_0 , in units of x_0^2/D . T^* is approximately linear for both small and large ϕ_0 (See (3.4.22) and (3.4.26)). <i>Inset:</i> expanded view of the crossover between the two linear regimes (logarithmic axes).	66
4.1 The elementary dynamical processes. (a) Hop: When a site contains only one particle, this particle hops onto the next site with rate $u(1)$, leaving behind an empty site. (b) Backchip: When a site contains n (3) particles, $n - 1$ (2) of these particles move together with rate $u(n)$ onto the next site and leave behind a <i>single</i> particle.	81
4.2 Plot of σ^2 against both ρ and b , for $L = 100$ and 1000 . There is a significant change of state when $b > 0.5$, and also a gradual, weaker change in state when $b \leq 0.5$ as ρ is increased.	83
4.3 Example occupancy distributions: (a) The fluid phase ($\rho = 0.5$, $L = 1000$, and $b = 0.25$). The distribution decays as a stretched exponential. (b) The standard condensate phase ($\rho = 2.0$, $L = 1000$, and $b = 0.25$). The distribution decays as a power law for low occupancies, but exhibits a ‘bump’ caused by a condensate at larger occupancies.	84
4.4 A sketch of the phase diagram suggested by the numerical measurements of the occupancy distribution $p(n)$	85

4.5	Illustration of the strong condensate phase. (a) A typical configuration sketched using data taken directly from a simulation ($L = 1000$, $N = 1000$, $b = 2.0$ and $\alpha = 1.0$). The columns represent the mass occupying the site, with the exact size shown above, and the direction of motion is indicated by the arrow. (b) The average mass \bar{n}_k at a site k sites <i>behind</i> the condensate ($\rho = 1, 2, 5, 10$, $b = 2.0$, $\alpha = 1.0$). Almost all of the system's mass is in the condensate, with any remaining trailing closely behind.	86
4.6	Plot of the occupancy distribution $p(n)$ in the strong condensate regime at a range of densities ($b = 2.0$, $L = 1000$, $\alpha = 1.0$). The points at and near $n/N = 1$ indicate the presence of a strong condensate which contains effectively all of the system's mass.	86
4.7	As the system size is increased, the position of the peak in the probability distribution decreases logarithmically with L . This means that the critical density ρ_c has L dependence of the form $\rho_c(L) \sim \ln(L)$	87
4.8	When a backchip occurs from a site with large occupancy, if the average occupancy, or density ρ , ahead is: (a) less than 1 the backchip will result in mass spreading out; (b) exactly 1 the mass distribution is unchanged; (c) greater than 1 the backchip will concentrate the mass.	93
4.9	Sketches of $r(S)$ against S for: (left) $\rho < 1$; (centre) $\rho = 1$; (right) $\rho > 1$	95
4.10	Plots of the occupancy distribution $p_k(n)$ at site k behind the condensate ($k = 1, 4, 6$). To the distribution for $k = 2$ (large blue +) we have fitted the function $c(1 - a)a^n$ (red solid line) to the middle of the tail, and $(1 - a)a^n$ (green dashed line) to the front of the tail. Above $n \sim 15$ the data is too noisy to be fit to reliably. ($\rho = 0.5$, $L = 1000$, $b = 1.0$, $\alpha = 1.0$).	97
4.11	Using the boundary condition $\bar{n}(x = 0) = n_0 = 1$ we see graphically that (a) if $n_c < n_0$ then as x increases, as we move further away from the condensate, so too does \bar{n} . It does so indefinitely, resulting in an infinite mean occupancy infinitely far from the condensate. (b) If $n_c > n_0$, then we see that as x increases, $\bar{n}(x)$ decreases to 0.	99
4.12	A plot of $b_c(\alpha)$ (red, solid). b_c increases monotonically from $b_c(0) = 1/3$ and asymptotically approaches $b_c = 1$ (blue, dashed).	102
4.13	Plots of σ^2 against b ($L = 1000$). (a) With $\alpha = 0$ all masses move with the same rate and no transition is observed in b . (b) Using the modified hop rate $u_{log}(n)$ given in (4.5.23) we can probe $b_c(\alpha)$ as $\alpha \searrow 0$. A transition occurs when b is in between 0.3 and 0.4, in good agreement with the prediction $b_c(\alpha = 0) = 1/3$ from (4.5.22).	103

4.14 Plot of σ^2 against b for (a) $\alpha = 2$ ($L = 500$) and (b) $\alpha = 10$ ($L = 1000$). The transition becomes less sharp as α is increased, and takes place over a range of values of b which are greater than the b_c predicted by (4.5.22). The formula (4.5.22) predicts that $b_c(\alpha = 2) = 0.8185$ and $b_c(\alpha = 10) = 0.9995$. (c) At $\alpha = 10$ the transition becomes sharper as L is increased, which is evidence that its gradual nature is a finite size effect. We can estimate $b_c \sim 1.6 \pm 0.1$ from the crossover of the curves.	104
4.15 Plot of σ^2 against b , for various L with $\rho = 0.5$. A transition is seen to occur for all system sizes, with a clear crossover point in the σ^2 - b curves at $b = 0.5$, which is indicative of the critical value $b_c = 0.5$	105
4.16 Plot of σ^2 against b , for various L with $\rho = 0.5$. We perform a finite size scaling procedure on b , rescaling it to $(b - b_c)L^X$. The choice of parameters for the best collapse of the data onto a single curve is $b_c = 0.5$ and $X = 0.75$	105
4.17 A plot of the mean occupancy at a site k behind the condensate site, measured numerically. The decay length in the region $0 < k < 500$ can be seen to slowly increase as $b \searrow 0.5$	106
4.18 The decay length $\lambda(b)$ measured from the tails in Figure 4.17 fits a power law in the scaling regime but flattens out as $b \searrow 0.5$. Numerically, the system size only affects the b dependence of $\lambda(b)$ as b approaches 0.5. As L is increased $\lambda(b)$ becomes closer to the power law at $b \searrow 0.5$	107
4.19 (Reproduced from [43]) A schematic diagram of the DACP. The first site is always active. Active sites become inactive with rate 1, or activate the site to their right with rate r	108
4.20 Plots of $\bar{n}(x)$, and its gradient, from the mean-field theory of Section 4.5 at different values of b . To see if it predicts a diverging length scale, I measured the distance from the origin at which the gradient of $\bar{n}(x)$ had the largest magnitude. We can see that this distance continually increases as $b \searrow b_c \simeq 0.619692$, and the function diverges when $b < b_c$	110
4.21 By numerically integrating (4.5.13) we measure a length scale in the tail to diverge logarithmically as $b \searrow b_c$	110
4.22 A sketch of the phase diagram for our system. Above the value b_c , the system exhibits a strong condensate phase. Below b_c and for low densities the system exists in a fluid phase. Above a certain value ρ_c , the system exhibits the characteristics of a standard condensate phase, but this critical density diverges as $L \rightarrow \infty$. . .	111

-
- 5.1 (Reproduced from [161]) **A:** A *Xenopus* keratocyte cell, moving in the upwards direction. The box highlights a section of the leading lamellipodium, which is expanded and shown in B. **B:** An image of the actin filaments in the leading lamellipodium. The top surface of the filamentous region has some rough structure. The arrangement of the filaments in the bulk appears disordered and shows different characteristics at different distances from the surface. **C:** An enlarged view of the box in B. At the surface the arrangement of filament tips appears to lack order. 116
- 5.2 The leading edge of the messy network of actin filaments in the lamellipodium is modelled using an interface, which grows up against a diffusing, infinite, solid wall, which represents the cell membrane. Absorption of an actin monomer by a filament is represented by the growth of a single point on the interface towards the membrane. 118
- 5.3 (Reproduced from [136]) A schematic diagram of the Brownian Ratchet, as presented in Ref [136]. A particle diffuses in one-dimension with diffusion constant D , under the influence of an external load force f . If the particle diffuses a distance δ or greater away from the tip of the actin filament, there is space for an actin monomer to be adsorbed, which occurs with rate α . With rate β an actin monomer can desorb from the tip, which can occur regardless of the position of the particle. 119
- 5.4 A diagram illustrating the MI model I study in this chapter. The membrane steps away (towards) the interface with rate u ($1 - u$). Particles in the ASEP, representing the slopes in the interface, hop to the right (left) with rate p ($1 - p$). Any move that would cause the interface to pass through the membrane is forbidden. 122
- 5.5 A plot of \bar{y} against u . Below $u_1 \simeq 0.62$, one sees that \bar{y} is small and independent of the system size. In the rough phase, between $u_1 \simeq 0.62$ and $u_2 = 3/4$ one sees that \bar{y} depends on the system size. One also sees additional structure becoming apparent at larger system sizes. When $u > u_2$, \bar{y} does not reach a steady state value as the membrane ‘escapes’ from the interface. 126
- 5.6 A plot of W against u . Far below $u_1 \simeq 0.62$, the width is very narrow and independent of L , which indicates a smooth interface. As we approach the rough phase, $u_1 < u < u_2$, the width develops a dependence on L , and within the rough phase itself it enters the KPZ scaling regime, with $W \sim L^{1/2}$. As expected, this scaling is maintained above $u_2 = 3/4$, where the interface is an unobstructed KPZ interface as the membrane drifts away. 127

- 5.7 A plot C against u . In the smooth phase, $u < u_1$, C scales linearly with L , and so the density of contacts scales independently of L . This is indicative of a smooth interface pushing up against the membrane. In the rough phase $C \sim L^0$, and so the density of contacts scales as $1/L$. In this case, the interface still pushes up against the membrane, but with a vanishing density of contacts. In the rough phase, $u > u_2 = 3/4$, the membrane escapes and there are no contacts at all. 128
- 5.8 A plot of J against u . In the smooth phase, the current increases almost linearly with u until it approaches u_1 . At u_1 itself the current saturates to its maximal value, $1/4$. When $u > u_1$, in both the rough and unbound phases, the current does not change with u as it is no longer reduced by interactions with the membrane, but also can increase no further. 129
- 5.9 A plot of v_m against u . In the smooth phase and rough phases it has the same functional form as the current, because the velocity of the membrane is determined by the speed at which the interface can push it forwards. The membrane velocity is measured to be $v_m = 2J$. The upper transition at $u_2 = 3/4$ occurs when the natural mean drift velocity of the membrane $2u - 1$ becomes greater than the velocity $1/2$ of the interface that is pushing it, and the two parts decouple as the membrane drifts away. 130
- 5.10 We perform a finite-size scaling procedure on the width W , plotting W/L^α against $(u - u_1)L^\chi$. The best data collapse was found for the parameters: $\alpha = 0.5$, $u_1 = 0.62$, and $\chi = 0.5$ 131
- 5.11 Numerical measurements of the roughness exponent α as a function of u show the expected behaviour at $u \geq 3/4$ and at small u , but unexpected behaviour around where I estimate the phase transition between the smooth and rough phases to be, $u_1 \simeq 0.62$ 132
- 5.12 A schematic diagram of the processes which occur in the simple mean-field theory. A point on the interface lies a distance y from the membrane. With rate $1/4$ the interface grows *two steps* towards the membrane, reducing y by 2. With rate u the membrane steps away from the interface, increasing y by 1. With rate $(1 - u)(1 - P(0))^L$ the membrane steps towards the interface, reducing y by 1. Any process which would make y negative is prohibited. 135

5.13 A visualisation of the underlying ASEP array for $L = 256$ over 500 time steps. Each row shows state of the ASEP at a single time step with vacant sites in white, occupied sites in black, and occupied sites where the particle cannot jump forward due to the effect of the membrane in red. Left: $u = 0.4$. This is the smooth phase. Regions of interface that are pinned to the membrane span the entire system. Centre: $u = 0.65$. In the rough phase, there are contiguous regions of interface pinned to the membrane that do not span the entire length. Jammed regions are likely to reoccur in the same or similar regions of the interface where they did previously. Right: $u = 0.8$. In the unbound phase there is no interaction between the membrane and interface.	143
5.14 Diagram of the Two Random Walker model. l can only increase in size if $m = 0$, and can only decrease in size if $m > 0$. In the ‘annealed’ case: l increases by 1 with probability $\lambda P^*(0)$ and decreases by 1 with probability $(1 - \lambda)(1 - P^*(0))$, where $P^*(0)$ is the steady state probability that $m = 0$	144
5.15 (A) There is no $P^*(0)$, so $m \rightarrow \infty$. Thus a steady state with $Q^*(0) = 1$ and $\bar{l} = 1$ is reached. (B) A steady state is reached with $\bar{l} = \rho(1 - \rho)^{-1}$, with $0 < \rho < 1$. $\rho = \lambda(1 - 2\mu)/(\mu(1 - \lambda))$. This phase is bounded by $\mu = 1/2$ from above and by $\mu = \lambda/(1 + \lambda)$ from below. (C) There is no steady state for $Q^*(0)$, $Q^*(m)$, and thus $\bar{l} \rightarrow \infty$	149

LIST OF FIGURES

List of Tables

2.1 The KPZ exponents in dimensions $d = 1, 2, 3$. $d = 1$: analytic results [12]. $d = 2, 3$: numerical results [3].	44
--	----

LIST OF TABLES

Chapter 1

Introduction

Calculating the exact dynamics of a microscopic system of many interacting constituents is practically impossible. Even though the constituents obey the laws of physics, solving the resulting equations of motion becomes prohibitively difficult not just because of the sheer number of them, but because they are also coupled together. The classic example of such a system is a gas. Around 20 litres of a typical gas will contain $\sim 10^{23}$ constituent atoms or molecules. A computer simulation of the dynamics of this many objects is infeasible, and solving 10^{23} coupled equations of motion is certainly a daunting task. A consequence of this difficulty has been to give rise to alternative approaches in which one can reduce the number of degrees of freedom to a more manageable size: *equilibrium thermodynamics* and *equilibrium statistical mechanics*.

A system is in thermodynamic equilibrium when any exchanges of volume, mass or heat with its environment are reversible, and it exhibits no net currents. In the field of thermodynamics, one attempts to understand the macroscopic properties of a system in thermodynamic equilibrium, such as the temperature, volume and pressure, without concerning oneself with the microscopic details [65]. In statistical mechanics one still attempts to understand the macroscopic properties of a system, but by explicitly giving consideration to the microscopic details of the system of interest, so that one can establish the link between micro- and macroscopic properties. By considering the microscopic properties of the system from a statistical point of view, one can often find ways to reduce the large number of variables to just a few.

Practically, in statistical mechanics one studies the probability $P(\mathcal{C})$ that a

system will be found in the exact microscopic configuration, or *microstate*, \mathcal{C} . In equilibrium, it is well known that $P(\mathcal{C})$ obeys the Boltzmann distribution (see e.g. [8])

$$P(\mathcal{C}) = \frac{\exp(-E(\mathcal{C})/k_B T)}{Z}, \quad (1.0.1)$$

where $E(\mathcal{C})$ is the energy of microstate \mathcal{C} , k_B is Boltzmann's constant, and T is the temperature of the system. The factor Z is the normalisation constant, known as the partition function, which is in general defined as

$$Z = \sum_{\mathcal{C}} P(\mathcal{C}). \quad (1.0.2)$$

The partition function is an important quantity in equilibrium statistical mechanics because from it all the macroscopic thermodynamic properties of a system can be calculated through its connection with the free energy $F = -k_B T \ln Z$ (see e.g. [8, 36, 68, 137]). It is because of the Boltzmann distribution and the link between the partition function and the free energy that equilibrium statistical mechanics provides a powerful, general framework for calculating the properties of equilibrium systems.

In contrast to systems in thermodynamic equilibrium, systems which are out of thermodynamic equilibrium exhibit net currents in their constituent quantities, such as mass, energy, charge or particle number. Furthermore, processes involving exchanges of these quantities are irreversible, which, in thermodynamic terms, means that there is some energy dissipated in the process which cannot be recovered. In statistical mechanics terms, irreversibility means that the probability of making the transition from microstate \mathcal{A} to microstate \mathcal{B} is not the same as from \mathcal{B} to \mathcal{A} . Broadly speaking there are two kinds of non-equilibrium dynamics [106]. The first is when systems experience fluctuations from an equilibrium state, or are in the process of relaxing to an equilibrium state [114, 134]. The second kind, and the subject of this work, are the dynamics of a system which is driven out of and typically far from equilibrium.

It is clear that ‘transport’ naturally describes a process which is driven out of equilibrium, where there exists a current of the constituent quantities being transported between locations. A particularly rich physical setting for the study of transport and non-equilibrium systems is in biology: life exists inherently out of

equilibrium, as living creatures and cells are constantly moving mass and energy from one place to another, and any organism in thermodynamic equilibrium is dead [153]. In the context of microbiology, for example, filaments of proteins, called microtubules, act as tracks upon which motor proteins called kinesins and dyneins travel carrying organelles from one region of the cell to another [32]. Also, in the process of filopodial growth in a variety of organisms the ‘building blocks’ are transported to the growing region from elsewhere in the cell [54, 159, 160, 177], and in the synthesis of DNA and RNA, specific enzymes travel along a DNA template, sequentially building the new DNA or RNA molecule [113].

The powerful, general framework for calculation offered by equilibrium statistical mechanics unfortunately does not yet exist for systems out of equilibrium. A consequence of this is that one must develop a new model for each system of interest, from which one can try to learn about things like the influence of the microscopic dynamics on the bulk phase behaviours. As such there is a long tradition of biological modelling [77], including for the specific processes listed above [17, 38, 54, 113, 159, 160, 177]. The usefulness and applicability of non-equilibrium transport models are not limited to biological contexts, and they have been applied extensively to more traditional and general studies of traffic flow [37, 151].

The need to define and study individual models in non-equilibrium statistical mechanics motivates the work in this thesis. I study a set of three distinct models with three distinct motivations, all of which display a conceptually different kind of transport, that additionally demonstrate both how varied and how closely connected different non-equilibrium models can be. A unifying theme across all of the research in this thesis is the endeavour to understand at a more fundamental level the role of stochasticity and fluctuations in the dynamics of these different systems.

The term *stochasticity* refers to the inherent ‘randomness’ in the behaviour of the particles or agents or whatever are the active constituents of the process. A simple example of this is the Poisson ‘hop’ or ‘jump’ rates in driven particle models such as the Zero Range Process (ZRP) or the Asymmetric Simple Exclusion Process (ASEP), which will be outlined in Chapter 2. In the context of this work, *fluctuations* are deviations from the mean of typical behaviours of the system. An example of the role fluctuations can play in the dynamics of a system also

comes from the ZRP. Under the right conditions, the ZRP exhibits a condensate phase where a finite fraction of the entire mass of the system occupies a single site. This condensate is static and maintained by the balance of mass current into and out of it from adjacent sites. If there is a large enough fluctuation in this current, then the condensate can dissolve and reform somewhere else in the system [75].

The first of these three models that I study, presented in Chapter 3, is a one-dimensional, continuous- space and time search process, where a searcher is ‘transported’ to a target. The dynamics of the searcher are diffusive and, as such, its average behaviour is strongly influenced by fluctuations. My primary focus here is to investigate the effect that a degree of imperfection, or stochasticity, in the interaction with or absorption by the target has on the effectiveness of the search process. This kind of search model is of interest in a variety of contexts, such as animal foraging [13], regulatory protein interactions with DNA [17], computer search algorithms [124], and searching for one’s keys [57, 58], in all of which one would expect an imperfection in the searcher-target interaction to be of physical significance.

In Chapter 4 I turn my attention to the role of the ‘hopping’ rate in a spatially-discrete model of driven, interacting particles that is strongly related to the ZRP, the archetypal model of this type [56]. Specifically I am interested in the effect that this hopping rate, combined with the dynamical rules, has on the existence of the *dynamic* condensate phase. This is a phase in which a finite but significant fraction of the mass becomes localised and the region into which this fraction of the mass is localised moves through the system. The model is motivated by the desire to understand what processes will permit or destabilise a moving condensate phase, and by what mechanisms they occur. There is already a broad literature of work (e.g. [85, 86, 110, 116, 172]) studying the existence of moving condensate phases with very different dynamical origins, which are different again to the origin of the condensation effect that I present in this chapter. Studies of these various condensate phases may prove useful in understanding the phenomena of dynamic condensation, or aggregation, in a broad variety of physical contexts (e.g. [63, 89, 112, 157]).

Finally, in Chapter 5 I study a growing interface which ‘ratchets’ a diffusing wall (the “membrane”), which was conceived as a very simple model for the

growth of the lamellipodium in a cell [139], a flat mesh of actin filaments which play a key role in cell motility. In the absence of the membrane, the structure and dynamics of the interfacial part of this spatially-discrete model would put it in the Kardar-Parisi-Zhang (KPZ) class of interfaces. Thus I have two motivations for studying this model. From a biological perspective, it is interesting to learn whether this membrane-interface (MI) model exhibits ratcheting properties similar to more established Brownian ratchets that have been studied in order to explain the observed motility of cells [88, 122, 123, 136, 179]. From a statistical physics point of view, it is of great interest to learn how the properties, in particular the scaling, of what would be a KPZ interface is affected by the presence of a diffusing wall, which is a problem that to my knowledge has not yet been investigated.

Next, in Chapter 2, I will briefly discuss some of the key concepts and methods used in statistical physics, and how they are used when studying non-equilibrium systems. Then I will discuss some of the paradigmatic non-equilibrium transport models which are most relevant to this work. I will begin by discussing random walks and diffusion, which are very simple models for stochastic transport, but become particularly relevant in the context of search processes when one considers their first-passage properties. I will then go on to review three of the most important models of non-equilibrium processes, the ASEP, ZRP and KPZ equation, which form the foundations of the models I study in Chapter 4 and Chapter 5.

Chapter 2

Concepts, Methods and Models

2.1 Introduction

In this thesis I present three distinct models of non-equilibrium transport processes with different backgrounds and motivations. Even so, there are some concepts and methods that are common to more than one. In all three models I study *master equations* that describe the dynamics of the systems, and in Chapter 4 and Chapter 5 I also use *mean-field* master equations to investigate the *phase behaviour* observed numerically. For this reason I first briefly introduce these concepts and methods before they are put into practice in later chapters.

A significant difference between the three models studied in this thesis is their context, and the fundamental models that they are based on. Therefore, in this chapter, I will also introduce these different models and will find that, rather than being distinct and unrelated, there are strong connections between each. I will begin with *diffusion* and *random walks*, which are fundamental models of transport processes. In particular, I will introduce the *first-passage properties* of these processes, which are of particular relevance to the search process studied in Chapter 3. Then I will briefly review the *Asymmetric Simple Exclusion Process* (ASEP), a simple multi-particle, driven diffusive system that is conceptually linked to the random walk. I will follow this with an introduction to the *Zero-Range Process* (ZRP), another driven diffusive system that is closely linked to the ASEP, and which forms the basis of the model in Chapter 4. The final topic of this chapter will be models of interfacial growth, which are important in the context of the Membrane-Interface model presented in Chapter 5. I focus particularly

on the *Kardar-Parisi-Zhang* (KPZ) class of growing, non-equilibrium interfaces, which also have a strong connection to the ASEP. Furthermore, the KPZ equation that provides a continuum description of such interfaces is a non-linear diffusion equation with an additional stochastic term, which links nicely back to diffusive processes, the first model to be discussed.

2.2 Concepts and Methods

We now proceed to discuss some of the key concepts and methods from statistical physics which are used in this thesis, particularly in Chapter 4 and Chapter 5. These are very general and well known, and covered in a wide range of texts, but the main sources I use here are [19, 65, 80, 132, 137, 178].

2.2.1 Master Equations

Despite the lack of a general framework for calculating thermodynamic properties of non-equilibrium systems, there are still some general methods which one can hope will yield some useful results. One such technique, that is used extensively in Chapter 4 and Chapter 5, is to study the *master equation*

$$\frac{\partial P(\mathcal{C}, t)}{\partial t} = \sum_{\mathcal{C}'} [P(\mathcal{C}', t)\omega(\mathcal{C}' \rightarrow \mathcal{C}) - P(\mathcal{C}, t)\omega(\mathcal{C} \rightarrow \mathcal{C}')] , \quad (2.2.1)$$

of the probability distribution $P(\mathcal{C}, t)$ for being in the microstate \mathcal{C} at time t . This equation describes the rate of change of the probability of being in microstate \mathcal{C} in terms of the probability current $\sum_{\mathcal{C}'} P(\mathcal{C}', t)\omega(\mathcal{C}' \rightarrow \mathcal{C})$ into state \mathcal{C} from all other configurations \mathcal{C}' and the probability current $\sum_{\mathcal{C}'} P(\mathcal{C}, t)\omega(\mathcal{C} \rightarrow \mathcal{C}')$ out of state \mathcal{C} into other configurations \mathcal{C}' , where $\omega(\mathcal{C} \rightarrow \mathcal{C}')$ is the rate at which the system makes the transition from state \mathcal{C} to \mathcal{C}' . This equation still holds for systems in equilibrium, but because all processes are reversible the probability of the transition from \mathcal{C} to \mathcal{C}' and its reverse must be equal. Thus in equilibrium we have the condition

$$P(\mathcal{C}', t)\omega(\mathcal{C}' \rightarrow \mathcal{C}) = P(\mathcal{C}, t)\omega(\mathcal{C} \rightarrow \mathcal{C}') , \quad (2.2.2)$$

known as *detailed balance* [22, 52, 132], and $\partial P(\mathcal{C}, t)/\partial t = 0$ at all times t . In systems out of equilibrium one can still have a *non-equilibrium steady state* (NESS) where, although the individual transitions between two states are not reversible, the net probability current into a state is zero. In this case the left hand side of (2.2.1) is 0, yielding an equation of the form

$$\sum_{\mathcal{C}'} [P(\mathcal{C}', t)\omega(\mathcal{C}' \rightarrow \mathcal{C}) - P(\mathcal{C}, t)\omega(\mathcal{C} \rightarrow \mathcal{C}')] = 0 , \quad (2.2.3)$$

which one can hope to solve for the steady state distribution $P(\mathcal{C})$.

2.2.2 Phase Transitions and Universality

In equilibrium systems, a *phase transition* between states occurs when there is a singularity in one or more of the derivatives of the *free energy* of the system, a thermodynamic potential which describes the amount of energy in the system available for work [65]. At a phase transition, as one changes a property of the system, for example temperature, one typically sees a sharp change in its properties and the system reconfigures itself from one phase to the other. Broadly speaking, there are two types of phase transition [19, 178]. The first is a *first-order* phase transition, where there is a discontinuity in the first derivative of the free energy, for example the magnetic moment, a property commonly referred to as the order parameter. The second type is called a *continuous* phase transition¹ is one in which the order parameter is continuous but there is a divergence in the second derivative at the transition, or ‘critical’, point. There is no sharp jump in the order parameter in this case, but it is instead characterised by a diverging susceptibility and correlation length, as well as a power law decay in the correlation function, as one approaches the critical point [178].

The key feature of the continuous transition is that one or more of the thermodynamic properties of the system is singular at the transition. If, for instance, one has the temperature T as the control parameter then, as T approaches its critical value T_c , these thermodynamic properties will have a functional form

$$\left(\frac{T - T_c}{T_c}\right)^x ,$$

¹historically also known as a ‘second-order’ phase transition, a name which has more recently been deemed unsatisfactory [178]

where the exponent x is different for each. These exponents x are called the ‘critical exponents’ of the model. For example, in a simple model magnet with no applied field one finds that as one approaches the critical point the specific heat C_H , isothermal susceptibility χ_T and the correlation length ξ can be written [178]

$$C_H \sim \left(\frac{T - T_c}{T_c} \right)^{-\alpha}, \quad \chi_T \sim \left(\frac{T - T_c}{T_c} \right)^{-\gamma}, \quad \xi \sim \left(\frac{T - T_c}{T_c} \right)^{-\nu}. \quad (2.2.4)$$

Another example is a fluid system where again, near T_C , the specific heat (at constant volume) C_V , isothermal compressibility κ_T , and the correlation length ξ also diverge with $T - T_C$ with critical exponents α , γ , ν . Importantly, these critical exponents and T_C are different across systems, but what is particularly interesting is that the value of T_C depends strongly on the details of the system in question, whereas the values of the exponents α , γ and ν depend only on a few of its fundamental properties. For models with short-range interactions, for example, these fundamental properties are the dimensionality of space and the symmetry of the order parameter [178]. It is this generic property of critical exponents which makes them the defining feature of what are called “universality classes”: classes of models which have different microscopic details but the same underlying fundamental features, which mean that they show the same ‘critical behaviour’ near the critical point, whatever it may be. This is a useful concept, because it allows us to more easily understand the behaviour of complicated, difficult-to-solve systems once their universality class has been identified.

In equilibrium, many universality classes are well known and describe a variety of systems. For instance, the Ising Model is a simple model for a magnet (see e.g. [8, 132, 178]), and the Edwards-Wilkinson (EW) equation describes a fluctuating interface in equilibrium [12, 50]. For systems out of equilibrium one can also find universality classes for different models, despite the general lack of a free energy function. For example, Directed Percolation (DP) is a simple lattice model which exhibits a transition between active and inactive phases. It has an absorbing state, meaning it does not satisfy detailed balance and is a non-equilibrium model. It is found that the transition between the inactive and active phases is continuous and characterised by critical exponents, making it one of the fundamental universality classes of non-equilibrium models [80]. Another well known non-equilibrium universality class is the KPZ universality class in 1+1

dimensions (space + time) which describes an interface whose growth is driven in one direction. The KPZ equation is very similar to the EW equation but has an additional non-linear growth term that breaks the symmetry in the growth direction and introduces lateral growth, growth in the direction along the length of the interface, which is not described by the EW equation. In the KPZ class, instead of describing the scaling of an order parameter at a phase transition, the universal exponents describe how the width of an interface scales with the system size and how long it takes for the width to saturate to its steady state value [12, 41, 101].

Although we broadly describe phase transitions as being either first-order or continuous, there are examples which are not exclusively either and show characteristics of both. These phase transitions are known variously as *mixed-order* or *hybrid* transitions. For instance, in a model of avalanche collapse of giant clusters in complex networks [14] it is found that below the transition into a phase with a giant cluster there is no precursor for its formation as more vertices are added, and thus the transition is first-order. However, above the transition, upon removal of vertices, the sizes of the avalanches which destroy the giant cluster diverge as the critical point is approached, and thus from above the transition is continuous. This transition is mixed-order in that above and below the critical point the nature of the phase transition is different. A different kind of mixed-order transition is seen in a spin model with long-range interactions [10,11]. At the phase transition the order parameter, the magnetisation, jumps discontinuously between 0 and ± 1 , while the correlation length between the spins diverges continuously. In contrast to Ref [14], in this case the characteristics of first-order and continuous transitions are seen simultaneously at the phase transition, rather than being seen separately on either side.

2.2.3 Mean-Field Theories

When developing a theory for a system of interest it is often too difficult to specify all the interactions between each constituent element and then make any useful analytic progress. A long established alternative technique is to develop what's known as a *mean-field theory* [137]. Generally speaking, a mean-field theory seeks to reduce the complexity of the theory by using average or statistical descriptions

of some or all of the interactions.

For equilibrium models, one way to do this is to find an approximation for the free energy in terms of a certain order parameter, and then minimise the free energy with respect to this order parameter in order to find the equilibrium steady state. One can also analyse the derivatives of the free energy with respect to this order parameter in order to learn about the existence and nature of phase transitions that the system may exhibit. A well known example of this approach is the general theory of phase transitions developed by Landau in 1936 [107, 137], where he uses the hypothesis that near a critical point one can expand the free energy in terms of powers of the order parameter. Then one can minimise this function to find the equilibrium value of the order parameter.

The key approximation in this and many other mean-field theories is that there are no correlations, or at least no long-range correlations, between the constituent elements. Even when out of equilibrium, when one cannot always find a free energy-like quantity, it is still possible to develop mean-field theories with this kind of approximation. One such example is the mean-field theory for the DP universality class, which can be used to predict the critical exponents at the inactive-to-active phase transition.

Directed Percolation

The DP model was originally presented in the mathematics literature primarily as a model for liquid flow through random, porous media, but also more generally as a model for a variety of processes such as disease spreading and electron mobility [33]. On a rotated lattice of sites, these sites can be connected by bonds between nearest neighbour sites, and starting from some original active site, bonds can be created to other sites only in one direction (Figure 2.1). For example, one can imagine that under gravity water entering a porous rock would only flow downwards. This can also be thought of as a process in 1+1 dimensions: one spatial and one temporal direction. The spatial direction corresponds to the width of the system along which the sites are distributed. The temporal direction corresponds to the vertical direction. One now considers the ‘water’ to be flowing downwards at a uniform velocity, activating a certain number of sites after time t . There is also a special state, the *absorbing state*, where no sites are active at a time step and thus no further sites will be active, which makes this a non-equilibrium

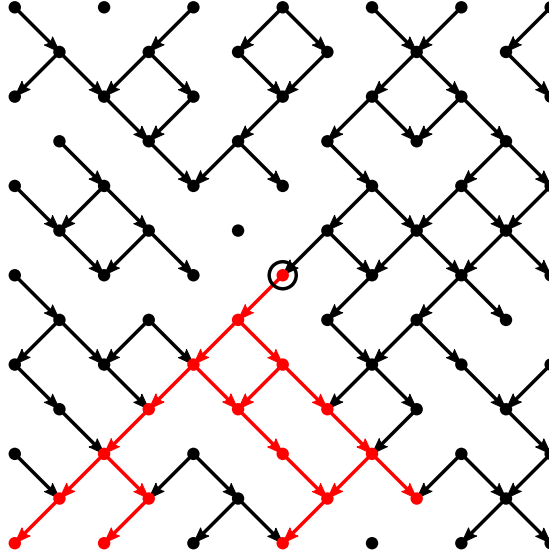


Figure 2.1: (Reproduced from [42]) Directed Percolation (DP) along bonds on a rotated square lattice. A cluster is defined as a set of points and bonds originating from a single source (shown in red). In what is known as “1+1 dimensions”, the vertical direction can be thought of as time instead of space.

model [80].

In this model, the control parameter is the probability p that a bond from an active site to a site at the next time step exists, and the order parameter is the percolation probability P_∞ , the probability that there will be at least one active site as $t \rightarrow \infty$. There is a phase transition in P_∞ at the numerically measured critical value $p_c = 0.644700185(5)$ [96]. When $p \leq p_c$, $P_\infty = 0$, meaning that the activity dies out and the system reaches the absorbing state. When $p > p_c$, P_∞ has some finite, non-zero value and there is an active phase. This phase transition is continuous, and certain properties diverge as $p \rightarrow p_c$, allowing us to define critical exponents to characterise the transition. These properties are: ρ , the density of active sites; ξ_{\parallel} the typical length of the cluster of active sites in the time direction; and ξ_{\perp} , the typical width of a cluster of active sites in the spatial direction. They are conventionally defined

$$\rho \sim |p - p_c|^\beta, \quad \xi_{\parallel} \sim |p - p_c|^{-\nu_{\parallel}}, \quad \xi_{\perp} \sim |p - p_c|^{-\nu_{\perp}}. \quad (2.2.5)$$

To date, no one has been able to analytically calculate the DP universality class

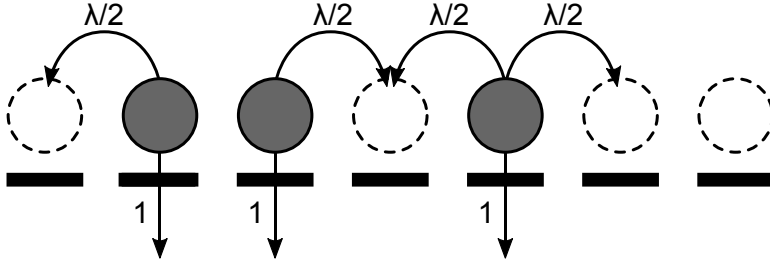


Figure 2.2: (Reproduced from [42]) Schematic diagram of the contact process. Active sites, those containing a particle, become inactive with rate 1, or make an adjacent inactive site active with rate $\lambda/2$.

exponents β , ν_{\parallel} and ν_{\perp} , although they have been numerically measured to be

$$\beta = 0.276486(8), \quad \nu_{\parallel} = 1.733847(6), \quad \nu_{\perp} = 1.096854(4), \quad (2.2.6)$$

in one dimension [96].

Contact Process

It is for this reason that constructing a mean-field equation is useful, as it can help us to predict what the critical exponents are analytically. The DP mean-field theory is easiest motivated from the context of the *contact process*, another model which is part of the DP universality class [80]. In one dimension, the contact process consists of a row of sites which are either active, labelled “1” here, or inactive, labelled “0”, that evolves continuously in time. Starting with a single active site, there are three processes which can occur:

$$\begin{aligned} 1 &\rightarrow 0 \quad \text{with rate } 1 \\ 10 &\rightarrow 11 \quad \text{with rate } \lambda/2 \\ 01 &\rightarrow 11 \quad \text{with rate } \lambda/2. \end{aligned} \quad (2.2.7)$$

Explicitly, these represent two processes: an active site becomes inactive with rate 1; and an active site activates an adjacent inactive site with rate $\lambda/2$. Depending on the choice λ there is a critical value λ_c , analogous to p_c , that separates an active phase, where there is a finite density of active sites as $t \rightarrow \infty$, and an inactive phase, where the system reaches the absorbing state with no active sites. Just as with the DP model described above, the cluster of active sites has the

same three properties $\rho \sim |\lambda - \lambda_c|^\beta$, $\xi_{\parallel} \sim |\lambda - \lambda_c|^{-\nu_{\parallel}}$, and $\xi_{\perp} \sim |\lambda - \lambda_c|^{-\nu_{\perp}}$.

To see how the mean field theory is motivated we can begin by writing down a master equation for the mean activity $\langle \tau_i \rangle$ of site i

$$\frac{\partial \langle \tau_i \rangle}{\partial t} = -\langle \tau_i \rangle + \frac{\lambda}{2} \langle \tau_{i-1}(1 - \tau_i) \rangle + \frac{\lambda}{2} \langle (1 - \tau_i) \tau_{i+1} \rangle , \quad (2.2.8)$$

where

$$\tau_i = \begin{cases} 1 & \text{if site } i \text{ is active} \\ 0 & \text{if site } i \text{ is inactive} \end{cases} , \quad (2.2.9)$$

and the terms on the right hand side are contributions from each of the processes listed in (2.2.7). This equation is difficult to solve because it has terms containing two-point correlations, such as $\langle \tau_{i-1}(1 - \tau_i) \rangle$, for which the master equation would involve 3-point correlation functions and so on. It is for this reason that we make our *mean-field approximation*,

$$\langle \tau_{i-1} \tau_i \rangle = \langle \tau_{i-1} \rangle \langle \tau_i \rangle , \quad (2.2.10)$$

in which we are asserting that there are no spatial correlations between the activities of sites. Now, writing $\langle \tau_i \rangle \equiv \rho_i$ the master equation becomes

$$\frac{\partial \rho_i}{\partial t} = -\rho_i + \frac{\lambda}{2} \rho_{i-1}(1 - \rho_i) + \frac{\lambda}{2} (1 - \rho_i) \rho_{i+1} . \quad (2.2.11)$$

This is still difficult to analyse, so one can make a further approximation that the activity is homogeneous across the system, and there is no i dependence. Thus

$$\frac{\partial \rho}{\partial t} = (\lambda - 1)\rho - \lambda\rho^2 . \quad (2.2.12)$$

It's easy to see from this that there are two steady state values

$$\rho = \begin{cases} 0 , & \lambda < 1 \\ \frac{\lambda-1}{\lambda} , & \lambda > 1 \end{cases} , \quad (2.2.13)$$

with a critical value $\lambda_c = 1$.

Using (2.2.12) and (2.2.13) we can begin to extract the scaling exponents. For $\lambda > \lambda_c$ we see that $\rho \sim (\lambda - \lambda_c)$, and so this simple mean-field predicts $\beta^{MF} = 1$.

Also, when $\lambda < \lambda_c$ both terms of (2.2.12) are negative and so the large t behaviour is $\rho(t) \sim \exp(-t/\xi_{\parallel}) \sim \exp(-|\lambda - \lambda_c|t)$, and so we see that $\xi_{\parallel} \sim |\lambda - \lambda_c|^{-1}$ and $\nu_{\parallel}^{MF} = 1$ [80].

To use the mean-field theory to estimate the spatial scaling exponent ν_{\perp} , one must include the effect of nearest neighbour interactions in the master equation. By expanding

$$\rho_{i\pm 1} \simeq \rho \pm \frac{\partial \rho}{\partial x} + \frac{1}{2} \frac{\partial^2 \rho}{\partial x^2} \quad (2.2.14)$$

and substituting this into (2.2.8), one finds the master equation (2.2.12) is modified by an additional diffusive term:

$$\frac{\partial \rho}{\partial t} = (\lambda - 1)\rho - \lambda\rho^2 + \frac{\lambda}{2} \frac{\partial^2 \rho}{\partial x^2}. \quad (2.2.15)$$

From the analysis of the Gaussian distribution, the root mean square distance L spanned by a diffusive process in one-dimension scales with time t as $L \sim t^{1/z}$ with $z = 2$. By comparing how they scale with $|\lambda - \lambda_c|$, one can see that $\xi_{\perp} \sim \xi_{\parallel}^{\nu_{\perp}/\nu_{\parallel}}$. Then one can identify L with ξ_{\perp} and t with ξ_{\parallel} to see that $z = \nu_{\parallel}/\nu_{\perp}$. Because the diffusion term is the only one contributing spatial correlations we must also have $z = 2$, and thus $\nu_{\parallel} = 2\nu_{\perp}$. So finally, we have found the mean-field scaling exponents for DP in one-dimension:

$$\beta^{MF} = 1, \quad \nu_{\parallel}^{MF} = 1, \quad \nu_{\perp}^{MF} = \frac{1}{2}. \quad (2.2.16)$$

Comparing the numerically calculated exponents in (2.2.6) we see that the mean-field predictions (2.2.16) are not very accurate, but this is not surprising given the level of approximation used in developing the theory. In higher spatial dimensions however correlations between sites become weaker and in fact the mean-field critical exponents are exact in four dimensions and above [80]. Also, improved mean-field theories have been developed, such as one which analyses the density of inactive intervals in the contact process [15] to find

$$\beta = \frac{1}{2}, \quad \nu_{\parallel} = \frac{3}{2}, \quad \nu_{\perp} = 1. \quad (2.2.17)$$

2.3 Random Walks and Diffusion

Many processes are encountered or observed at a level which makes their dynamics seem random, even though the underlying processes are not necessarily so. For example, observed through a microscope, a pollen grain in water seems to follow a random trajectory, known as Brownian motion, without obvious cause (see e.g. [69, 93]). For such a process, although we may know the origin of the randomness, we can model the behaviour at the level of the random trajectory itself. Depending on the nature of the process, we can build appropriate models by approximating the observed behaviour with a *random walk* or *diffusion*, two of the fundamental models for stochastic transport processes, which are actually equivalent in the appropriate limits. A feature of these processes that we are particularly interested in is the *first-passage* probability $F(x, t)$, the probability that the process reached x *for the first time* at time t , the associated *survival probability*, $S(x, t)$, and *Mean First Passage Time*, $T(x)$. The ability to measure first passage statistics is a useful tool for both characterising and optimising search processes. The standard text for these concepts is Ref [144], which we shall follow throughout this section.

2.3.1 Random Walks

A random walker exists of a discrete space of sites and takes what are variously known as ‘hops’, ‘steps’ or ‘jumps’ between adjacent sites at discrete time steps [69, 144, 145, 173]. For simplicity, we will consider here a random walk on a one-dimensional lattice, but generalisations to higher dimensions and different geometries are possible(see e.g. [126, 145]).

As this is stochastic process, what one is interested in knowing is the probability $P(n, \tau)$ that after τ (time) steps, the walker occupies site n . For a random walk where the walker steps from $n \rightarrow n + 1$ with probability p , and from $n \rightarrow n - 1$ with probability $q = 1 - p$, the evolution of the occupation probability can be described by the simple master equation [144]

$$P(n, \tau + 1) = pP(n - 1, \tau) + qP(n + 1, \tau) . \quad (2.3.1)$$

The first term on the right-hand side represents the probability that the walker was at $n - 1$ at the previous time step and hopped on to n at this time step,

and the second represents same same process but in the opposite direction, from $n + 1$. By noticing that the number of steps taken in one direction is binomially distributed, one can find [145]

$$P(n, \tau) = \frac{\tau!}{\left(\frac{\tau+n}{2}\right)! \left(\frac{\tau-n}{2}\right)!} p^{\frac{\tau+n}{2}} q^{\frac{\tau-n}{2}} . \quad (2.3.2)$$

Furthermore, by using Stirling's approximation $\ln(x!) \simeq x \ln x - x$, for large x , one finds [144] that at large times the occupancy probability approaches the Gaussian distribution:

$$P(n, \tau) \rightarrow \frac{1}{\sqrt{2\pi\tau pq}} \exp\left(-\frac{(n - \tau(p - q))^2}{2\tau pq}\right) . \quad (2.3.3)$$

One can also study discrete space random walks in continuous time [144]. In this case, the hops the random walker makes from $n \rightarrow n \pm 1$ are a Poisson process with rate w_{\pm} . By defining the continuous time $t = \tau\delta t$, one can Taylor expand the left hand side of (2.3.1) to first order in δt ,

$$P(n, \tau + 1) \simeq P(n, t) + \frac{\partial P(n, \tau)}{\partial t} \delta t + \mathcal{O}(\delta t) , \quad (2.3.4)$$

to find the continuous time master equation

$$\frac{\partial P(n, \tau)}{\partial t} = w_+ P(n - 1, t) + w_- P(n + 1, t) - w_0 P(n, t) , \quad (2.3.5)$$

where $w_+ = p/\delta t$ and $w_- = q/\delta t$ are the hopping rates in the \pm direction, and $w_0 = 1/\delta t$ is the total hopping rate. It can be shown that, in the appropriate limit, the solution for $P(n, t)$ is also the Gaussian distribution [144].

2.3.2 Diffusion

Diffusion is the fundamental description of transport in continuous time and space, and is equivalent to a random walk in the appropriate limits. A direct link to the random walk can be made clear by further Taylor expansion of (2.3.1) in the spatial coordinate. Writing $x = n\delta x$, and keeping the definition $t = \tau\delta t$, we expand to first order in δt and second order in δx to find

$$P(x, t) + \frac{\partial P(x, t)}{\partial t} \delta t = (p + q)P(x, t) - (p - q)\frac{\partial P(x, t)}{\partial x} \delta x + \frac{(p + q)}{2} \frac{\partial^2 P(x, t)}{\partial t^2} \delta x^2 . \quad (2.3.6)$$

Then, using the fact that we chose $p + q = 1$, we find that we can recover the *advection-diffusion* equation

$$\frac{\partial P(x, t)}{\partial t} = -v \frac{\partial P(x, t)}{\partial x} + D \frac{\partial^2 P(x, t)}{\partial t^2}, \quad (2.3.7)$$

where $v = (p - q)\delta x/\delta t$ is the velocity, and $D = \delta x^2/2\delta t$ is the diffusion constant [144]. The first term on the right-hand side is the advective term, represents a drift at constant velocity v in the positive x direction. The second term is the diffusive term. This causes a broadening and flattening of the distribution, with diffusion constant D . In the case $p = q = 1/2$, then $v = 0$ and we are left simply with the diffusion equation.

To arrive at this continuum limit, the expansion was taken with $\delta x, \delta t \rightarrow 0$, such that $\delta x^2/\delta t$ remains finite. A problem is that v/D diverges as $1/\delta x$, which means that the advective term dominates the dynamics ahead of the diffusive term, and the flattening effect becomes insignificant. For the diffusion effect to be significant one requires that $p - q \propto \delta x$, thus allowing the diffusion to occur at an appreciable rate relative to the advection.

The standard method of solution of (2.3.7) is to use the Fourier transform $P(k, t)$ of $P(x, t)$ to simplify the equation. Once a solution for $P(k, t)$ has been found this can be inverted and integrated directly, after completing the square in the exponent, to find the Gaussian distribution solution

$$P(x, t) = \frac{1}{\sqrt{4\pi Dt}} \exp\left(-\frac{(x - vt)^2}{4Dt}\right). \quad (2.3.8)$$

2.3.3 First-Passage Properties

In many situations one is not just interested in the probability that a quantity has a certain value at some time, but also the *first time* said value was reached. For instance, a particle might undergo diffusion until the first time it reaches an absorbing boundary, or the first time a stock price reaches a certain value may trigger a decision on the part of a buyer or seller.

The first-passage probability $F(x, t|x_0)$ describes the probability that the random walker or diffusing particle reached position x for the first time at time t , given that it started at x_0 . In this section we will choose $x_0 = 0$ and simplify the notation to $F(x, t)$. Although conceptually the first-passage probability is a

simple idea, its explicit connection to the occupation probability $P(x, t)$ is not obvious. One can derive the relationship as by first finding $P(x, t)$ in terms of $F(x, t)$ and then inverting the expression, as described in Ref [144] and outlined in Appendix A.1.

In the context of search processes however it is more useful to study the survival probability $S(x, t)$ of the process. This is the probability that the location x has not been visited up to time t , and is related to the first-passage probability by

$$\begin{aligned} 1 - S(x, t) &= \text{probability that } x \text{ has been reached up to time } t \\ &= \int_0^t F(x, t') dt' , \end{aligned} \quad (2.3.9)$$

or

$$F(x, t) = -\frac{\partial S(x, t)}{\partial t} , \quad (2.3.10)$$

with $S(x, 0) = 1$.

Another related quantity is the Mean First Passage Time (MFPT), $T(x)$. This describes the mean time it takes for the random walker or diffusing particle to first visit x , and is of particular interest in processes where some quantity is being transported to a binding or an absorption site. Furthermore, in search processes this is normally the quantity one wants to minimise, with respect to some control parameter, in order to optimise the search.

The MFPT has a simple and intuitive integral definition

$$T(x) = \int_0^\infty t F(x, t) dt , \quad (2.3.11)$$

but can also be expressed in terms of the survival probability. One can use the relationship (2.3.10) between F and S to write

$$T(x) = - \int_0^\infty t \frac{\partial S(x, t)}{\partial t} dt , \quad (2.3.12)$$

which one can then integrate by parts to find

$$T(x) = -[tS(x, t)]_0^\infty + \int_0^\infty S(x, t) dt . \quad (2.3.13)$$

If one then assumes that $t \rightarrow \infty$ and $S(x, t) \rightarrow 0$ faster than $1/t$, one can integrate by parts to find

$$T(x) = \int_0^\infty S(x, t) dt . \quad (2.3.14)$$

Now with the definition of the Laplace transform

$$\tilde{S}(x, s) = \int_0^\infty S(x, t) e^{-st} dt , \quad (2.3.15)$$

we see that

$$T(x) = \tilde{S}(x, 0) , \quad (2.3.16)$$

the Laplace transform of $S(x, t)$ with $s = 0$. This is a useful connection to make because the Laplace transform can be used to obtain the (temporal) moments of $S(x, t)$.

As an example we will now briefly overview the first passage properties of a diffusive particle which starts at $x_0 > 0$ and is absorbed at the boundary $x = 0$. The probability distribution $P(x, t)$ of the particle obeys the diffusion equation

$$\frac{\partial P(x, t)}{\partial t} = D \frac{\partial^2 P(x, t)}{\partial x^2} , \quad (2.3.17)$$

with the *absorbing boundary condition*

$$P(0, t) = 0 , \quad (2.3.18)$$

which models the absorption at the boundary by enforcing zero probability density there. The solution to this equation [144], by the method of images, is

$$P(x, t) = \frac{1}{\sqrt{4\pi t}} \left[\exp\left(-\frac{(x - x_0)^2}{4Dt}\right) - \exp\left(-\frac{(x + x_0)^2}{4Dt}\right) \right] . \quad (2.3.19)$$

Now the probability $F(0, t)$ of first-passage to the absorbing boundary at $x = 0$ at time t is simply the probability flux into the boundary at time t :

$$\begin{aligned} F(0, t) &= D \frac{\partial P(x, t)}{\partial x} \Big|_{x=0} , \\ &= \frac{x_0}{\sqrt{4\pi t^3}} \exp\left(-\frac{x_0^2}{4Dt}\right) . \end{aligned} \quad (2.3.20)$$

Now we can see that the MFPT is

$$T(0) \sim \int_0^\infty t \cdot t^{-3/2}, \quad (2.3.21)$$

which diverges. Next, we compute the survival probability $S(0, t)$, the probability that the particle has not been absorbed. From (2.3.9),

$$\begin{aligned} S(0, t) &= 1 - \int_0^t \frac{x_0}{\sqrt{4\pi t'^3}} \exp\left(-\frac{x_0^2}{4Dt'}\right), \\ &= 1 + \frac{2}{\sqrt{\pi}} \int_{\infty}^{x_0/\sqrt{4Dt}} e^{-u^2} du, \\ &= \frac{2}{\sqrt{\pi}} \int_0^{x_0/\sqrt{4Dt}} e^{-u^2} du, \\ &= \operatorname{erf}\left(\frac{x_0}{\sqrt{4Dt}}\right), \end{aligned} \quad (2.3.22)$$

where the substitution $u^2 = x_0^2/4Dt'$ was used. When $t \rightarrow \infty$, $\operatorname{erf}(t^{-1/2}) \rightarrow t^{-1/2}$ (see e.g. [24]), and so we have found that the survival probability decays to 0 as $t \rightarrow \infty$. This means that the particle *will* eventually be absorbed at the origin, but the MFPT (2.3.21) diverges, meaning that the mean time it takes to do so is infinite! The implications of this result for a one-dimensional search process is that diffusion, or a random walk, alone is not a very good strategy for locating a target, because of the diverging MFPT. This has helped motivate the development of more advanced strategies (see e.g. [13, 57–59, 119, 125, 135]) which go beyond purely diffusive motion.

The first-passage properties of a diffusive process actually vary with dimension d . It has been shown [144], for the return to the origin, that

$$S(t) \sim \begin{cases} \frac{1}{t^{1-d/2}}, & d < 2 \\ \frac{1}{\ln t}, & d = 2 \\ t^{1-d/2}, & d > 2 \end{cases} \quad (2.3.23)$$

and

$$F(0, t) \sim \begin{cases} \frac{1}{t^{2-d/2}}, & d < 2 \\ \frac{1}{t \ln^2 t}, & d = 2 \\ t^{-d/2}, & d > 2 \end{cases} \quad (2.3.24)$$

and so a diffusive particle only returns to the origin when $d \leq 2$.

2.4 The Asymmetric Simple Exclusion Process (ASEP)

Diffusion and the random walk, as described above, are single particle descriptions of a transport process. It is often of interest however to build models of transport processes with many particles. One such model, conceptually similar to the random walk and described as a ‘driven diffusive system’, is the Asymmetric Simple Exclusion Process (ASEP) [22, 52].

The ASEP, also sometimes also known as the Totally Asymmetric Simple Exclusion Process (TASEP), is a very simple model of non-equilibrium transport that is widely accepted to be “*a fundamental model of non-equilibrium statistical physics*” [22]. The model describes a one-dimensional lattice of ‘hard-core’ particles that undergo biased diffusion and spatially exclude each other, which is the simplest interaction that can be introduced into a model of this type. The model was first proposed in 1968 by MacDonald and Gibbs [113] as a model for the synthesis of proteins, DNA and RNA in a process called biopolymerisation. In the transcription process of RNA, for example, RNA polymerase binds to a piece of DNA and takes sequential steps along its length, synthesising new RNA as it goes. Typically, there are many such enzymes on the DNA strand at once, which causes traffic because RNA polymerase molecules cannot pass through each other, just as is the case with the exclusion interaction (see e.g. [4]).

The model itself is simple to define. There is a one-dimensional lattice of L sites containing N particles. If there is a vacant site ahead, a particle can ‘hop’ onto this site from its current site with Poisson rate p , for which $p = 1$ can be chosen without loss of generality. The dynamics occur in continuous time, so there is a probability pdt that a particle which is able to hop forwards will do in an infinitesimal interval of time dt . If the site ahead is occupied then the particle

must wait for it to become vacant once more before it can move to it.

There are two distinct types of boundary condition which can be applied to complete the model. The first is a periodic boundary condition. In this case there is a fixed density of particles, all travelling in the same direction around a ring of discrete sites. The second boundary condition is an open boundary condition. In this case, particles enter the system at the first site with rate α and travel towards the final site, where they leave the system with rate β .

2.4.1 Periodic Boundary Conditions

It is relatively straightforward to find the steady state of the ASEP with periodic boundary conditions in which there is a uniform current of particles [22]. For a system with L sites and N particles, one first notices that each of the $\binom{L}{N}$ particle configurations are equally likely, occurring with a probability $1/\binom{L}{N}$. The current J_i between sites i and $i+1$ is the hopping rate $p = 1$ multiplied by the probability of there being a particle at site i and a vacancy at site $i+1$. This probability is the number of configurations of the remainder of the sites, $\binom{L-2}{N-1}$, multiplied by the probability of a single configuration given above. Thus, one finds

$$J_i = J = \frac{\binom{L-2}{N-1}}{\binom{L}{N}} = \frac{N(L-N)}{L(L-1)}. \quad (2.4.1)$$

The fact that the current between each pair of adjacent sites is equal tells us that J is the steady state current. Furthermore, by taking the thermodynamic limit, where $N, L \rightarrow \infty$ with the density $\rho = N/L$ remaining finite, one finds the steady state current takes the form

$$J = \rho(1 - \rho). \quad (2.4.2)$$

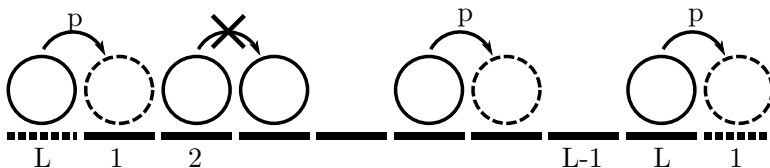


Figure 2.3: A schematic diagram of the ASEP with periodic boundaries. Particles hop forwards with rate p , but cannot hop onto a site that is already occupied.

From this expression it is straightforward to calculate the maximum current $J_{max} = 1/4$ that the ASEP with periodic boundaries can exhibit, which occurs when the density of particles $\rho = 1/2$.

2.4.2 Open Boundary Conditions

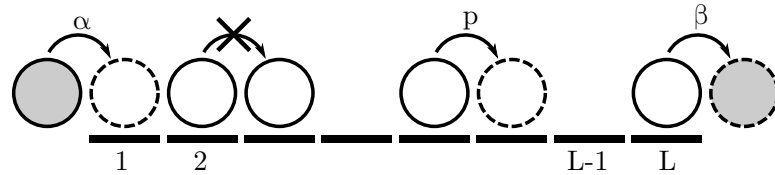


Figure 2.4: A schematic diagram of the ASEP with open boundaries. Particles enter at the left with rate α , hop to adjacent sites with rate p , and leave at the right with rate β .

Analysis of the ASEP with open boundaries is not as simple as with periodic boundaries. The entry and exit rates α and β are equivalent to having an extra site 0 with density α and another site $L + 1$ with density $1 - \beta$, with $\alpha, \beta < 1$.

The key features of the phase diagram can be extracted from a simple mean-field theory [22, 44] which assumes that the steady state probability distribution has a factorised form

$$P(\tau_1, \tau_2, \dots, \tau_L) = \prod_{i=1}^L \mu_i(\tau_i). \quad (2.4.3)$$

In this formalism,

$$\tau_i = \begin{cases} 1 & \text{if site } i \text{ is occupied} \\ 0 & \text{otherwise} \end{cases} \quad (2.4.4)$$

and the density of particles at site i is $\rho_i = \langle \tau_i \rangle$, the mean occupancy τ_i . The function

$$\mu_i(\tau) = \begin{cases} \rho_i & \text{if } \tau = 1 \\ 1 - \rho_i & \text{if } \tau = 0 \end{cases} \quad (2.4.5)$$

simply gives the probability that the site i is occupied ($\mu_i(1)$) or not ($\mu_i(0)$). Higher order correlations are neglected in this approximate theory, meaning that we use the mean-field approximation $\langle \tau_i \tau_j \rangle = \langle \tau_i \rangle \langle \tau_j \rangle = \rho_i \rho_j$, in a similar way as was used in the DP mean-field theory described in Section 2.2.3.

One can use this factorised distribution to write down a master equation for

the density ρ_i at site i . The transition into a state where i is occupied requires a configuration with $\tau_{i-1} = 1$ and $\tau_i = 0$. Similarly, a transition out of a state where i is occupied require $\tau_i = 1$ and $\tau_{i+1} = 0$. This means we can write

$$\frac{\partial \rho_i}{\partial t} = \mu_{i-1}(1)\mu_i(0) - \mu_i(0)\mu_{i+1}(1) = \rho_{i-1}(1 - \rho_i) - \rho_i(1 - \rho_{i+1}), \quad (2.4.6)$$

where the contributions from the occupancies of the other sites not involved in the transition have been ‘integrated out’. In the steady state the currents into and out of a site must be balanced, so we can see from this equation that we have a mean-field current

$$J = \rho_i(1 - \rho_{i+1}). \quad (2.4.7)$$

This expression for the current gives us the recursion relation

$$\rho_{i+1} = 1 - \frac{J}{\rho_i} \quad (2.4.8)$$

relating the densities at adjacent sites that can be used to obtain and understand the phase diagram for the model.

There are two fixed points, corresponding to $\rho_{i+1} = \rho_i$, given by

$$\rho_{\pm} = \frac{1}{2} \left(1 \pm \sqrt{1 - 4J} \right). \quad (2.4.9)$$

When $J < 1/4$, these fixed points are real, ρ_+ being stable and ρ_- unstable, and lead to the existence of two phases: *high density* and *low density*.

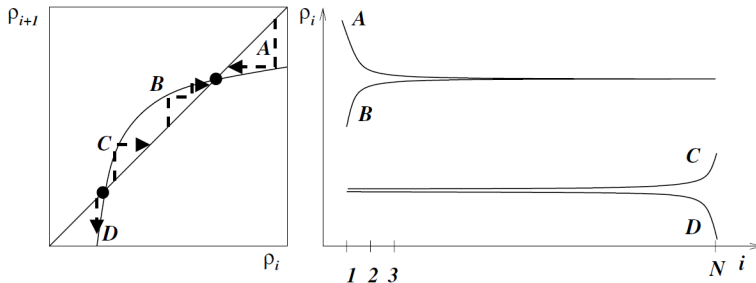


Figure 2.5: (Reproduced from [22]) The iterative density mapping in the mean-field theory for the ASEP. Profiles A and B quickly iterate close to the high-density fixed point ρ_+ . Profiles C and D begin infinitesimally close to the low-density fixed point until close to the right boundary, where they iterate away.

In the *high density* phase, densities close to ρ_+ are iteratively mapped according to (2.4.8) arbitrarily close to ρ_+ . As a result, the bulk density of particles in the system is approximately ρ_+ . The exit rate β is equivalent to having a boundary site $\rho_{L+1} = 1 - \beta$ and so $\rho_+ = 1 - \beta$. The bulk current $J = \rho(1 - \rho)$ and therefore because the bulk density is approximately ρ_+ , $J = \beta(1 - \beta)$. Also, from (2.4.9), $J = \rho_+ \rho_-$. This means that $\rho_- = \beta$ and, because $\rho_- < \rho_+$, we find that $\beta < 1/2$ in this phase. Furthermore, the entry rate α is equivalent to having a boundary site with $\rho_0 = \alpha$ and, because the density started in the region near ρ_+ , we find that $\alpha > \rho_- = \beta$. This means that we see the high density phase when $\beta < 1/2$ and $\alpha > \beta$.

A similar argument follows for the *low density* phase. In this case the bulk density is $\rho_- = \alpha$, and so the current is $J = \alpha(1 - \alpha)$ in the bulk. This means that this time $\rho_+ = 1 - \alpha$ and the condition $\rho_+ > \rho_-$ tells us that $\alpha < 1/2$. Furthermore, because $\rho_{L+1} < \rho_+$ we find that $1 - \beta < 1 - \alpha$, and so $\beta > \alpha$. Thus the *low density* phase exists when $\alpha < 1/2$, $\beta > \alpha$.

There is also a third phase, when $J > 1/4$, called the *maximal current* phase. There are no fixed points in (2.4.8) in this case, but by analysis of the density profile one can show [22] that $J \approx \frac{1}{4} + \mathcal{O}\left(\frac{1}{L^2}\right)$ in the bulk. In the maximal current phase it has been shown [70] that the relaxation time τ to the steady state scales like $\tau \sim L^{3/2}$, with dynamic exponent $z = 3/2$. This is the same dynamic exponent as is seen in the KPZ equation for non-equilibrium surface growth (Section 2.6.2) and highlights the connection between the two, as will be discussed in Section 2.6.3. This same dynamic exponent $z = 3/2$ has also been found in the ASEP with periodic boundaries [47].

The three phases can be also be extracted by applying a phenomenological theory of kinematic waves, first developed in order to study traffic flow [112]. Without going into details (see [22]), what this theory tells us is that the phases can be described in terms of the dynamics of a shock front, a discontinuous boundary between a region of high and low density. In the low density phase, when $\alpha < 1/2$ and $\alpha < \beta$, this shock front propagates towards the right boundary, and thus the region of lower density α propagates from the left boundary into the bulk. In the high density phase, the opposite happens and the shock propagates to the left boundary, causing the bulk to have density $1 - \beta$. When $\alpha = \beta < 1/2$,

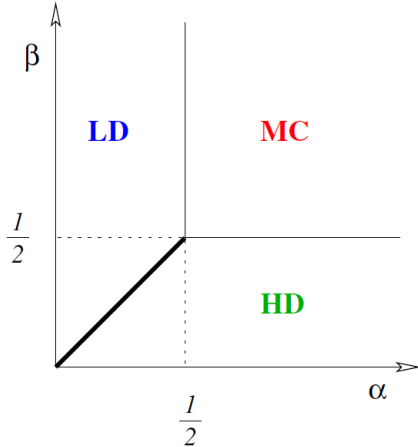


Figure 2.6: (Reproduced from [22]) The phase diagram for the ASEP predicted by the mean-field theory. The discontinuous-transition line between the high-density (HD) and low-density phases (LD) is indicated by the bold line. The transition between HD/LD and the maximal current (MC) phase is continuous.

the system is in the *coexistence phase* and the shock front is stationary somewhere in the bulk, with density $\alpha < 1/2$ to the left and density $1 - \beta > 1/2$ to the right. Beyond this phenomenological analysis, in the stochastic model what actually happens is that the shock front performs a random walk, or diffuses, through the bulk and its *average position* is stationary [22].

In fact the ASEP can be solved exactly by analysis of matrix product states [46], and it can also be shown that it exhibits two different kinds of phase transition [52]. From the low- and high-density phases the transition to the maximal current phase is continuous, with a discontinuity in the second derivative of the current. The transition *between* the low- and high-density phases however is *discontinuous*. In this case the current is continuous but there is a discontinuity in both the bulk density of the current and the first derivative.

There are also some interesting generalisations of the ASEP which have been studied in detail. For instance, in the Partially Asymmetric Exclusion Process (PASEP) particles hop to the right with rate p but can also hop to the left with rate q (see e.g. [23, 71, 148, 149]). There have also been studies of the ASEP with second class particles, which have exhibited shocks in the particle density and long-range correlations in the positions of the second-class particles [45, 48]. Similarly the density profile and phase diagram of the ASEP on a ring with a single defect particle have been calculated [150]. Furthermore, in studies with a

single defect particle [94, 95] and with equal densities of two species of particle [6, 7] the phenomenon of spatial condensation of particles is observed. Spatial condensation is a key feature of the model discussed next in Section 2.5.

2.5 The Zero-Range Process (ZRP)

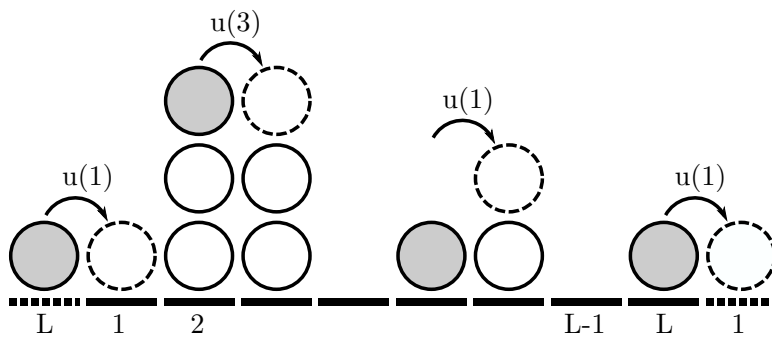


Figure 2.7: Schematic diagram of the ZRP. One particle from a site containing n hops to the next site with rate $u(n)$.

The Zero-Range Process (ZRP) is a model of transport of discrete mass units in discrete space and continuous time [55, 56], which is closely related to the ASEP. Like the ASEP, single mass units, or *particles*, ‘hop’ between sites. Unlike the ASEP, there is no exclusion between particles, meaning there is no limit to how many particles are allowed to be on any one site at any one time, and particles hop with a Poisson rate $u(n_l)$, which depends only on the occupancy n_l of the site l that is being hopped from. The simplest ZRP set-up is on a one-dimensional, periodic lattice of L sites and N particles, with particle density $\rho = N/L$, where the particles are only allowed to hop in one direction.

One motivation for studying the ZRP is its mapping onto the ASEP [56] in one-dimension. In this mapping, the sites in the ZRP are identified as particles in the ASEP, and the number of particles on a site in the ZRP represents the number of vacant sites between the corresponding ASEP particle and the next. The ZRP can then be used to study the ASEP with the condition that the hop rates are no longer constant, but depend on the gaps between one particle and the next. This type of formalism has found applications in various contexts, such as in the bus route model [133], a two-species driven system which describes the jamming of ‘sticky’ particles or gelling fluid, and another two-species driven

diffusive system where the ZRP hopping is analogous to the current through domains of particles [53]. It has also been used to find a general criterion for phase separation in driven, density conserving, one-dimensional driven systems [100].

An important and useful property of the ZRP, which makes it amenable to analysis, is that the steady state probability distribution $P(\{n_l\})$ of the configuration $\{n_l\}$ can be written in a factorised form [56]

$$P(\{n_l\}) = \frac{1}{Z_{L,N}} \prod_{l=1}^L f(n_l) , \quad (2.5.1)$$

where $Z_{L,N}$ is the normalisation constant, given by

$$Z_{L,N} = \sum_{\{n_l\}} \prod_{l=1}^L f(n_l) \delta \left(\sum_{l=1}^L n_l - N \right) , \quad (2.5.2)$$

which plays the same role as an equilibrium canonical partition function, and is thus referred to as such. The factors $f(n)$ are functions of the hop rate $u(n)$ and are given by

$$f(n) = \prod_{m=0}^n \frac{1}{u(m)} , \quad n > 0 , \quad f(0) = 1 . \quad (2.5.3)$$

This form of $f(n)$ can be found by substituting $P(\{n_l\})$ from (2.5.1) into the steady state master equation. One can then cancel terms to find the recursion relation

$$f(n) = \frac{f(n-1)}{u(n)} , \quad (2.5.4)$$

which can be iterated to find (2.5.3), where $f(0) = 1$ can be chosen without loss of generality.

2.5.1 Condensation

Another interesting property of the Zero-Range Process is that under certain conditions it exhibits a transition to a phase with real space condensation, where a single site contains a finite fraction of the total number of particles in the thermodynamic limit [55, 56]. Condensation phenomena are of broad interest as they are seen in a wide range of contexts, such as economic models [34], traffic

flow [37, 102, 111, 133], and complex networks [5, 104].

In the ZRP, the existence of a condensate depends on the behaviour of the function $f(n)$, the details of which depend on the exact choice of $u(n)$. Condensation in the ZRP also has some similarities to Bose-Einstein (BE) condensation, which we briefly review in Appendix A.2. However, in the ZRP condensation takes place over spatially equivalent sites and there is no site selection preference, whereas BE condensation occurs in state space, and the ground state is always selected. Another important difference is that there is no grand-canonical condensation in the ZRP [56].

The nature of the condensation transition can be revealed from analysis of the particle density ρ using the grand canonical partition function [56]

$$\mathcal{Z}_L = \sum_N z^N Z_{L,N} , \quad (2.5.5)$$

where, similarly to BE condensation, the fugacity z is used to set the mean density of particles via

$$\rho = \frac{z}{L} \frac{\partial \ln \mathcal{Z}_L}{\partial z} . \quad (2.5.6)$$

One can exploit the fact that $P(\{n_l\})$ factorises to find $\mathcal{Z}_L = [F(z)]^L$, where

$$F(z) = \sum_{m=0}^{\infty} z^m f(m) , \quad (2.5.7)$$

and consequently that

$$\rho = \frac{z F'(z)}{F(z)} , \quad (2.5.8)$$

where $F'(z) = \partial F / \partial z$.

The right hand side of (2.5.8) can be shown to be an increasing function of z , so as one increases z , one increases the average density ρ . However, the sum $F(z)$ has a radius of convergence, $z = \beta$, above which there is no solution for $z(\rho)$. Thus,

$$\rho_c = \frac{\beta F'(\beta)}{F(\beta)} \quad (2.5.9)$$

is the maximum average density which can be specified by a choice of z . If ρ_c is infinite then there is always a solution for z for any density ρ . If, however, ρ_c is finite then for $\rho > \rho_c$ there is no solution, and the excess $L(\rho - \rho_c)$ particles

form a condensate. Thus, the existence of a condensation transition depends on whether or not ρ_c is finite or infinite.

This condition can be used to find a condition on the hop rate $u(n)$ which would allow for condensation. $F(\beta)$ converges, so the convergence of ρ_c depends on the convergence of the sum $\beta F'(\beta) = \sum_{m=0}^{\infty} m\beta^m f(m)$; if this quantity converges then ρ_c has a finite value and we have a condensate. We can use the recursion (2.5.4) to show that the ratio of successive terms is

$$\frac{(n-1)f(n-1)}{\beta n f(n)} = \frac{u(n)}{\beta} \left(1 - \frac{1}{n}\right). \quad (2.5.10)$$

By the ratio test (see e.g. [24]), for $\beta F'(\beta)$ to converge we require that in the limit $n \rightarrow \infty$ the ratio (2.5.10) is greater than 1, which is satisfied if it decays slower than $1 + 1/n$. This means that, for large n

$$u(n) > \beta \frac{(n+1)}{(n-1)} \simeq \beta \left(1 + \frac{2}{n} + \mathcal{O}\left(\frac{1}{n^2}\right)\right), \quad (2.5.11)$$

which tells us that we have condensation as long as $u(n)$ decays *slower* than $\beta(1 + 2/n)$. If one considers the generalised hop rate

$$u(n) = \beta \left(1 + \frac{b}{n^\alpha}\right), \quad (2.5.12)$$

then we find that a condensation transition occurs when $0 < \alpha < 1$, and for $b > 2$ when $\alpha = 1$, in which case the critical density

$$\rho_c = \frac{1}{b-2} \quad (2.5.13)$$

can be found exactly [75, 76].

The condensate phase has been studied extensively and it has been found to have many interesting properties. At lower occupancies n the occupancy distribution $p(n)$ scales like a power law $p(n) \sim n^{-\gamma}$, but at higher occupancies the distribution exhibits a Gaussian ‘bump’, representing the contribution to $p(n)$ from the condensate [115]. The area under the Gaussian bump representing the condensate is $1/L$, which indicates that the condensate occupies a single site, but it has also been proved rigorously that this is the case [76]. When

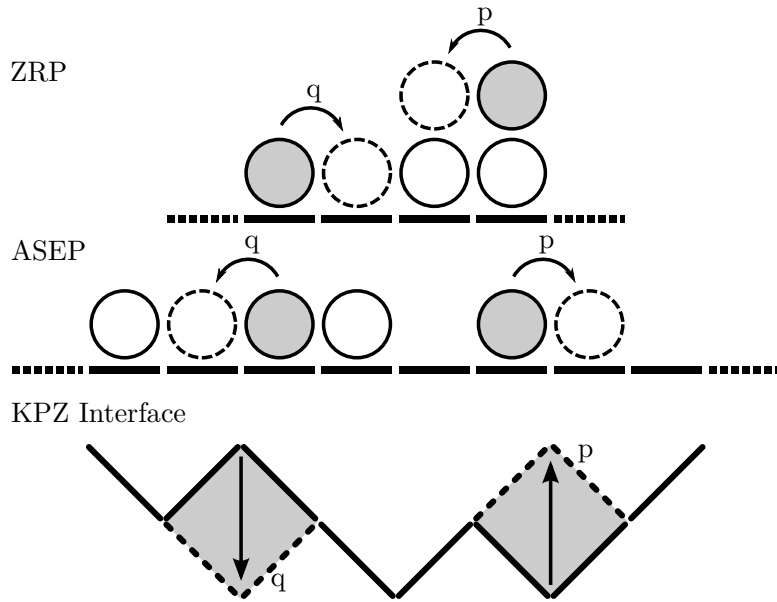


Figure 2.8: Illustration of the correspondence between the ZRP, ASEP, and KPZ interface.

one is at the critical density itself, $p(n) \sim n^{-\gamma}$ with no additional condensate piece, and in the fluid phase, below the critical density $p(n)$ decays exponentially, $p(n) \sim \exp(-n/n^*)$. Starting from a homogeneous initial distribution of particles, the steady state condensate phase is reached via a non-trivial process of coarsening [133]. In the steady state itself the condensate is essentially static, but after residing at the same point in space for a long period it can dissolve due to a large fluctuation and reform somewhere else [75]. As will be discussed further in Chapter 4, many variations of the ZRP have been developed and studied which exhibit a condensate phase which is not static but moves through the system. This movement can happen in many ways, for example diffusively [110, 116, 117, 140, 141], with a ‘slinky-like’ motion [85–87], or ballistically [62, 172, 174].

In the next section, Section 2.6, we discuss stochastic modelling of interfacial growth. A non-equilibrium, growing interface appears to be a very different kind of transport process to the ZRP but, as will be discussed in Section 2.6.3, the dynamics of a growing interface can also be linked to the ASEP (Figure 2.8).

2.6 Interfacial Growth

The growth of an interface is a dynamic process which appears in a variety of contexts, and the physical shape of an interface, whether between two materials or encapsulating one, can have interesting properties. Interfaces are seen, for example, when: soaking up a liquid with a porous material, like tea with kitchen towel; on a piece of paper, burnt at the edges; in the surfaces created by molecular beam epitaxy; at the edges of a bacterial colony, growing outwards from a Petri dish. All of these can show a familiar, rough surface or interface. It is of great interest to classify and understand the shapes and properties of such structures, once formed and during the dynamic processes of formation and continued growth. We will now introduce some of the theory behind interfacial growth, with particular focus on the Edwards-Wilkinson (EW) equation and the Kardar-Parisi-Zhang (KPZ) equation. A good text on the subject, from which we draw on extensively in this section, is Ref [12], and two comprehensive reviews can be found in Ref [79] and Ref [105].

Two important properties of interfaces that can be measured and analysed are their mean heights and their widths. A one-dimensional interface is one which has only one spatial dimension in its domain x and has a height $h(x, t)$ above the surface at x which evolves in time, t . In general, though, one can have a higher dimensional interface with height $h(\vec{r}, t)$ above some point \vec{r} on a higher-dimensional surface. For simplicity, we will discuss only one-dimensional interfaces and, furthermore, we will discuss interfaces in terms of a set of heights over L discrete sites. In this case, the mean height is given by

$$\bar{h}(t) = \sum_{l=1}^L h(l, t) . \quad (2.6.1)$$

The rate of change of the mean height could describe the rate of deposition of atoms, or the rate at which a bacterial colony is growing outwards. Perhaps a more interesting measure, the width $W(t)$ of an interface is simply the root mean

square height, given by

$$W(t) = \sqrt{\frac{1}{L} \sum_{l=1}^L (h(l, t) - \bar{h}(t))^2}. \quad (2.6.2)$$

The width characterises the *roughness* of an interface. A very *smooth* interface will have very small fluctuations from the mean height along its length, and thus the width will be small. An interface with a large width is one where the root mean square variations in height from the mean height are large, and as such the interface is *rough*.

The strategy for classifying different kinds of interface that we will discuss here is to study the *scaling* of the interface properties. In this way, no matter what the microscopic physical details are, one can look at the generic fundamental properties of different interfaces and try and group them into *universality classes*, within which all the members exhibit the same scalings of certain properties. In particular, we will discuss the scaling of the width, with respect to time t and the interface size, or length, L . Understanding how an interface's morphology scales with a certain length scale, in this case the interface length L , is an important idea. If one were to look at the side of a snow capped mountain range from close up, its surface might look very smooth. At a distance however, it would probably look very jagged and rough. It's clear then that describing the roughness of an interface only makes sense if one gives due consideration to length scales [12].

A simple model for the growth of a *non-equilibrium* interface is the *Ballistic Deposition* (BD) model, which had early applications as a model for the sedimentation volume of colloids (e.g. [171]) and has since been studied in the context of surface scaling properties [9, 64, 99]. In one-dimension, there is a (flat) lattice of L sites, onto which a particle is dropped from above. The site above which the particle is dropped is chosen at random and the particle travels in a straight line downwards. The particle either sticks to the first particle it makes contact with, whether sticking to another at its side or by coming down to rest on the highest particle on the site it has been released above (see Figure 2.9). The height at site l is then measured to the highest point in the column of particles above it, even though the column may contain some gaps where there are no particles.

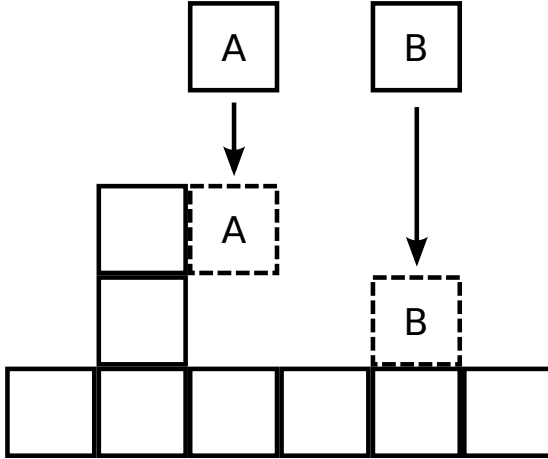


Figure 2.9: Schematic diagram of Ballistic Deposition (BD). New particles dropped onto the surface stick to the first particle they come into contact with. (Inspired by figure in Ref [12].)

Typically, when one plots the time evolution of the width of the growing surface from an initially smooth state, one sees the growth profile is characterised by two regions. In the first, the width grows as a power of time, like

$$W(L, t) \sim t^\beta , \quad (2.6.3)$$

where β is known as the *growth exponent*. Then the second region is seen after some *crossover time*, t_c , where the width saturates to its (time-independent) saturation value

$$W_s \sim L^\alpha , \quad (2.6.4)$$

where α is known as the *roughness exponent*. There is typically also a third exponent, z , known as the dynamic exponent which characterises the crossover time

$$t_c \sim L^z . \quad (2.6.5)$$

After collecting data from different system sizes L , one can perform a collapse of this data to learn more about the functional form of the width W . First, by plotting $W(L, t)/W_s(L)$, one will see that all the interface data saturates at the same value. Similarly, by plotting $W(L, t)$ against the rescaled time $t/t_c(L)$ one will see that the data sets saturate at the same rescaled crossover time. By performing both scaling procedures together, we find that the data sets will

collapse onto each other, and have the functional form

$$W(L, t) \sim L^\alpha f(t/L^z), \quad (2.6.6)$$

where the scaling function $f(u)$ behaves like

$$f(u) \sim \begin{cases} u^\beta, & u \ll 1 \\ \text{const.}, & u \gg 1 \end{cases} \quad (2.6.7)$$

The expression (2.6.6) is commonly known as the *Family-Vicsek scaling relation* and it describes the finite size scaling of an interface [64].

One can also find a scaling law for this scaling function (2.6.6) that relates the three exponents α , β and z , which are not independent, by considering the crossover time t_c . Approaching t_c from earlier times, $W(L, t_c) \sim t_c^\beta$, but approaching from later times $W(L, t_c) \sim L^\alpha$. Because W is continuous, these expressions must be equivalent. Thus, using $t_c \sim L^z$,

$$L^{z\beta} = L^\alpha, \quad (2.6.8)$$

and so

$$\alpha = \frac{z}{\beta}. \quad (2.6.9)$$

In fact, this scaling law holds for any system which has the scaling relation (2.6.6), not just the BD model. For the BD model, numerical simulations [9, 120] have been used to measure the exponents to be

$$\alpha = 0.47 \pm 0.02, \quad \beta = 0.33 \pm 0.006. \quad (2.6.10)$$

The L dependence of the saturation width and the crossover time is called a *finite size effect* and has its origins in the correlations between the heights along the interface. One can define a correlation length ξ , the characteristic distance along the interface over which the heights are correlated. As the interface grows, ξ grows with time, but it cannot grow indefinitely because there can be no correlations over length scales greater than L . At t_c itself, $t_c \sim \xi^z$, because $\xi \sim L$, and so $\xi(t_c) \sim t_c^{1/z}$. This relationship actually holds for $t < t_c$ [12] and

thus

$$\xi \sim \begin{cases} t^{1/z}, & t \ll t_c \\ L, & t \gg t_c \end{cases}. \quad (2.6.11)$$

2.6.1 The Edwards-Wilkinson (EW) Equation

To attempt to calculate the scaling exponents α and β analytically, one can attempt to write down a stochastic growth equation to describe the evolution of the height in the form

$$\frac{\partial h(x, t)}{\partial t} = G(h, x, t) + \eta(x, t), \quad (2.6.12)$$

where $G(h, x, t)$ is a general function which includes derivatives of $h(x, t)$ and $\eta(x, t)$ is the white noise term, which has the properties

$$\langle \eta(x, t) \rangle = 0, \quad \langle \eta(x, t) \eta(x', t') \rangle = 2D\delta(x - x')\delta(t - t'), \quad (2.6.13)$$

meaning its average contribution to the rate of change of the height is zero, and it is uncorrelated in space and time.

The simplest such equation which is used to describe a growing interface is the Edwards-Wilkinson (EW) equation [50]

$$\frac{\partial h(x, t)}{\partial t} = \nu \frac{\partial^2 h(x, t)}{\partial t^2} + \eta(x, t), \quad (2.6.14)$$

which is presented here in one-dimension, but can be generalised to higher dimensions. The term $\nu \frac{\partial^2 h(x, t)}{\partial t^2}$ has the effect of smoothing the interface and so ν is often referred to as the surface tension. It is important to note that this term smooths the interface by ‘redistributing’ the height while leaving the mean height unchanged. This means that the EW equation describes an *equilibrium* interface, which has average velocity

$$v = \int_0^L dx \left\langle \frac{\partial h(x, t)}{\partial t} \right\rangle = 0, \quad (2.6.15)$$

because $\langle \eta(x, t) \rangle = 0$ and with periodic boundary conditions the integral of the surface tension term is also zero on average.

Although this equation describes an equilibrium interface, starting from flat

initial conditions it still displays similar scaling features to the BD model. At early times the width $W \sim t^\beta$ and it eventually saturates to $W_s \sim L^\alpha$.

An object which has some inherent randomness in its shape can exhibit statistical similarities in its shape at different length scales. Such shapes are described as being *self-affine*, which means that upon the application of some anisotropic rescaling of its dimensions its shape remains statistically the same, or *invariant* [12]. We can apply this description to a random interface described by the EW equation. By rescaling x by some scaling factor b , such that

$$x \rightarrow bx , \quad (2.6.16)$$

and by rescaling the height as

$$h \rightarrow b^\alpha h , \quad (2.6.17)$$

one should find that the new, rescaled interface is statistically indistinguishable from the original. Furthermore, to compare the dynamics of the rescaled interface with the original we must also rescale time

$$t \rightarrow b^z t . \quad (2.6.18)$$

Applying these transformations to (2.6.14), and multiplying by $b^{z-\alpha}$ we find

$$\frac{\partial h(x, t)}{\partial t} = \nu b^{z-2} \frac{\partial^2 h(x, t)}{\partial t^2} + b^{-\alpha-(1-z)/2} \eta(x, t) . \quad (2.6.19)$$

The rescaling of the derivatives is clear, but the rescaling of the noise term η comes from a rescaling of the correlation function

$$\langle \eta(bx, b^z t) \eta(bx', b^z t') \rangle = \frac{1}{b^{z+1}} \langle \eta(x, t) \eta(x', t') \rangle , \quad (2.6.20)$$

where we have used the identity

$$\delta(ax) = \frac{1}{a} \delta(x) ,$$

and assumed that η rescales like the square root of (2.6.20). By demanding that the rescaled interface be statistically identical to the original, the EW equation must be *invariant* under this transformation of variables. Thus, there should be

no dependence on the choice of scaling factor b in (2.6.19), meaning that each exponent of b should be equal to zero. This leads to two equations

$$z - 2 = 0 , \quad \alpha + \frac{(1-z)}{2} = 0 , \quad (2.6.21)$$

from which we can calculate the scaling exponents

$$z = 2 , \quad \alpha = \frac{1}{2} , \quad \beta = \frac{1}{4} . \quad (2.6.22)$$

These are the results for the one-dimensional EW equation, but the procedure above can be generalised to any dimension d [12] to find

$$z = 2 , \quad \alpha = \frac{2-d}{2} , \quad \beta = \frac{2-d}{4} . \quad (2.6.23)$$

In fact, the exact solution to (2.6.14) can be found using Fourier transforms in both space and time [131] to find

$$\langle h(x,t)h(x',t') \rangle = \frac{D}{2\mu} |x-x'| f\left(\frac{\nu|t-t'|}{|x-x'|^2}\right) , \quad (2.6.24)$$

where

$$f(u) \rightarrow \begin{cases} u^{1/2} & u \rightarrow 0 \\ \text{const.} & u \rightarrow \infty \end{cases} , \quad (2.6.25)$$

from which the same scaling exponents (2.6.23) can be calculated.

These scaling exponents (2.6.23) characterise the EW universality class of equilibrium interfaces, but comparing these to the measured BD scaling exponents (2.6.10) we can see that the EW model does not accurately predict the growth exponent β , and so BD is not in this universality class. One key aspect of the BD model that the EW equation does not capture is its non-equilibrium property which comes from the “sticking” effect, where particles adhere to the first part of the surface they encounter, whether or not it is the top of the column they are falling towards. A feature that is modelled by the sticking is the effect of *lateral growth*, where the interface grows in the direction of the local normal.

2.6.2 The Kardar-Parisi-Zhang (KPZ) Equation

This insight that the lateral growth is significant was presented by Kardar, Parisi and Zhang in the paper describing their formulation of the eponymous Kardar-Parisi-Zhang (KPZ) equation [101]. For growth which occurs in the direction of the local normal of the surface with velocity v , the distance grown in an infinitesimal time step δt is $v\delta t$. This distance forms a right-angled triangle with hypotenuse δh , the distance grown in the ‘height-direction’, and the remaining side of length $v\delta t(\partial h/\partial x)$. Using the Pythagorean theorem, one can write down an expression for the resulting height increase δh as

$$\delta h = \sqrt{(v\delta t)^2 + \left(v\delta t \frac{\partial h}{\partial x}\right)^2} = v\delta t \sqrt{1 + \left(\frac{\partial h}{\partial x}\right)^2}. \quad (2.6.26)$$

When $|\partial h/\partial x| \ll 1$ this can be expanded to find

$$\frac{\partial h(x, t)}{\partial t} \simeq v + \frac{v}{2} \left(\frac{\partial h(x, t)}{\partial x} \right)^2. \quad (2.6.27)$$

This tells us that to capture the non-equilibrium effect of lateral growth, one must include a non-linear term $(\partial h/\partial x)^2$ in the growth equation (2.6.14). This motivates the KPZ equation

$$\frac{\partial h(x, t)}{\partial t} = \nu \frac{\partial^2 h(x, t)}{\partial t^2} + \frac{\lambda}{2} \left(\frac{\partial h(x, t)}{\partial x} \right)^2 + \eta(x, t), \quad (2.6.28)$$

where $\lambda/2$ is the conventional constant prefactor. The non-linear term makes the equation describe non-equilibrium growth because it breaks the symmetry in the h direction. This means that the growth equation is now no longer invariant under the transformation $h \rightarrow -h$, and the mean velocity

$$v = \frac{\lambda}{2} \left\langle \left(\frac{\partial h(x, t)}{\partial x} \right)^2 \right\rangle \quad (2.6.29)$$

is now non-zero (unless the interface is flat).

Calculating the scaling exponents predicted by the KPZ equation cannot be done using the same technique as given above for the EW equation because in this case the constants ν , λ and D do not renormalise independently of each other.

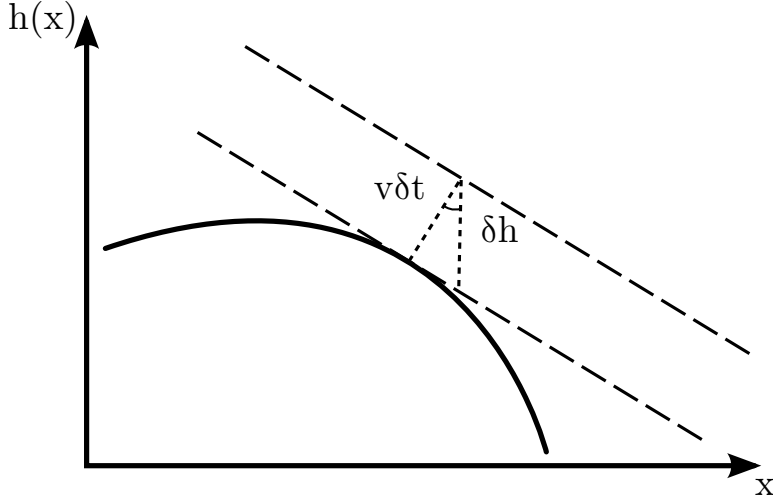


Figure 2.10: Schematic diagram showing the geometric relationship between growth in the direction of the local normal of the surface normal and the associated increase in height. (Inspired by illustration in Ref [12].)

In fact, no one has yet been able to calculate the KPZ exponents exactly in dimensions $d > 1$, and only numerical measurements exist [3, 12]. In one dimension however, one can calculate the exponents by approaching the problem from multiple angles.

The first step is to notice that the height in the KPZ equation maps to the stochastic Burgers equation [35, 101]

$$\frac{dv(x, t)}{dt} = \nu \frac{\partial^2 v}{\partial x^2} - \frac{\partial \eta(x, t)}{\partial x} \quad (2.6.30)$$

under the transformation

$$v = -\frac{\partial h(x, t)}{\partial x}, \quad (2.6.31)$$

with $\lambda = 1$ and the total derivative

$$\frac{dv(x, t)}{dt} = \frac{\partial v(x, t)}{\partial t} + v \frac{\partial v}{\partial x}. \quad (2.6.32)$$

Because there is a direct mapping, the scaling exponents for the burgers equation and the KPZ equation should be linked. After rescaling the total derivative (2.6.32) becomes

$$\frac{dv(x, t)}{dt} = \frac{\partial v(x, t)}{\partial t} + v b^{\alpha+z-2} \frac{\partial v}{\partial x}. \quad (2.6.33)$$

This derivative should remain invariant under rescaling, which gives us the relationship

$$\alpha + z = 2 . \quad (2.6.34)$$

To find another relationship between the exponents, we first consider the scaling relationship

$$b^\alpha h(x) \sim h(bx) \quad (2.6.35)$$

which is described by (2.6.16) and (2.6.17). A consequence of scale invariance is that

$$\Delta h(\Delta x) \sim (\Delta x)^\alpha , \quad (2.6.36)$$

where $\Delta h(\Delta x) \equiv |h(x_2) - h(x_1)|$ and $\Delta x^\alpha \equiv |x_2 - x_1|^\alpha$. That is, the height difference between two points scales as a power α of the separation distance. Now, consider a random walk which moves upwards or downwards with probability $p = 1/2$ at every time step t . This is one of the simplest self-affine random structures, and as such obeys the scaling relationship (2.6.35) [12]. As discussed in Section 2.3, the probability of being at position y after t steps (for large y, t) is

$$P(y, t) = \frac{1}{\sqrt{2\pi t}} \exp\left(-\frac{y^2}{2t}\right) . \quad (2.6.37)$$

From this equation, one can calculate the standard deviation

$$\langle (y(t_2) - y(t_1))^2 \rangle^{1/2} \sim |t_2 - t_1|^{1/2} . \quad (2.6.38)$$

Now, consider mapping the time coordinate t onto the interface length coordinate x , and the space coordinate y onto the interface height coordinate h . One can see then that generically,

$$\langle \Delta h^2 \rangle^{1/2} \sim (\Delta x)^{1/2} , \quad (2.6.39)$$

which implies that $\alpha = 1/2$ for any interface which is invariant under the rescaling (2.6.35). This scaling relation is obeyed by the EW equation, and the random walk prediction for α agrees with that calculated in (2.6.23). Furthermore, KPZ interfaces are also invariant under this transformation, and so we have our prediction

$$\alpha = \frac{1}{2} \quad (2.6.40)$$

for the KPZ in one-dimension.

Combining this result with (2.6.34) we find

$$z = \frac{3}{2}, \quad \alpha = \frac{1}{2}, \quad \beta = \frac{1}{3}, \quad (2.6.41)$$

for the KPZ in one-dimension. There are other methods for calculating the exponents in one-dimension which agree with this result [26, 154] and in $d = 2$ compare well with numerical measurements made for higher dimensions [3] (see Table 2.1).

d	α	β	z
1	1/2	1/3	3/2
2	0.38	0.24	1.58
3	0.30	0.18	1.66

Table 2.1: The KPZ exponents in dimensions $d = 1, 2, 3$. $d = 1$: analytic results [12]. $d = 2, 3$: numerical results [3].

2.6.3 Connection to the ASEP

The KPZ interface actually has a strong connection to the ASEP described in Section 2.4. There is a direct mapping [52, 105, 120] between the occupancy τ_i of site i in the ASEP and the slope between sites i and $i + 1$ in a discrete KPZ interface:

$$h_{i+1} - h_i = 1 - 2\tau_i. \quad (2.6.42)$$

In this representation a site i in the ASEP which is occupied by a particle ($\tau_i = 1$) represents a downwards slope, $h_{i+1} - h_i = -1$, in the interface between site i and site $i + 1$, and a vacancy in the ASEP represents an upwards slope in the same way. A particle hop from site $i - 1$ to site i in the ASEP corresponds to the slope between sites $i - 1$ and i switching from down to up, and the slope between sites i and $i + 1$ switching from up to down. Thus, when an ASEP particle hops from $i - 1$ to i , the interface height h_i increases by 2. This means that the rate at which h_i increases is twice the current through ASEP bond $i \rightarrow i + 1$, and the average interfacial growth velocity is

$$v = 2J. \quad (2.6.43)$$

For an interface with periodic boundaries, the total number of up slopes must be the same as the total number of down slopes, which is equivalent to having an ASEP on a ring with particle density $\rho = 1/2$. The current in the ASEP on a ring is $J = \rho(1 - \rho)$, and so we can immediately see that the interfacial growth rate is $1/2$.

Chapter 3

Partial Absorption in a Diffusive Search Process

3.1 Introduction

Diffusion is a simple example of a transport process and is a natural choice for the mechanism to underlie a search process, where, from a starting location, a searcher is transported to the target it is searching for. In this chapter I present a simple model for such a process. As a strategy for locating an absorbing boundary (the ‘target’), a particle (the ‘searcher’) undergoes diffusive motion on the real line and stochastically ‘resets’ its position to an arbitrary, but uniquely defined, position.

This model was studied in detail in [57–59] for a system with a ‘totally absorbing’ target, in the context, for instance, of a strategy one might employ to find one’s keys. If your keys are not in the usual location, as a strategy to find them you might ‘diffuse’ around the room, house, office, or wherever you might be, occasionally returning to the usual key location if unsuccessful to start the process again. I extend this model to the case where the target is only ‘partially’ absorbing. What this means is not that some fraction of a single searcher gets absorbed, but rather that upon reaching the target there is a probability that it is absorbed, and if it is not it continues its motion. This modification of the original model is easy to motivate in the context of searcher-target relationships where the mutual detection is imperfect. In the example with keys, this may represent the chance that you did not notice your keys when they were right in front of you.

The results of this chapter have been published in Ref [175].

3.1.1 Background and Motivation

In dimensions $d \leq 2$ a diffusing (point) particle is certain to return to its origin eventually, but the mean time it takes for this to happen diverges [144], because of the contributions to the mean of trajectories which take the particle infinitely far away. Therefore, a purely diffusive search strategy will be impractical, even if it theoretically guarantees success. Better search strategies typically involve a mixture of local steps and long-range moves [13]. In defining these strategies, the local part of the search is often taken to be a diffusive process, whereas the long-range moves can take more varied forms, such as being drawn from some Lévy distribution [135] or being the stochastic process of ‘resetting’ the search to some preferred position [57, 58, 119, 125]. A search process can then be modelled as a random walker that also incorporates one or more of these long-range moves, and is absorbed by the target when it arrives at the target’s position.

Search processes can also involve ‘many-body’ effects, such as there being many searchers, many targets, or both. Systems of this type have been studied for many years in the reaction kinetics literature [28–30, 169], focusing in particular on large numbers of two species of particles, which react and/or annihilate upon contact, as well studies of systems of many diffusing particles and many static or mobile traps [2, 108, 164]. In the general search process context there has also been interest in systems with many targets and a single searcher [21, 31] and many searchers and a single target [20, 59].

One simplification inherent in this description is that absorption occurs instantaneously: the searcher instantaneously interacts with the target upon contact. Of course real searches are less reliable and other factors come into play. For example, human or animal error may occur in foraging or searching for a face in a crowd, or there may be stochasticity in the biochemical binding reaction of a protein searching for a target promoter site on a length of DNA [156]. In the context of chemical reactions, ionic recombination processes take a finite time during which the two reactants will have the opportunity to move away from each other [147]. Furthermore, in certain situations the target itself may switch stochastically between states that are visible or invisible to the searcher,

for example a fleeing prey hiding from a predator, or a binding site that switches from being available to unavailable through external factors.

As such, in this chapter I investigate the effect of stochastic or ‘partial’ absorption of a searcher at the target, particularly in the context of the model of diffusion with resetting presented in [57, 58]. I calculate the Mean Time to Absorption (MTA) of a searcher at the target, and investigate the robustness of the results of [57, 58] to partial absorption. I find that generally for high absorption rate the changes are small, so that the results are indeed robust to the previous work. However, the changes in some properties are more significant than others. For example the MTA differs from the Mean First Passage Time (MFPT), the mean time to absorption at a *totally* absorbing boundary, by an additive constant whereas the survival probability of the target decays with time exponentially with a rate that depends on the absorption rate.

3.2 Model

The model search process that I study, an extension of the model described in [57, 58], and illustrated in Figure 3.1, is a diffusive particle with initial position z , which stochastically resets its position to a predetermined, uniquely defined location x_0 . At the origin, $x = 0$, is the target that the particle is searching for. To better understand the construction of the model I will first briefly review the dynamics in the case where the absorption at the boundary is perfect, called ‘total absorption’. Then I will present the model, where I introduce the feature that the boundary is imperfectly or ‘partially’ absorbing. The difference in the absorption properties at the boundary (target) is specified by the boundary conditions, which I will discuss in Section 3.2.3. An interesting feature of the model is the emergence of dimensionless quantities that relate the dynamical processes to each other. These will appear naturally later in the calculations, but for convenience will be presented first in Section 3.2.4.

3.2.1 Total Absorption

In the process with total absorption [57] the diffusive searcher is instantly absorbed upon contact with the target without fail, and stochastically resets its position to its initial position x_0 . The master equation for the probability

distribution of this particle reads

$$\frac{\partial p(x, t|x_0)}{\partial t} = D \frac{\partial^2 p(x, t|x_0)}{\partial x^2} - rp(x, t|x_0) + r\delta(x - x_0) , \quad (3.2.1)$$

with initial condition $p(x, 0|x_0) = \delta(x - x_0)$. On the right hand side of this equation, the first term represents the diffusive motion of the particle, with diffusion constant D . The second term represents loss of probability density from all space x which is a consequence of the particle stochastically resetting its position to x_0 with rate r , and the final term represents the gain of probability density at x_0 as a consequence of this resetting. To impose the effects of total absorption at the boundary, at $x = 0$, one uses an absorbing boundary condition

$$p(0, t|x_0) = 0 . \quad (3.2.2)$$

Setting aside this boundary condition for the moment, it is straightforward to show that in the long-time limit the stationary distribution $p^*(x|x_0)$ with *no absorption* is

$$p^*(x|x_0) = \frac{\alpha_0}{2} \exp(\alpha_0|x - x_0|) , \quad (3.2.3)$$

where

$$\alpha_0 = \sqrt{\frac{r}{D}} , \quad (3.2.4)$$

and $1/\alpha_0$ is the typical distance diffused between reset events.

To calculate the Mean First Passage Time (MFPT), the mean time it takes for the particle to be absorbed at the boundary, one first calculates the particle's survival probability, $q(x_0, t)$. This is the probability that, up to time t , a particle which began at x_0 has not been absorbed. The master equation for this probability is derived as follows [57].

Considering the survival probability $q(z, t + \Delta t)$ at time $t + \Delta t$ of a particle which originated at z , the history of the particle is split into two intervals: $[0, \Delta t]$ and $[\Delta t, t + \Delta t]$. There are two possible events which can occur in the first interval: either the particle resets its position to x_0 with probability $r\Delta t$, or it diffuses to a new position $z + \epsilon$ with probability $1 - r\Delta t$. In the first case, the particle's survival probability at the end of the second interval will simply be

$q(x_0, t)$. In the second case, ϵ is a random variable with a Gaussian distribution

$$P(\epsilon) = \frac{1}{\sqrt{4\pi D\Delta t}} \exp\left(-\frac{\epsilon^2}{4D\Delta t}\right), \quad (3.2.5)$$

and at the end of the second interval the survival probability will be

$$\int d\epsilon P(\epsilon) q(z + \epsilon, t). \quad (3.2.6)$$

Thus the total survival probability at $t + \Delta t$ is

$$q(z, t + \Delta t) = r\Delta t q(x_0, t) + (1 - r\Delta t) \int d\epsilon P(\epsilon) q(z + \epsilon, t). \quad (3.2.7)$$

From this one can write

$$\begin{aligned} \frac{q(z, t + \Delta t) - q(z, t)}{\Delta t} &= rq(x_0, t) - r \int d\epsilon P(\epsilon) q(z + \epsilon, t) \\ &+ \frac{1}{\Delta t} \int d\epsilon P(\epsilon) (q(z + \epsilon, t) - q(z, t)). \end{aligned} \quad (3.2.8)$$

The Gaussian distribution for ϵ means that

$$\begin{aligned} \langle \epsilon \rangle &= 0 \\ \langle \epsilon^2 \rangle &= 2D\Delta t, \end{aligned} \quad (3.2.9)$$

which can be used after expanding $q(x + \epsilon, t)$ in terms of ϵ to find

$$\frac{q(z, t + \Delta t) - q(z, t)}{\Delta t} = rq(x_0, t) - rq(z, t) + D \frac{\partial^2 q(z, t)}{\partial t^2} + \mathcal{O}(\Delta t). \quad (3.2.10)$$

Thus, in the limit $\Delta t \rightarrow 0$, the backward master equation

$$\frac{\partial q(z, t)}{\partial t} = D \frac{\partial^2 q(z, t)}{\partial z^2} - rq(z, t) + rq(x_0, t) \quad (3.2.11)$$

is obtained.

The absorption at the origin gives rise to the boundary condition $q(0, t) = 0$, which ensures that the particle does not survive if it meets the origin. Similarly, one has the initial condition $q(z, 0) = 1$ which says that initially, the particle has not been absorbed by the target. It is important to note that these conditions

are incompatible if $z = 0$. One must assume that the particle's initial position doesn't coincide with the target location for the analysis to be meaningful.

From this master equation, and the initial and boundary conditions, one derives the MFPT $T(z)$ for a particle which originates at x to be

$$T(z) = \frac{e^{\alpha_0|x_0|}}{r} [1 - e^{-\alpha_0|z|}] . \quad (3.2.12)$$

This MFPT has an intuitive dependence on the resetting rate r . First, when $r \rightarrow 0$, $T(z)$ diverges. This is just a reduction to the purely diffusive searcher, for which $T(z)$ is known to diverge owing to the possible diffusive trajectories which take the searcher infinitely far from the target. Secondly, $T(z)$ diverges as $r \rightarrow \infty$ as well. In this case, the particle is effectively pinned to the resetting position as the characteristic distance diffused between resets, $1/\alpha_0$, goes to 0. Finally, $T(z)$ is minimised with respect to r by the optimal resetting rate r^* which satisfies the transcendental equation

$$\frac{\theta^*}{2} = 1 - e^{\theta^*} . \quad (3.2.13)$$

From this equation, $\theta^* = 1.5936$ and

$$r^* = D \left(\frac{\theta^*}{x_0} \right)^2 . \quad (3.2.14)$$

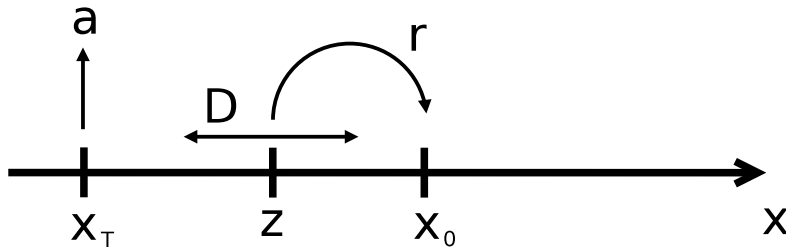


Figure 3.1: Schematic diagram of the system studied. The particle starts at z and diffuses (diffusion constant D) along the x axis. With rate r it stochastically resets to x_0 , and when it reaches the target location x_T (in this case 0) it is absorbed at a rate proportional to a .

3.2.2 Partial Absorption

We now return to the definition of the model (Figure 3.1). Just as in the model described above and in [57, 58] the searcher is a diffusive particle which

stochastically resets its position, except now the particle might not be absorbed on arrival at the target at the origin. The probability density, $p(x, t|z)$, of the particle being at position x at time t after having started from initial position z obeys the same (forward) master equation as (3.2.1), but with an additional final term:

$$\frac{\partial p(x, t|z)}{\partial t} = D \frac{\partial^2 p(x, t|z)}{\partial x^2} - rp(x, t|z) + r\delta(x - x_0) - ap(0, t)\delta(x). \quad (3.2.15)$$

This final so-called sink term represents the partial absorption process at the origin, and is used instead of a boundary condition. The particle is absorbed with rate $a\delta(z)$, where the constant a has dimensions of velocity and we refer to it as the absorption velocity. It can be shown [163, 176] that a sink term of this type is equivalent to a radiation boundary condition, which for this process would be

$$\left. \frac{\partial p(x, t)}{\partial x} \right|_{x=0} = \frac{a}{D} p(0, t). \quad (3.2.16)$$

As I will discuss, a radiating boundary absorbs only part of the probability or particle flux and reflects the remainder, and so naturally describes a partially absorbing boundary.

In principle the diffusion equation can be solved with the radiation boundary condition by using the appropriate Green function, but it may be that this Green function is difficult to find, and so it may be more convenient to use a sink term instead. In general terms, a sink term represents the loss of probability density from a region of space as a consequence of absorption, attenuation, or some other similarly natured process.

To see the equivalence between the radiation boundary condition and the sink term explicitly refer to Ref [163, 176] and to Appendix B where I present the calculation. What one finds is that a sink term of the form

$$-a\delta(x)p(x, t) \quad (3.2.17)$$

in a master equation of the form of (3.2.15) is equivalent to the radiation boundary condition (3.2.16).

In order to learn about the processes of searching for and finding the target, I study the survival probability $q(z, t)$ of a diffusive searcher (particle) after time t given that it started at position z . This is the probability that the searcher

has *not* found, or been absorbed by, the target. It is convenient to work with the backward master equation for the survival probability itself, which reads as follows:

$$\frac{\partial q(z, t)}{\partial t} = D \frac{\partial^2 q(z, t)}{\partial z^2} - rq(z, t) + rq(x_0, t) - aq(0, t)\delta(z). \quad (3.2.18)$$

Again, this is the same master equation as (3.2.11), except with the additional sink term in lieu of the boundary condition. I will proceed in my calculations with this equation, using the sink term in the master equation instead of applying a boundary condition to the solution.

3.2.3 Absorption and Boundary Conditions

Before presenting the calculations with this model, I first elucidate the nature the boundary condition. The most commonly studied boundary condition in the diffusive process literature is the *totally absorbing boundary condition* wherein, once the particle meets the boundary, it is certain that the particle is absorbed and leaves the system instantaneously. The totally absorbing boundary condition is therefore defined in terms of the probability density $p(x, t)$ of the particle at the boundary x_B as

$$p(x_B, t) = 0. \quad (3.2.19)$$

To describe a system which includes a ‘reflecting wall’, it is natural to use what is commonly referred to as the *reflecting boundary condition*. Here, because all particles which try to reach the boundary location are reflected back away from the boundary, the net flux into the boundary site is zero. This means that this boundary condition can be straightforwardly expressed as

$$\left. \frac{\partial p(x, t)}{\partial x} \right|_{x=x_B} = 0. \quad (3.2.20)$$

In the reaction kinetics literature a partial reaction is often modelled by a so-called *radiation boundary condition* where the probability density flux into the target site is proportional to the probability density at the target site [16,144,147]. A radiating boundary exhibits properties of both an absorbing boundary, where the probability density at the boundary or target site x_B is 0, and a reflecting boundary where there is no probability density flux into x_B , and has the general

form [144, 147]

$$\left. \frac{\partial p(x, t)}{\partial x} \right|_{x=x_B} = kp(x_B, t) . \quad (3.2.21)$$

The constant k is a parameter which characterises the boundary. In the limit $k \rightarrow 0$, the reflecting boundary condition is recovered. In the limit $k \rightarrow \infty$, the totally absorbing boundary is recovered. As can be seen in Appendix B.1, for this model the form of k in the boundary condition which corresponds to the sink term (3.2.17) is

$$k = \frac{a}{D} , \quad (3.2.22)$$

as given in (3.2.16).

3.2.4 Significant Dimensionless Quantities

Throughout the following calculations two dimensionless variables, with straightforward physical interpretations, will repeatedly be present.

The first, which is directly linked to the partial absorption property of the target is

$$\phi_0 = \frac{D/a}{1/\alpha_0} = \frac{\sqrt{rD}}{a} , \quad (3.2.23)$$

where we have used the definition of the length scale $1/\alpha_0 = \sqrt{D/r}$, the typical distance diffused between reset events, as given in (3.2.4). The length D/a is equivalent to the attenuation length in a composite medium [144]. The composite medium is used to model the propagation of light in turbid media such as concentrated suspensions or human tissues [173]. In this medium there is a boundary at $x = 0$, in the region $x > 0$ particles can undergo free diffusion, and for $x < 0$ the density of particles is attenuated [16]. It can be shown for this system that the probability density within the attenuating region decreases linearly to 0 at the depth $x = -D/a = -l$, hence we refer to l as the attenuation depth. This furnishes a physical interpretation of the characteristic length scale D/a , and thus the dimensionless variable ϕ_0 represents the ratio of these two length scales. In all the results the dynamics of the totally absorbing system are only modified in terms of this ratio and not the absolute strength of the imperfection which has been introduced to the target.

The second, providing a notion of distance in the system, is

$$\theta = \alpha_0 |x_0| . \quad (3.2.24)$$

This quantity measures the ratio of the characteristic diffusion length $1/\alpha_0$ to the distance of the resetting position x_0 from the target, which is the origin in this case.

3.3 Survival Probability Calculation

To solve the master equation (3.2.18) for the survival probability with partial absorption we perform the Laplace Transform on the variable t . We define the Laplace Transform of the survival probability as

$$\tilde{q}(z, s) = \int_0^\infty q(z, t) e^{-st} dt , \quad (3.3.1)$$

and use this definition with the initial condition $q(z, 0) = 1$ to take the Laplace Transform of equation (3.2.18):

$$D \frac{\partial^2 \tilde{q}(z, s)}{\partial z^2} - (r + s) \tilde{q}(z, s) = -1 - r\tilde{q}(x_0, s) + a\tilde{q}(0, s)\delta(z) . \quad (3.3.2)$$

First we find the solution to the homogeneous equation

$$D \frac{\partial^2 \tilde{q}(z, s)}{\partial z^2} - (r + s) \tilde{q}(z, s) = 0 , \quad (3.3.3)$$

which yields

$$\tilde{q}(z, s) = A e^{\alpha z} + B e^{-\alpha z} , \quad (3.3.4)$$

where

$$\alpha = \alpha(s) = \left(\frac{r + s}{D} \right)^{1/2} , \quad (3.3.5)$$

and $\alpha(0) = \alpha_0$ as defined in (3.2.4). From the full equation (3.3.2), for $z \neq 0$, we find the particular solution

$$\tilde{q}(z, s) = A e^{\alpha z} + B e^{-\alpha z} + \frac{1 + r\tilde{q}(x_0, s)}{r + s} . \quad (3.3.6)$$

We require that our solution be finite in the limits $z \rightarrow \pm\infty$, which implies separate solutions $\tilde{q}_+(z, s)$ and $\tilde{q}_-(z, s)$ for the regions where z is greater than and less than zero respectively. Using the required continuity at $z = 0$ to find that $A = B$, we obtain the result

$$\tilde{q}_{\pm}(z, s) = Ae^{\mp\alpha z} + \frac{1 + r\tilde{q}(x_0, s)}{r + s}. \quad (3.3.7)$$

Now we can use the discontinuity in the derivative which comes from the delta function in (3.2.18) to find A . We integrate (3.3.2) with respect to z over a small region of width 2ϵ about the origin. This yields

$$D \left[\frac{\partial \tilde{q}}{\partial z} \right]_{-\epsilon}^{\epsilon} = -2\epsilon(1 + r\tilde{q}(x_0, s)) + a\tilde{q}(0, s). \quad (3.3.8)$$

The first term is evaluated using the derivatives of \tilde{q}_+ and \tilde{q}_- :

$$\left[\frac{\partial \tilde{q}}{\partial z} \right]_{-\epsilon}^{\epsilon} = -2\alpha A e^{-\alpha\epsilon}. \quad (3.3.9)$$

Then by taking $\epsilon \rightarrow 0$ we find

$$A = \frac{-a\tilde{q}(0, s)}{2\alpha D}, \quad (3.3.10)$$

and by substituting this back into the particular solution (3.3.6) we obtain

$$\tilde{q}(z, s) = \frac{-a\tilde{q}(0, s)}{2\alpha D} e^{-\alpha|z|} + \frac{1 + r\tilde{q}(x_0, s)}{r + s}. \quad (3.3.11)$$

The self consistent solution for $z = 0$ gives

$$\tilde{q}(0, s) = \frac{1}{1 + a/2\alpha D} \frac{1 + r\tilde{q}(x_0, s)}{r + s}. \quad (3.3.12)$$

Substituting this back into (3.3.11) we find

$$\tilde{q}(z, s) = \left(1 - \frac{ae^{-\alpha|z|}}{2\alpha D + a} \right) \frac{1 + r\tilde{q}(x_0, s)}{r + s}. \quad (3.3.13)$$

For convenience we define

$$\tilde{Q}(z, s) = \frac{ae^{-\alpha|z|}}{2\alpha D + a} = \frac{e^{-\alpha|z|}}{1 + 2\phi(s)} , \quad (3.3.14)$$

where $\phi(s)$ is given by

$$\phi(s) = \frac{D\alpha(s)}{a} = \frac{\sqrt{(r+s)D}}{a} , \quad (3.3.15)$$

and $\phi(0) = \phi_0$. Now, we can set $z = x_0$ in (3.3.13) to find

$$\tilde{q}(x_0, s) = \frac{1 - Q(x_0, s)}{s + rQ(x_0, s)} . \quad (3.3.16)$$

Finally, substituting this into (3.3.13) we find

$$\tilde{q}(z, s) = \frac{1 - \tilde{Q}(z, s)}{s + r\tilde{Q}(x_0, s)} . \quad (3.3.17)$$

Thus, we have derived the form Laplace transform of the survival probability. As will be discussed in Section 3.4, $\tilde{q}(z, s)$ is used to determine the Mean Time to Absorption of the searcher by the target, as well as being a route to calculating $q(z, t)$ itself.

3.3.1 Inverting the Laplace Transform

To find the full solution for the survival probability $q(z, t)$ one would need to invert (3.3.17). This is generally difficult to do, so instead we examine the long time behaviour only, which simplifies the inversion. As illustrated in Fig. 3.2, the analytic structure of this function in the complex s plane is a branch point $s = -r$, which comes from the square root of $r + s$ in α , and a simple pole at $s = s_0$ which satisfies

$$s_0(1 + 2\phi(s_0)) + re^{-\alpha(s_0)|x_0|} = 0 , \quad (3.3.18)$$

where

$$-r < s_0 \leq 0 . \quad (3.3.19)$$

We can look for solutions in the $t \rightarrow \infty$ limit by noting that for large t the sum

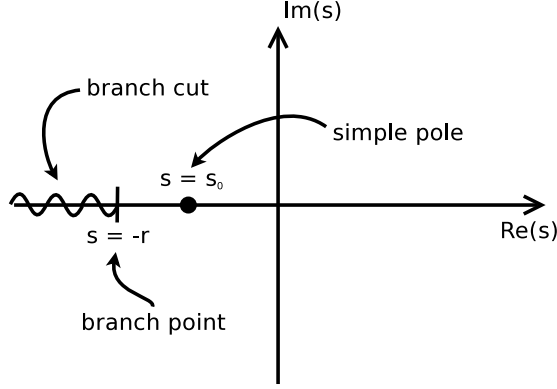


Figure 3.2: Sketch of the singularities of the function (3.3.17) in the complex s plane.

of the residues will be dominated by the pole with the largest (most positive) real part, which in this case is s_0 . Thus, in the large time limit, the residue from s_0 dominates the solution to the Bromwich inversion formula,

$$q(z, t) = \frac{1}{2\pi i} \int_{c-i\infty}^{c+i\infty} \tilde{q}(z, s) e^{st} ds , \quad (3.3.20)$$

(where $c > \text{Re}(s_0)$ is some real constant) for this function. For convenience we consider the case where the initial position coincides with the resetting position, $z = x_0$, which is the initial position for all the dynamics following the first resetting event. In this case

$$q(x_0, t) \simeq \lim_{s \rightarrow s_0} (s - s_0) \frac{1 - \tilde{Q}(x_0, s)}{s + r\tilde{Q}(x_0, s)} e^{st} . \quad (3.3.21)$$

For further convenience, we make a change of variable

$$s = r(u - 1) . \quad (3.3.22)$$

Under this substitution

$$s_0 = r(u_0 - 1) , \quad (3.3.23)$$

$$\phi(s) = \phi_0 \sqrt{u} , \quad (3.3.24)$$

$$\alpha(s) = \alpha_0 \sqrt{u} , \quad (3.3.25)$$

and equation (3.3.18) becomes

$$(u_0 - 1)(2\phi_0\sqrt{u_0} + 1) + \exp(-\theta\sqrt{u_0}) = 0 , \quad (3.3.26)$$

where we have used $\theta = \alpha_0 x_0$ as defined in (3.2.24). Now we can write

$$q(x_0, t) \simeq e^{r(u_0-1)t} \lim_{u \rightarrow u_0} \left[\frac{(u - u_0)(1 + 2\phi_0 u^{1/2} - e^{-\theta u^{1/2}})}{(u - 1)(1 + 2\phi_0 u^{1/2}) + e^{-\theta u^{1/2}}} \right] . \quad (3.3.27)$$

A more convenient way to take the limit is to define $u = u_0 + \epsilon$ and take $\epsilon \rightarrow 0$ instead. We expand

$$u^{1/2} = u_0^{1/2} \left(1 + \frac{\epsilon}{2u_0} \right) + \mathcal{O}(\epsilon^2) , \quad (3.3.28)$$

to rewrite the numerator of (3.3.27) as

$$(1 + 2\phi_0 u_0^{1/2} - e^{-\theta u_0^{1/2}})\epsilon + \mathcal{O}(\epsilon^2) , \quad (3.3.29)$$

and the denominator as

$$\begin{aligned} & (u_0 - 1)(1 + 2\phi_0 u_0^{1/2}) + e^{-\theta u_0^{1/2}} \\ & + \left(1 + 2\phi_0 u_0^{1/2} + (u_0 - 1) \frac{\phi_0}{u_0^{1/2}} - \frac{\theta}{2u_0^{1/2}} e^{-\theta u_0^{1/2}} \right) \epsilon \\ & + \mathcal{O}(\epsilon^2) . \end{aligned} \quad (3.3.30)$$

Then, using

$$-\exp(-\theta\sqrt{u_0}) = (u_0 - 1)(2\phi_0\sqrt{u_0} + 1) \quad (3.3.31)$$

from (3.3.26), we see that the order ϵ^0 term in the denominator is 0. Thus we have

$$q(x_0, t) \simeq e^{r(u_0-1)t} \lim_{\epsilon \rightarrow 0} \left[\frac{(1 + 2\phi_0 u_0^{1/2} - e^{-\theta u_0^{1/2}})\epsilon + \mathcal{O}(\epsilon^2)}{\left(1 + 2\phi_0 u_0^{1/2} + (u_0 - 1) \frac{\phi_0}{u_0^{1/2}} - \frac{\theta}{2u_0^{1/2}} e^{-\theta u_0^{1/2}} \right) \epsilon + \mathcal{O}(\epsilon^2)} \right] . \quad (3.3.32)$$

Now, with some algebra, we find

$$q(x_0, t) \simeq \frac{2u_0^{3/2}[1 + 2\phi_0 u_0^{1/2}]e^{r(u_0-1)t}}{2\phi_0[2u_0 + (\theta u_0^{1/2} + 1)(u_0 - 1)] + [2u_0^{1/2} + \theta(u_0 - 1)]}. \quad (3.3.33)$$

This solution is somewhat unwieldy, but the important point to note is that the survival probability decays exponentially and the rate of decay increases with absorption velocity a . That is, as a is increased, u_0 decreases, and $(u_0 - 1)$ becomes more negative. If one expands to leading order in $1/a$ one finds

$$u_0 \simeq u^* + \frac{4u^*(1-u^*)}{2(u^*)^{1/2} - \theta(1-u^*)} \frac{\alpha_0 D}{a}, \quad (3.3.34)$$

where u^* is the solution of

$$(u^* - 1) + \exp\left(\theta\sqrt{u^*}\right) = 0. \quad (3.3.35)$$

This is the equation for the poles of $\tilde{q}(z, s)$, as given in (3.3.18) and (3.3.26), once the limit $a \rightarrow \infty$ has been taken, and is the same expression as was obtained in the study of the totally absorbing case [57, 58]. As such, in the limit $a \rightarrow \infty$ we recover the same decay rate $s^* = r(u^* - 1)$ as was found for total absorption.

3.4 Mean Time to Absorption

Intuitively, the survival probability at a time $t + \Delta t$ is the survival probability at t less the probability that the searcher was absorbed at time t . Thus, the survival probability $q(t + \Delta t, z)$ at time $t + \Delta t$ can be expressed as

$$q(t + \Delta t, z) = q(z, t) - F(t)\Delta t, \quad (3.4.1)$$

where $F(t)$ is the probability that the searcher is absorbed for the first time at time t , known as the first-passage probability. By expanding about Δt and neglecting terms of $\mathcal{O}(\Delta t^2)$, one finds that

$$F(t) = -\frac{\partial q(z, t)}{\partial t}, \quad (3.4.2)$$

and the probability of absorption during an infinitesimal interval dt after time t is

$$-\frac{\partial q(z, t)}{\partial t} dt .$$

Therefore, we can write the Mean Time to Absorption (MTA) $T(z)$ of a particle which originated at z as

$$T(z) = \int_0^\infty t \left(-\frac{\partial q(z, t)}{\partial t} \right) dt , \quad (3.4.3)$$

which, after integrating by parts, can be expressed [144] as

$$T(z) = \int_0^\infty q(z, t) dt = \tilde{q}(z, s=0) . \quad (3.4.4)$$

In our analysis we are considering the mean first time to *absorption* of the searcher by the target, not just the mean first time to coincidence (the MFPT) as in the case where the absorption is perfect. This means that it is possible for the searcher to pass *through* the target site without interacting with it. Even so, the MTA as defined above in (3.4.4) is still the appropriate measure of this process. Using equation (3.3.17) and the definition in equation (3.4.4) we can write down an expression for the MTA:

$$T(z) = \frac{1 - \tilde{Q}(z, 0)}{r \tilde{Q}(x_0, 0)} . \quad (3.4.5)$$

Explicitly,

$$Q(z, 0) = \frac{e^{-\alpha_0|z|}}{1 + 2\phi_0} , \quad (3.4.6)$$

which we use to write

$$T(z) = \frac{e^{\alpha_0|x_0|}}{r} [2\phi_0 + 1 - e^{-\alpha_0|z|}] , \quad (3.4.7)$$

and, setting $z = x_0$,

$$T(x_0) = \frac{1}{r} [e^{\alpha_0|x_0|} - 1] + \frac{2\phi_0}{r} e^{\alpha_0|x_0|} . \quad (3.4.8)$$

Comparing with the total absorption result [57, 58]

$$T(z) = \frac{e^{\alpha_0|x_0|}}{r} [1 - e^{-\alpha_0|z|}] \quad (3.4.9)$$

from (3.2.12), we see that the effect of partial absorption is to increase the mean time to absorption through the additive second term in (3.4.8), which is inversely proportional to the absorption velocity a . In the limit $a \rightarrow \infty$ ($\phi_0 \rightarrow 0$) this term goes to 0 and so we see that the first term in (3.4.8) is simply the total absorption result (3.4.9), the mean time to first incidence with the target. Now if we consider the case where $x_0 = 0$, meaning that the searcher starts at *and resets to* the same position as the target, the first term of (3.2.12) is 0 and we have

$$T(0) = \frac{2\phi_0}{r} . \quad (3.4.10)$$

This quantity can be interpreted as the mean time it takes for the searcher to be absorbed by the target, given that it started at the target's location. Furthermore, by expressing it in terms of r , D and a we see that

$$T(0) = \frac{1}{a} \sqrt{\frac{D}{r}} = \frac{1/\alpha_0}{a} , \quad (3.4.11)$$

where $1/\alpha_0$ is again the typical distance diffused between resetting events. From this we see that the mean time to be absorbed by the target starting from the target's location is controlled by the competition between how far the particle can diffuse away before being reset to the target and the velocity at which it is absorbed.

Another way to try to understand the additional contribution to the MTA that comes from the partial absorption property, which provides a more general interpretation, is to consider a more general problem involving a resetting *distribution* $\mathcal{P}(x)$ [57]. In this case, the particle resets with rate r to a random position drawn from the distribution $\mathcal{P}(x)$. The resetting term $rq(x_0, t)$ in the backward master equation (3.2.18) becomes $r \int dx \mathcal{P}(x)q(x, t)$ and so, for the survival probability $q(z, t)$, the master equation itself reads

$$\frac{\partial q(z, t)}{\partial t} = D \frac{\partial^2 q(z, t)}{\partial z^2} - rq(z, t) + r \int \mathcal{P}(x)q(x, t)dx - aq(0, t)\delta(z) . \quad (3.4.12)$$

The calculation of the mean time to absorption is a straightforward generalisation of that presented above and so we leave it for Appendix B.2. The result we find is

$$T(z) = \frac{1}{2\sqrt{rD}p^*(0)} (1 - e^{-\alpha_0|z|}) + \frac{\phi_0}{\sqrt{rD}} \frac{1}{p^*(0)}, \quad (3.4.13)$$

where, similarly to (3.2.3), $p^*(x)$ is the stationary distribution of the diffusive process with resetting to a position drawn from $\mathcal{P}(x')$ but without any absorption [57], and is given by the integral

$$p^*(x) = \frac{\alpha_0}{2} \int dx' \mathcal{P}(x') e^{-\alpha_0|x-x'|}. \quad (3.4.14)$$

Remembering that

$$\frac{\phi_0}{\sqrt{rD}} = \frac{1}{a}, \quad (3.4.15)$$

(3.4.13) tells us that the effect of partial absorption is to increase the mean time to absorption by an additional term proportional to $1/a$.

In the limit $a \rightarrow \infty$, $\phi_0 \rightarrow 0$, and this expression becomes identical to the expression to the Mean First Passage Time (MFPT) found in the total absorption case [57, 58]. If the particle starts at the target site, then we have

$$T(z=0) = \frac{1}{ap^*(0)}, \quad (3.4.16)$$

and we keep the second term of (3.4.13) only. The mean time it takes for the searcher to get absorbed at the origin is inversely proportional to a , which takes into account the ‘strength’ of the absorption, and is also inversely proportional to $p^*(0)$, which takes into account how resetting events, dictated by r and $\mathcal{P}(x)$, and diffusion take it away from the target again.

It is clear then that the MTA, (3.4.8) or (3.4.13), can be interpreted as the sum of two timescales: the first is the mean time to the first meeting of the positions of the searcher and target, when the searcher had an arbitrary starting position z , and the second is the mean time to absorption given that the searcher started at the target.

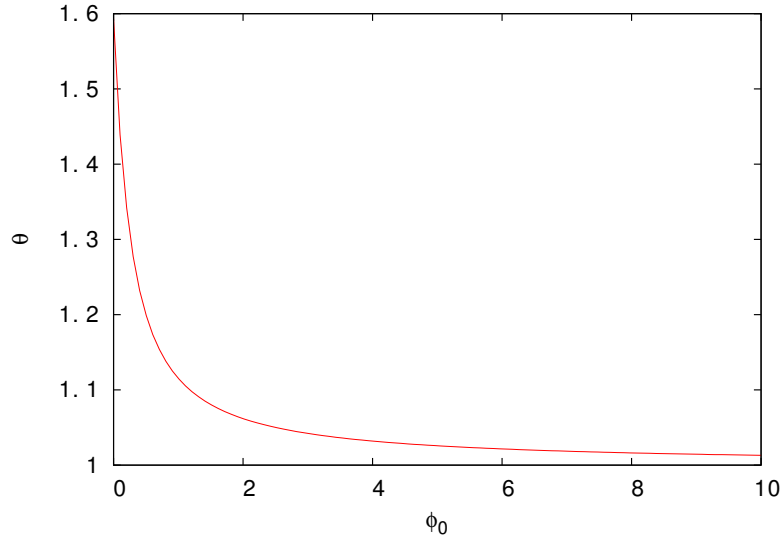


Figure 3.3: Plot of the value of θ that minimises the MTA for a given ϕ_0 . The value of θ at $\phi_0 = 0$, found numerically to be $\theta^* = 1.5936$, is indicated.

3.4.1 Minimisation of the MTA with respect to resetting rate r

When developing search strategy it is often important to optimise it in some way, for example to locate a target in the quickest time or to find the greatest number of targets within a certain time. In this search process, we are interested in finding the choice of r which minimises $T(z)$, as given in (3.4.8). The resetting process is the perturbation away from pure diffusion which improves the search, and so it is natural to ask what the best way to implement it is.

We start by considering the minimum of $T(x_0)$ with respect to r . Setting $\frac{\partial T(x_0)}{\partial r} = 0$ yields

$$e^{-\theta} = 1 + \phi_0 - \frac{\theta}{2} - \phi_0\theta, \quad (3.4.17)$$

where the dimensionless quantities ϕ_0 and θ are defined in (3.2.23) and (3.2.24) respectively. The solutions of (3.4.17) are shown in Fig. 3.3. In the following we analyse the solution of (3.4.17) in the regimes $a \gg \alpha_0 D$ and $a \ll \alpha_0 D$ corresponding to strong and weak absorption.

First, when the absorption is strong, $a \gg \alpha_0 D$ ($\phi_0 \ll 1$) and (3.4.17) reduces

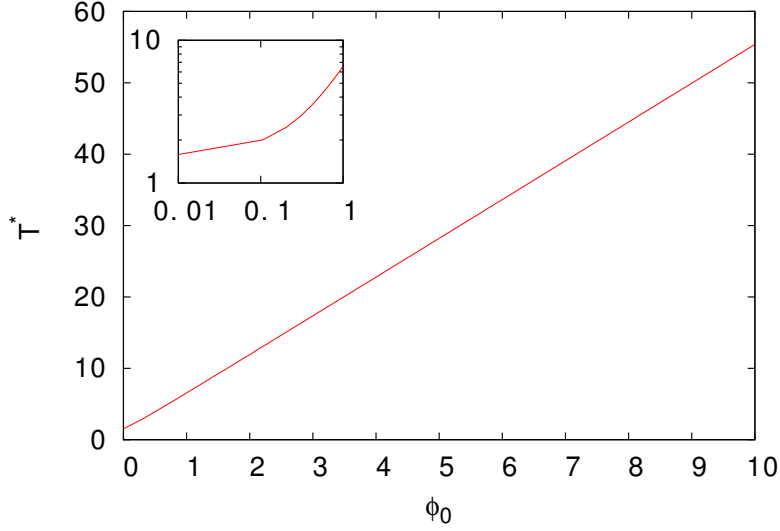


Figure 3.4: The minimised MTA, T^* , as a function of ϕ_0 , in units of x_0^2/D . T^* is approximately linear for both small and large ϕ_0 (See (3.4.22) and (3.4.26)). *Inset:* expanded view of the crossover between the two linear regimes (logarithmic axes).

to the transcendental equation (3.2.13) found in the study of total absorption [58]:

$$\frac{\theta^*}{2} = 1 - e^{-\theta^*}. \quad (3.4.18)$$

We then find that, to second order in ϕ_0 ,

$$\theta = \theta^* - 2\phi_0 + \frac{2\theta^*}{\theta^* - 1}\phi_0^2 \quad (3.4.19)$$

satisfies (3.4.17). It is helpful to rewrite the expression for the MTA, given in (3.4.8), as

$$T(x_0) = \frac{x_0^2}{D\theta^2} [(2\phi_0 + 1)e^\theta - 1], \quad (3.4.20)$$

where we have used

$$r = \frac{D\theta^2}{x_0^2}. \quad (3.4.21)$$

Then, by substituting (3.4.19) into (3.4.20) and Taylor expanding, it can be shown using that for $\phi_0 \ll 1$ the MTA minimised with respect to r is

$$T^*(x_0) \simeq \frac{x_0^2}{D} \frac{1}{\theta^*(2 - \theta^*)} \left[1 + \frac{4}{\theta^*} \phi_0 + \frac{4(3 - \theta^*)}{(\theta^*)^2} \phi_0^2 \dots \right]. \quad (3.4.22)$$

To study the weak absorption regime, $a \ll \alpha_0 D$, $\phi_0 \gg 1$, we first rewrite (3.4.17) as

$$1 - \theta = \frac{1}{\phi_0} \left(e^{-\theta} - 1 + \frac{\theta}{2} \right). \quad (3.4.23)$$

Then we can see that because $\phi_0 \gg 1$, then left hand side of (3.4.23) must be a power series

$$1 - \theta = \frac{c_1}{\phi_0} + \frac{c_2}{\phi_0^2} + \dots . \quad (3.4.24)$$

and $\theta \rightarrow 1^+$. By Taylor expanding the exponential and equating orders of ϕ_0 in (3.4.23), explicitly we find that to first order in $1/\phi_0$

$$\theta \simeq 1 + \frac{1 - 2e^{-1}}{2\phi_0}. \quad (3.4.25)$$

We can then substitute this back into (3.4.20) and perform some more Taylor expansions to find that the minimised MTA is, to leading order in $1/\phi_0$,

$$T^*(x_0) \simeq 2e \frac{x_0^2}{D} \phi_0. \quad (3.4.26)$$

We plot T^* as a function of ϕ_0 in Fig. 3.4. Whether the imperfection in the target is weak or strong, the imperfection increases the minimum MTA and does so linearly with ϕ_0 . Again this fits with our intuition that the imperfection in the absorption at the target increases the MTA.

3.5 Many Independent Searchers

We now consider a ‘many-body’ search process. In particular we are interested in the situation where there are many searchers searching for a single target, which is of particular interest in the study of biological processes such as the search for specific sequences of DNA by binding proteins [27, 156].

We study the multi-particle version of the search process with a single immobile target at the origin and many searchers which are initially uniformly distributed on the line with density ρ . The searchers are independent of each other and the position of each searcher evolves stochastically starting at its own initial position to which it resets.

The survival probability of the target, $P_s(t)$, is simply the probability that

none of the searchers have been absorbed by the target, given by

$$P_s(t) = \prod_{i=1}^N q(z_i, t) , \quad (3.5.1)$$

where the survival probability of the i^{th} particle $q(z_i, t)$ is the survival probability in the single searcher problem [58]. The initial position of each particle is taken to be its resetting position:

$$z_i = x_{0,i} \equiv x_i . \quad (3.5.2)$$

The positions x_i are independent and distributed uniformly within the box $[-L/2, L/2]$. The average probability $P_s^{\text{av}}(t) = \langle P_s(t) \rangle_x$ and the typical probability $P_s^{\text{typ}}(t) = \exp[\langle \ln P_s(t) \rangle_x]$, where $\langle \cdot \rangle_x$ denotes averages over x_i 's. In random additive processes the average of the random variable and its typical or most probable value exhibit the same behaviour. For multiplicative processes (where a product of random variables is considered such as is described here), there exist extreme events which, although exponentially rare, are exponentially different from the typical value of the product [143]. Thus, for multiplicative processes, it is important to consider both average and typical values.

As a simple example consider rolling two fair, 6-sided dice. The quantity A is the sum of the totals shown, and the quantity B is the product. The typical, or most probable, value for A obtained is 7, but also, if one calculates the mean value of A one finds that it is also 7, so the typical and mean values of A are the same. For B however, one can calculate that its mean value is 12, and its typical value is approximately 8.96. Although it's just as likely to roll two ones as it is two sixes, the difference in the values of B produced by these two results is large, and so the distribution of possible values is skewed towards the lower values.

3.5.1 Average Survival Probability of the Target

First we calculate the average survival probability of the target, $P_s^{\text{av}}(t)$, given by

$$P_s^{\text{av}}(t) = \langle q(x, t) \rangle_x^N = \exp(N \ln[1 - \langle 1 - q \rangle_x]) , \quad (3.5.3)$$

where

$$\langle 1 - q \rangle_x = \frac{1}{L} \int_{-L/2}^{L/2} dx [1 - q(x, t)] . \quad (3.5.4)$$

As we are interested in the thermodynamic limit, we take $N, L \rightarrow \infty$ while keeping the density of searchers $\rho = N/L$ fixed. We also exploit the fact that the survival probability is symmetric in x about the target, meaning $q(x, t) = q(-x, t)$. Under these conditions, we find that

$$P_s^{av}(t) \rightarrow \exp \left(-2\rho \int_0^\infty dx [1 - q(x, t)] \right) \equiv \exp(-2\rho M(t)) , \quad (3.5.5)$$

with

$$M(t) = \int_0^\infty dx [1 - q(x, t)] . \quad (3.5.6)$$

Now we define the Laplace transformed function

$$\tilde{M}(s) = \int_0^\infty M(t) e^{-st} dt , \quad (3.5.7)$$

and we can use the equation

$$\tilde{q}(z, s) = \frac{1 - \tilde{Q}(z, s)}{s + r\tilde{Q}(x_0, s)} . \quad (3.5.8)$$

from (3.3.17) to rewrite this as

$$\tilde{M}(s) = \frac{r+s}{s} \int_0^\infty dx \left[\frac{\tilde{Q}(x, s)}{s + r\tilde{Q}(x, s)} \right] , \quad (3.5.9)$$

which can be expressed as

$$\tilde{M}(s) = \frac{r+s}{s} \int_0^\infty dx \left[\frac{e^{-\alpha x}}{s(2\phi + 1) + re^{-\alpha x}} \right] . \quad (3.5.10)$$

The integral can be computed directly to find

$$\tilde{M}(s) = \frac{r+s}{rs\alpha(s)} \ln \left(1 + \frac{r}{s(2\phi(s) + 1)} \right) . \quad (3.5.11)$$

In principle this may be inverted to find $P_s^{av}(t)$. Rather than present the formula which takes the form of a double convolution it is more instructive to examine the effect of partial absorption on asymptotic behaviour directly from (3.5.11).

First, for convenience, we write

$$\phi(s) = k(r+s)^{\frac{1}{2}}, \quad \text{where } k = \frac{\sqrt{D}}{a}, \quad (3.5.12)$$

so that we can then expand (3.5.11) to leading order in s to find

$$\tilde{M}(s) = \sqrt{\frac{D}{r}} \frac{1}{s} (-\ln s + \ln r - \ln[2k\sqrt{r} + 1] + O(s)) . \quad (3.5.13)$$

Using the identity [146]

$$\mathcal{L}^{-1} \left[-\frac{\ln s}{s} \right] = \ln t + \gamma , \quad (3.5.14)$$

where $\gamma = 0.577$ (to three significant figures) is Euler's constant, we find then that for long times

$$P^{av}(t) \sim \exp [-2\rho (\ln rt + \gamma - \ln (2\phi_0 + 1))] . \quad (3.5.15)$$

Thus the effect of partial absorption is to change the asymptotic decay of the average survival probability by a multiplicative factor $(1 + 2\phi_0)^{2\rho}$. As we expect, this multiplicative factor increases $P^{av}(t)$, meaning that on average the target survives longer, but what is interesting is that at large t , there is no effect from the imperfection on its time dependence, suggesting that the dominant contributions from partial absorption on $P^{av}(t)$ take effect at early times. This may be because relatively unlikely instances of the target being found very quickly by a searcher have a very strong influence on $P^{av}(t)$ because it is a multiplicative process.

3.5.2 Typical Survival Probability

Now we turn our attention to the typical survival probability of the target, $P_s^{typ}(t)$, which can be expressed as

$$P_s^{typ}(t) = \exp \sum_{i=1}^N \langle \ln q(x_i, t) \rangle_x = \exp \left[2\rho \int_0^{L/2} dx \ln q(x, t) \right] . \quad (3.5.16)$$

We found in (3.3.33) that in the long time limit,

$$q(x_0, t) \sim e^{-|s_0|t} , \quad (3.5.17)$$

which we can use to write

$$\int_0^\infty dx_0 \ln q(x_0, t) \simeq const - t \int_0^\infty dx_0 |s_0(x_0)| , \quad (3.5.18)$$

where the constant comes from the constant factors multiplying $q(x_0, t)$ which are not important. When we exponentiate this, the constant part becomes a constant multiplying factor in $P^{typ}(t)$ that is still not important. We can now write as $P^{typ}(t) \sim \exp(-2I\rho t)$, where

$$I = \int_0^\infty dx_0 |s_0(x_0)| . \quad (3.5.19)$$

We can calculate the integral I using the following procedure. To begin, we simply rewrite (3.5.19) as an integral over θ ,

$$I = \frac{1}{\alpha_0} \int_0^\infty d\theta |s_0(\theta)| , \quad (3.5.20)$$

and then make the substitution

$$\sigma(\theta) = -\frac{s_0(\theta)}{r} , \quad (3.5.21)$$

which satisfies

$$\sigma(2\phi_0(1-\sigma)^{1/2} + 1) = \exp(-\theta(1-\sigma)^{1/2}) \quad (3.5.22)$$

from (3.3.18) and

$$0 \leq \sigma < 1 \quad (3.5.23)$$

from (3.3.19). We also note here that

$$\theta = -\frac{1}{(1-\sigma)^{1/2}} [\ln(\sigma) + \ln(2\phi_0(1-\sigma)^{1/2} + 1)] . \quad (3.5.24)$$

Now we can rewrite the integral again to eliminate θ :

$$I = \sqrt{rD} \int_{\sigma_0}^{\sigma_\infty} \frac{d\theta}{d\sigma} d\sigma \sigma(\theta) . \quad (3.5.25)$$

From (3.5.22), the upper limit of the integral, σ_∞ , must satisfy

$$\sigma_\infty(2\phi_0(1-\sigma_\infty)^{1/2} + 1) = 0 . \quad (3.5.26)$$

The solution which satisfies this and (3.5.23) for all ϕ_0 is

$$\sigma_\infty = 0 . \quad (3.5.27)$$

Similarly, the lower limit σ_0 satisfies

$$\sigma_0(2\phi_0(1 - \sigma_0)^{1/2} + 1) = 1 , \quad (3.5.28)$$

which is a quadratic with solutions

$$\sigma_{0\pm} = \frac{-1}{8\phi_0^2} \pm \frac{\sqrt{1 + 16\phi_0^2}}{8\phi_0^2} . \quad (3.5.29)$$

The solution σ_{0-} is negative and does not satisfy (3.5.23), so

$$\sigma_0 = -\frac{1}{8\phi_0^2} \left(1 - \sqrt{1 + 16\phi_0^2} \right) . \quad (3.5.30)$$

We can now write

$$I = \sqrt{rD} \int_{\sigma_0}^0 d\sigma \left[\frac{d}{d\sigma} \left(-\frac{\ln(\sigma)}{(1-\sigma)^{1/2}} - \frac{\ln(2\phi_0(1-\sigma)^{1/2} + 1)}{(1-\sigma)^{1/2}} \right) \right] \sigma . \quad (3.5.31)$$

The next step is to integrate by parts. The first term

$$\int_{\sigma_0}^0 d\sigma \left[\frac{d}{d\sigma} \left(-\frac{\ln(\sigma)}{(1-\sigma)^{1/2}} \right) \right] \sigma = -\frac{\sigma_0 \ln(\sigma_0)}{(1-\sigma_0)^{1/2}} + \int_{\sigma_0}^0 d\sigma \left(\frac{\ln(\sigma)}{(1-\sigma)^{1/2}} \right) , \quad (3.5.32)$$

and the second

$$\begin{aligned} \int_{\sigma_0}^0 d\sigma \left[\frac{d}{d\sigma} \left(-\frac{\ln(2\phi_0(1-\sigma)^{1/2} + 1)}{(1-\sigma)^{1/2}} \right) \right] \sigma &= -\frac{\sigma_0 \ln(2\phi_0(1-\sigma_0)^{1/2} + 1)}{(1-\sigma_0)^{1/2}} \\ &\quad + \int_{\sigma_0}^0 d\sigma \left(\frac{\ln(2\phi_0(1-\sigma)^{1/2} + 1)}{(1-\sigma)^{1/2}} \right) . \end{aligned} \quad (3.5.33)$$

Now, using (3.5.28), we see that

$$-\frac{\sigma_0 \ln(2\phi_0(1-\sigma_0)^{1/2} + 1)}{(1-\sigma_0)^{1/2}} = \frac{\sigma_0 \ln(\sigma_0)}{(1-\sigma_0)^{1/2}} , \quad (3.5.34)$$

so the first term of (3.5.32) cancels the first term of (3.5.33). This means that, after our integration by parts, we can now write I more simply as

$$I = \sqrt{rD} \int_{\sigma_0}^0 d\sigma \left[\frac{\ln(\sigma)}{(1-\sigma)^{1/2}} + \frac{\ln(2\phi_0(1-\sigma)^{1/2} + 1)}{(1-\sigma)^{1/2}} \right]. \quad (3.5.35)$$

We make one more change of variable before computing the integral, which is

$$\sigma = 1 - y^2. \quad (3.5.36)$$

Under this substitution, I simplifies further to become

$$I = 2\sqrt{rD} \int_1^{y_0} dy [\ln(1-y^2) + \ln(2\phi_0 y + 1)], \quad (3.5.37)$$

where

$$y_0^2 = 1 - \sigma_0. \quad (3.5.38)$$

We label the first term of this integral I_0 ,

$$I_0 = 2\sqrt{rD} \int_1^{y_0} dy [\ln(1-y) + \ln(1+y)], \quad (3.5.39)$$

and the second I_1 ,

$$I_1 = 2\sqrt{rD} \int_1^{y_0} dy \ln(2\phi_0 y + 1). \quad (3.5.40)$$

I_0 can be computed directly to give

$$I_0 = 4\sqrt{rD} \left[1 - \ln 2 - y_0 + \frac{(1+y_0)}{2} \ln(1+y_0) - \frac{(1-y_0)}{2} \ln(1-y_0) \right]. \quad (3.5.41)$$

The second term, I_1 , can also be computed directly, giving

$$I_1 = -\frac{\sqrt{rD}}{\phi_0} [(2\phi_0 + 1) \ln(2\phi_0 + 1) - (2y_0\phi_0 + 1) \ln(2\phi_0 y_0 + 1) - 2\phi_0(1 - y_0)]. \quad (3.5.42)$$

To compare with the previous results [57, 58] for total absorption, we are interested in looking at the leading order dependence on a , and therefore ϕ_0 , of $P^{typ} \sim \exp(-2(I_0 + I_1)\rho t)$ for a weakly imperfect target, which has large absorption velocity a ($\phi_0 \ll 1$). First, we find the leading order dependence on

ϕ_0 of y_0 :

$$y_0^2 = 1 + \frac{1}{8\phi_0^2} \left(1 - \sqrt{1 + 16\phi_0^2} \right) \simeq 4\phi_0^2. \quad (3.5.43)$$

Now we consider I_0 . For small y_0 ,

$$-y_0 + \frac{(1+y_0)}{2} \ln(1+y_0) - \frac{(1-y_0)}{2} \ln(1-y_0) = -\frac{y_0^3}{6} + \mathcal{O}(y_0^4). \quad (3.5.44)$$

Thus, using $y_0^3 \simeq 8\phi_0^3$, we find

$$I_0 \simeq 4\sqrt{rD} \left(1 - \ln 2 - \frac{4\phi_0^3}{3} + \mathcal{O}(\phi_0^4) \right). \quad (3.5.45)$$

For I_1 , by using (3.5.43) again we see that, for $\phi_0 \ll 1$,

$$I_1 \simeq -4\sqrt{rD} \left[\frac{\phi_0}{2} + \mathcal{O}(\phi_0^2) \right]. \quad (3.5.46)$$

Combining the results (3.5.45) and (3.5.46) we find that

$$I \simeq 4\sqrt{rD} \left(1 - \ln 2 - \frac{\phi_0}{2} \right), \quad (3.5.47)$$

to leading order in ϕ_0 , for $\phi_0 \ll 1$. In this limit, from (3.5.45) and (3.5.46), the correction to the total absorption decay rate is linear in ϕ_0 :

$$P^{typ}(t) \sim \exp \left[-8\sqrt{rD} \left(1 - \ln 2 - \frac{\phi_0}{2} \right) \rho t \right]. \quad (3.5.48)$$

The decay rate becomes smaller as the absorption velocity a is decreased (ϕ_0 increased) and the absorption at the target becomes ‘less perfect’. The result is intuitive: it tells us that as the absorption at the target weakens, its survival probability over time decays more slowly, because the target is less likely to react with a searcher.

The fact that the target imperfection affects the rate of decay of $P^{typ}(t)$ at large times indicates that its effect is still felt significantly on a typical searcher trajectory at long times. In contrast, there no effect on the time dependence of the average survival probability of the target $P^{av}(t)$ at large times. This suggests that there are relatively rare trajectories involving interactions between the target and searchers at short times which are strongly influenced by the imperfection at

the target. These could be events such as the searchers which start closest to the target finding it relatively quickly, before the contributions to the overall search process from searchers which begin far away become significant.

For completeness, we present the full result

$$\begin{aligned} P^{typ}(t) \sim & \exp \left\{ -8\rho t \sqrt{rD} \left[1 - \ln 2 - y_0 + \frac{(1+y_0)}{2} \ln(1+y_0) \right. \right. \\ & - \frac{(1-y_0)}{2} \ln(1-y_0) - \left(\frac{2\phi_0+1}{4\phi_0} \right) \ln(2\phi_0+1) \\ & \left. \left. - \left(\frac{2y_0\phi_0+1}{4\phi_0} \right) \ln(2\phi_0y_0+1) - \left(\frac{1-y_0}{2} \right) \right] \right\}, \end{aligned} \quad (3.5.49)$$

which shows the all the corrections to the decay rate from ϕ_0 .

3.6 Discussion and Conclusions

In this chapter I have studied the dynamics of a diffusive searcher in a system with a partially absorbing target, as defined in (3.2.15), which gives a more realistic description of many, varied search processes. This study has revealed some straightforward, significant and intuitive consequences for the dynamics as a direct result of imperfection in the absorption at the target.

We see from Section 3.3, and equations (3.3.33) and (3.3.34) in particular, that the survival probability of the searcher (or target) decreases exponentially with time, with a decay rate which increases as the absorption constant a increases. As the target comes closer to being perfectly absorbing, the survival probability decays much faster with time.

The study of the MTA in Section 3.4 has revealed that the mean time to absorption is increased by an additive term $1/ap^*(0)$ (see (3.4.13)). As a decreases and the target is made more ‘imperfect’ the mean time to absorption increases, as expected. The MTA is also increased by reducing $p^*(0)$, whether by changing the diffusion constant D , the resetting rate r , or the resetting distribution $\mathcal{P}(x)$.

For multiplicative processes, such as the many searcher problem analysed in Section 3.5, the distinction between *typical* and *average* probabilities becomes significant. This is emphasised by the difference in the form of effects of imperfect absorption on the typical and average survival probabilities of the target in the many searcher system. We see from Section 3.5.1 that $P^{av}(t)$ is modified by

multiplicative factor $(1 + 2\phi_0)^{2\rho}$, whereas in Section 3.5.2 it is the decay rate of $P^{typ}(t)$ which is decreased by factor proportional to $1/a$.

An important quantity that has emerged from this work is the dimensionless ratio $\phi_0 = \alpha_0 D/a$. This quantity is a ratio of length scales characteristic to the system: the length scale $1/\alpha_0 = \sqrt{D/r}$ has already been established as the characteristic displacement of the searcher due to diffusion between reset events [57]; the length D/a is the attenuation depth in the composite medium discussed in [144] and Section 3.2.4. The dimensionless variable ϕ_0 represents the ratio of these two length scales, and in all the results the dynamics are only modified in terms of this ratio and not the absolute strength of the imperfection that has been introduced to the target. This is clear evidence that it is the competition between resetting and the absorption that controls the dynamics of the system.

The effect of resetting is not just of interest in the study of search processes. Its effect on a growing interface has been shown to have the effect of creating non-Gaussian fluctuations in its heights. In particular the widths of interfaces which experience stochastic resetting no longer scale with the system size, but instead with the resetting rate r as $r \rightarrow 0$ [78]. The phenomenon of the resetting of an interface is of particular interest in biochemistry and medicine. Stochastic cell division, such as in bacteria or tumours, creates cell colonies bound by a rough interface. Upon application of chemicals, the colonies can be suddenly reduced in size, ‘resetting’ their bounding interface to some earlier less developed configuration.

Resetting has also been studied in a spatially discrete, one-dimensional model of coagulation and diffusion [49]. In this study, resetting is shown to result in modified non-equilibrium steady states. Furthermore, it is found that the influence of resetting on the behaviour is more significant at larger length scales, whereas the behaviour without resetting dominates at smaller length scales.

Chapter 4

A Moving Condensate in a Zero-Range Chipping Model

4.1 Introduction

In this chapter I present a minimal mass-transport model in the spirit of the Zero-Range Process (ZRP), but which allows large-mass hopping events. My primary interest is in the study of a phenomenon called *condensation*, where a finite fraction of the total mass becomes localised, and in particular how a *moving* condensate phase can be maintained.

The defining feature in this model is the incorporation of a ‘backchip’ move where all of the mass bar a single unit move together to the next site. Understanding this process, in the context of earlier similar studies (e.g. [85, 86, 110, 116, 172]), is important for building a broader understanding of what kinds of processes and conditions create or destabilise a moving condensate phase, which itself is relevant to the study of collective behaviour such as flock formation [168].

I find that the model exhibits a moving condensate phase with a distinctive mechanism of formation and maintenance. The moving condensate is a *strong* condensate, in the sense that the fraction of the total particles in the condensate tends to one in the large system size limit, which travels through the system followed by a tail of low occupancy sites that collectively comprise of a vanishing fraction of the mass.

As I show, the dynamics of the mass within this tail is responsible for

maintaining the structure of the condensate. Using numerical simulations, I find that above a critical value for a rate parameter, b , and at all densities, a strong condensate forms. Numerically I am able to classify the transition as being of mixed order, exhibiting features of both first and second order phase transitions. I further provide an approximate theory of the mechanism which gives a reasonable prediction for the critical value, and also discuss the behaviour of the system below this critical rate.

In this chapter I present results that have been published in [174]. In addition to these, I also present a mean-field theory analysis in Section 4.4.

4.1.1 Background and Motivation

In non-equilibrium statistical physics, condensation is used as a general term to describe the localisation of a finite fraction of some quantity, typically mass, in a wide variety of fundamental models of dynamical processes. These include the flow of wealth [34], traffic flow [37, 102, 111, 133], and the formation of hubs in complex networks [5, 104]. The archetypal model of this class is the ZRP [55, 56], as described in Section 2.5.

In this model single units of mass hop between sites at a rate which is a function only of the total mass on the site they are leaving. Furthermore the ZRP satisfies the conditions required for the steady state to factorise, which simplifies the analysis of its condensate phase [60, 61, 115]. As discussed in Section 2.5, with an appropriate choice of the hopping rate $u(n)$ there exists a *static* condensate phase in which a finite fraction of the total mass of the system occupies a single site. For the case $u(n) = 1 + b/n^\alpha$ the transition has been extensively studied. When $\alpha = 1$, a condensation transition occurs when $b > b_c = 2$ and the particle density $\rho > \rho_c = 1/(b - 2)$. For $\rho < \rho_c$, the system is in a fluid phase where the mass is evenly distributed across sites, and for $\alpha < 1$ a condensation transition occurs for all b [55].

There are certain cases in which the nature of the condensate phase is different from the ‘standard’ condensation described above. For example: the fraction of the total system mass in the condensate can be equal to 1, creating a *strong* condensate [97, 98]; the condensed phase can exhibit a subextensive number of smaller mesocondensates [155] or an extensive number of finite-sized quasi-

condensates [167]. Also, it should be noted that the existence of a condensate phase is not unique to models based on the ZRP or with factorised steady states. For example, a non-Markovian simple exclusion process has been shown to exhibit an immobile condensate phase [39].

In all these examples, the condensates are static: they reside at the same point in space for a long period until dissolving through a large fluctuation and reforming elsewhere [75]. However, in physical settings *moving* condensates or aggregates are often observed, for example in traffic jams [112], gravitational clustering [157], sedimentation [89] and droplet formation [63], and some understanding of these has been gained. In the study of traffic flow [112], for instance, the authors study the mechanism by which a high-density traffic phase travels along a low-density road and see that it is maintained by a steady current of cars into and out of the high-density region, which moves slower than the average traffic speed. In general, however, moving condensates are less well understood than the static variety and it is unclear what the physical mechanisms that will maintain the condensate are.

In this chapter I investigate conditions under which a condensate may maintain its order as it moves through the system. To understand why this is a pertinent question I first review how condensates move in a variety of simple model systems related to the ZRP.

Majumdar, Krishnamurthy and Barma [116] introduced a chipping model in which all the mass from a site can move, or ‘diffuse’, to an adjacent site, or a single unit of mass can ‘chip’ off from the departure site and hop to an adjacent site. For symmetric diffusion of the mass, a condensed phase was observed. However for asymmetric diffusion, which leads to a condensate that moves on average, a careful analysis revealed that, although a condensate is still observed on a finite system [117], the critical density at which the condensation transition occurs diverges in the thermodynamic limit [141]. This is because the chipping process (in one-dimension) dissipates clusters faster than the diffusion process creates them [140]. However subsequent work on a chipping model with a chipping rate of the classical zero-range type, $u(n) = 1+b/n$, suggests that a condensate may be possible for large enough b with the critical value b_c somewhere close to two [110].

Also, Hirschberg *et al.* have investigated what kinds of dynamical processes

will permit a moving condensate phase using variants of the ZRP with non-Markovian hopping rates [85, 86] and with hopping rates affected by spatial correlations [87]. Both models exhibit a condensate phase which drifts with a finite, non-vanishing velocity. In the former, temporal correlations between departure and arrival sites allow the formation of a condensate over two adjacent sites, which then moves with a ‘slinky’-like motion through the system, where the mass is ‘poured’ sequentially from one site to the next. In the latter, the effect of spatial correlations is that the condensate also moves with a slinky-like motion, but with certain differences in the details depending on the values of certain hopping parameters. Condensate motion of a similar slinky nature has also been observed in a totally asymmetric model [62, 172] in which the hopping rate is a monotonically increasing function of the mass at both departure and arrival sites. The condensation in this model is found to be “explosive” in as much as the condensate moves with a superextensive velocity and forms instantaneously in an infinite system.

Taken together these studies pose the intriguing question that I pursue here: What are the key dynamical processes that permit a moving condensate phase, and which processes will destabilise the phase?

To motivate the specific features of the model let us first consider the limit of zero chipping rate in the models of [110, 117]. In the absence of any chipping, the dynamics is simply diffusion combined with irreversible aggregation. The stationary state of this process on a finite system comprises a single condensate containing all the system’s mass. The work of [140, 141] has shown that the condensate is unstable to the effect of single particles chipping away from an aggregate with rate $u = 1 + b/n$, where n is the number of particles contained within the aggregate, unless b is greater than a critical value $b_c > 0$. Therefore it is of interest to consider what other perturbations may destabilise the condensate exhibited in diffusion with irreversible aggregation.

4.2 Model

In this model, the specific perturbation we consider is as follows: when the aggregate moves forward it leaves one unit of mass behind (Figure 4.1). We consider a system of N particles on a one-dimensional lattice of L discrete sites

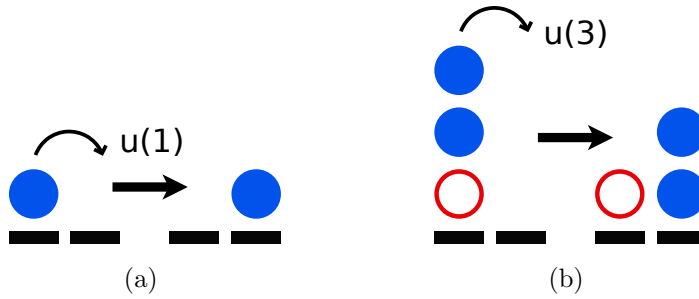


Figure 4.1: The elementary dynamical processes. (a) Hop: When a site contains only one particle, this particle hops onto the next site with rate $u(1)$, leaving behind an empty site. (b) Backchip: When a site contains n (3) particles, $n - 1$ (2) of these particles move together with rate $u(n)$ onto the next site and leave behind a *single* particle.

that hop, as an aggregate, from one site to the next. We retain the zero-range feature that the rate of movement $u(n)$ only depends on the number of particles within the aggregate, and we are particularly interested in the large N , L behaviour where the density $\rho = N/L$ is fixed.

In the case where the site has occupancy $n > 1$, a ‘backchip’ takes place: $n - 1$ of the particles move to the next site, and leave behind a single particle (Figure 4.1(b)). This occurs with rate with rate $u(n)$ given by

$$u(n) = 1 + \frac{b}{n^\alpha}, \quad (4.2.1)$$

where n is the total number of particles on the departure site. With this form, larger values of the rate parameter b bias the dynamics towards faster hopping from sites occupied by fewer particles, causing larger groups of mass to move slowly in comparison.

The dynamical rule must of course be modified when there is just single unit of mass at a site, when $n = 1$. This single particle moves to the next site and leaves behind an empty site (Figure 4.1(a)) with rate $u(1)$.

The choice of hop rates allows us to compare the model to the standard formulation of the ZRP where only a single particle can hop at a time. This type of hop is often referred to as a ‘chip’, as in [116, 117, 140, 141], and is in some sense symmetric to the definition of a backchip. The name ‘chip’ can be conceptually understood in the context of a single mass unit chipping off from a site with large occupancy. We study the case where $\alpha = 1$, as it can be shown exactly

that with the hop rate given in (4.2.1) and $\alpha = 1$ the standard ZRP undergoes a condensation transition at $\rho_c = 1/(b - 2)$ for $b > 2$ [56].

4.3 Numerical Analysis

I implemented Monte Carlo simulations of the system on a one-dimensional periodic lattice, using a continuous time Monte Carlo algorithm [25, 132]. The simulations were run until equilibrated, and measurements were taken over many regular temporally separated intervals. These were then averaged over to obtain the numerical results. I then used two methods to try to identify and characterise any phases observed.

The first was to look at plots of the measured occupancy distribution of system, $p(n/N)$, which is the probability that any given site holds a fraction n/N of the total number of particles, or *mass*, N . In the ZRP there is a clear difference in this distribution between the fluid and condensate phases. In the fluid phase, one finds that this distribution decays exponentially [56]. In the condensate phase, the distribution decays as a power law for small n/N , but then there is a Gaussian ‘bump’ in the distribution, peaked around

$$\frac{n_{\text{peak}}}{N} = (\rho - \rho_c) \frac{L}{N} , \quad (4.3.1)$$

where ρ_c is the critical density, and the density of mass in the background fluid (the sites which do not hold the condensate) [56].

I also measure the normalised variance, defined

$$\sigma^2 = \frac{1}{\rho^2 L} (\bar{n}^2 - \bar{n}^2) , \quad (4.3.2)$$

such that

$$0 \leq \sigma^2 < 1 , \quad (4.3.3)$$

making it comparable across data sets from numerical simulations of different system sizes L and densities ρ . To get a conceptual understanding of what different kinds phenomena different values of σ^2 represent, consider two possible example states. The first is one where all the mass is distributed homogeneously throughout the system. In this case, the variance σ^2 would be close to 0, if not 0,

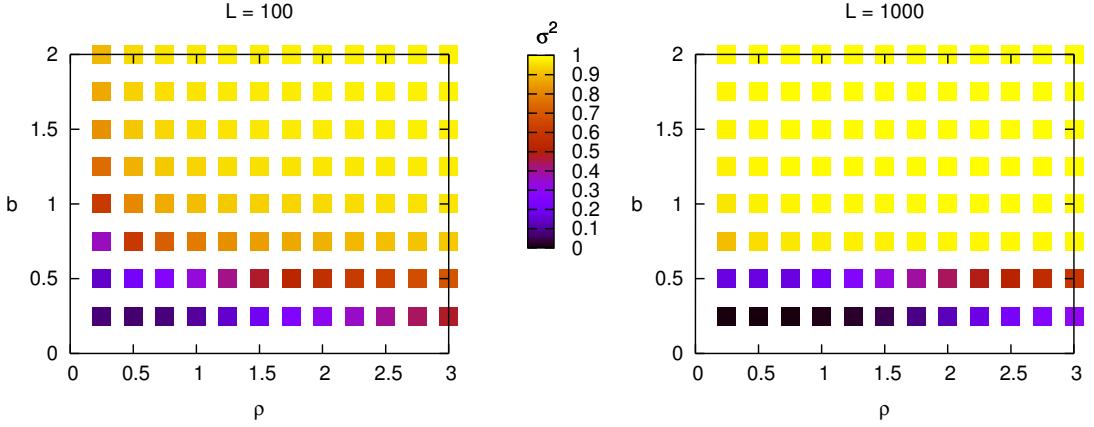


Figure 4.2: Plot of σ^2 against both ρ and b , for $L = 100$ and 1000 . There is a significant change of state when $b > 0.5$, and also a gradual, weaker change in state when $b \leq 0.5$ as ρ is increased.

because the occupancy distribution will be sharply peaked about a single value of n/N . The second, is the case where all of the mass is on a single site. In this case, there are two peaks at opposite ends of the distribution. The empty sites contribute $P(n/N = 0) \sim 1 - 1/L$ to the distribution, and the single site with all of the mass contributes $P(n/N = 1) \sim 1/L$. In this case, $\sigma^2 = 1 - 1/L$, which tends to 1 as $L \rightarrow \infty$. So we see that the measure σ^2 tells us whether the system is highly ordered ($\sigma^2 \rightarrow 1$) or very disordered ($\sigma^2 \rightarrow 0$).

4.3.1 Identifying Phases

Using the measure σ^2 , and by inspecting the occupancy distributions, we begin to understand the different phases exhibited by this system. First, by looking at heat plots of σ^2 as a function of both ρ and b in Figure 4.2 we see a transition in the b direction between a phase with small σ^2 to one with large σ^2 . This means that for small b we see a homogeneous phase, which gradually becomes less homogeneous as ρ is increased, and for b greater than some critical value b_c we see a highly ordered phase. To understand this phase further, we can look at the occupancy distribution and compare it to the distributions seen in the ZRP. Well into the ordered phase, $b = 2$, Figure 4.6, we see that the distribution has two striking features: sharp peaks at $n/N = 0$ and 1. In fact, $P(0) \sim 1 - 1/L$ and $P(1) \sim 1/L$. This tells us that we have a *strong* condensate, where essentially all of the mass occupies a single site.

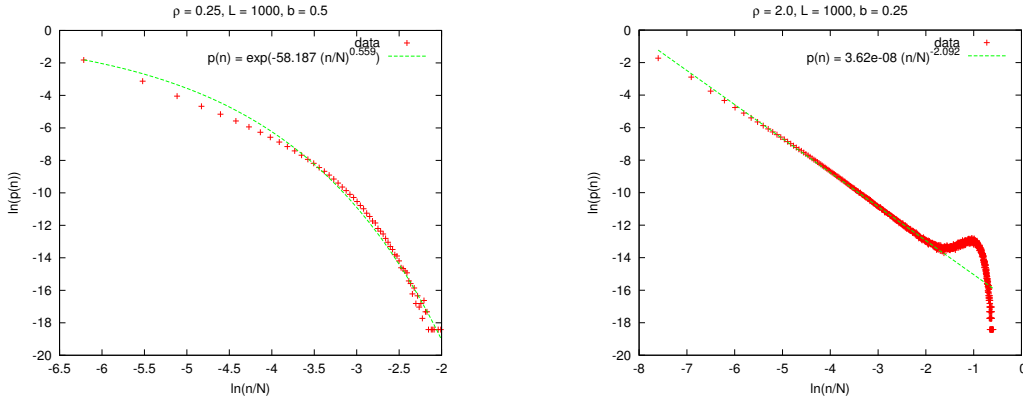


Figure 4.3: Example occupancy distributions: (a) The fluid phase ($\rho = 0.5$, $L = 1000$, and $b = 0.25$). The distribution decays as a stretched exponential. (b) The standard condensate phase ($\rho = 2.0$, $L = 1000$, and $b = 0.25$). The distribution decays as a power law for low occupancies, but exhibits a ‘bump’ caused by a condensate at larger occupancies.

Looking at the occupancy distribution also hints at what happens to the system as the density is varied. At small values of ρ , where σ^2 is close to 0, the distribution is similar to the fluid phase seen in the ZRP, and decays as a stretched exponential (Figure 4.3(a)). As ρ is increased, one sees the emergence of a peak in the distribution which indicates the existence of a condensate. One also sees that the distribution decays as a power law at low occupancies, instead of an exponential or a stretched exponential.

Now, we can sketch a simple phase diagram for the system, Figure 4.4. From this starting point, we will investigate the nature of the phases and transitions in greater depth.

4.3.2 Strong Condensate Phase

From the simulations we see that, above a critical value of b , the system exhibits a *strong* condensate, where almost all the mass occupies a single site, which moves through the system. This is immediately followed by a short tail of sites with very low occupancy, leaving all other sites empty (Figure 4.5). This behaviour can also be seen from a plot of the site occupancy distribution (Figure 4.6), which is strongly peaked at $n/N = 1$, indicating that we have a strong condensate. It tells us that typically at an instant in time nearly all of the mass occupies a single site.

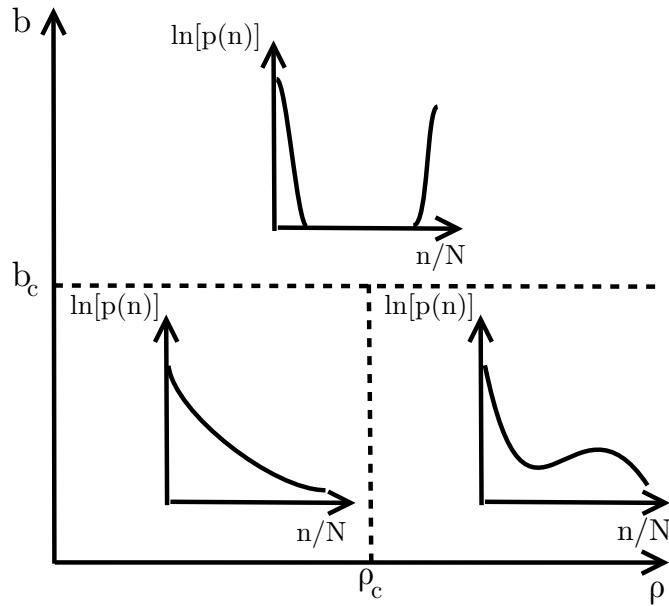


Figure 4.4: A sketch of the phase diagram suggested by the numerical measurements of the occupancy distribution $p(n)$.

Mechanism of Maintenance of the Strong Condensate

The maintenance of the structure of the strong condensate phase can be attributed to the dynamics of this tail of mass which trails directly behind the condensate itself. Since a larger hopping rate b biases the rate function $u(n)$ towards hops from sites with a low occupancy n , these hops will occur much more frequently than from those sites with large n . When the condensate hops, it leaves behind a site of occupancy 1. A single unit of mass has the largest possible hop rate, and thus it seems plausible that it is much more likely for the single mass unit immediately behind the condensate to recombine with it than it is for the condensate to hop again and away from the mass it left behind. In this way, it appears that the strong condensation is a consequence of the condensate being unable to escape from the tail of mass trailing behind. As such, the structure of a very strongly occupied condensate and its very short tail of a few masses is maintained as they move through the system. We provide further evidence for this intuitive picture of strong condensation within a theoretical treatment below.

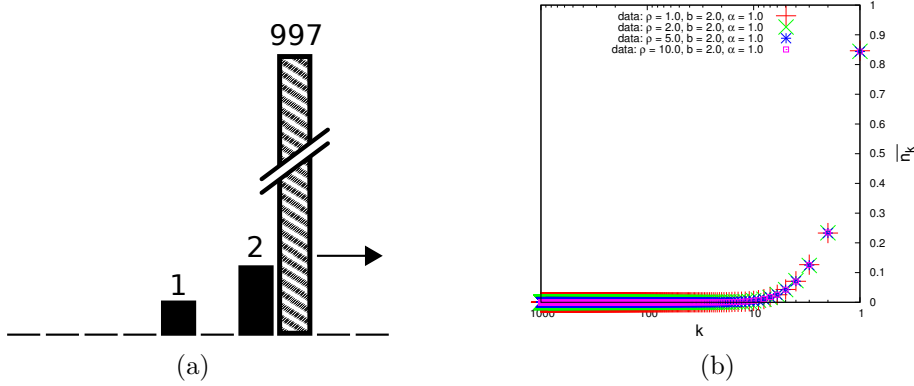


Figure 4.5: Illustration of the strong condensate phase. (a) A typical configuration sketched using data taken directly from a simulation ($L = 1000$, $N = 1000$, $b = 2.0$ and $\alpha = 1.0$). The columns represent the mass occupying the site, with the exact size shown above, and the direction of motion is indicated by the arrow. (b) The average mass \bar{n}_k at a site k sites *behind* the condensate ($\rho = 1, 2, 5, 10$, $b = 2.0$, $\alpha = 1.0$). Almost all of the system's mass is in the condensate, with any remaining trailing closely behind.

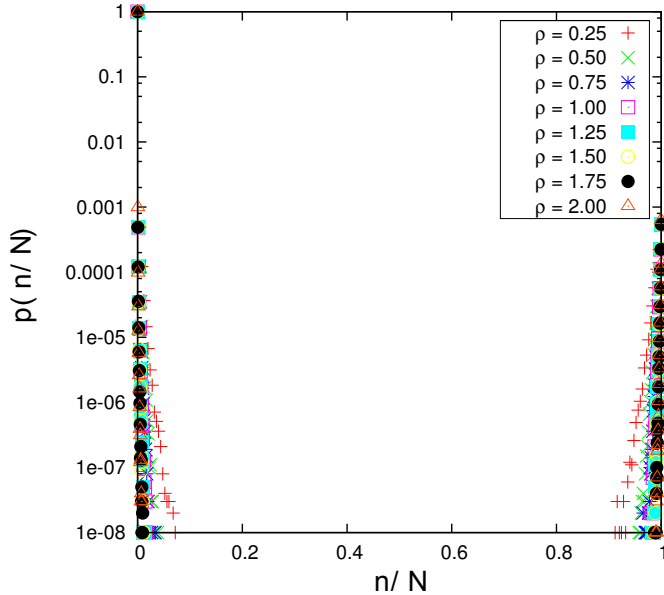


Figure 4.6: Plot of the occupancy distribution $p(n)$ in the strong condensate regime at a range of densities ($b = 2.0$, $L = 1000$, $\alpha = 1.0$). The points at and near $n/N = 1$ indicate the presence of a strong condensate which contains effectively all of the system's mass.

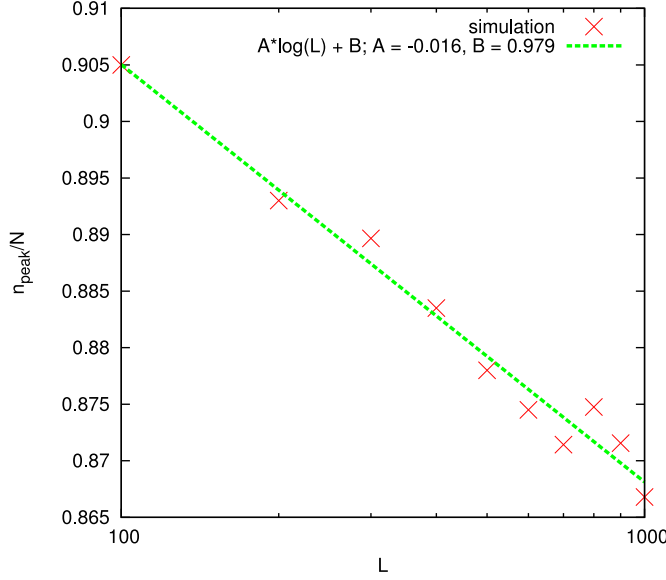


Figure 4.7: As the system size is increased, the position of the peak in the probability distribution decreases logarithmically with L . This means that the critical density ρ_c has L dependence of the form $\rho_c(L) \sim \ln(L)$.

4.3.3 Standard Condensate Phase

When $b < b_c$ we find a transition from a homogeneous fluid phase when $\rho \lesssim 1$ to a ‘standard’ condensate phase. From the heat plots in Figure 4.2 one might guess that this transition takes place in the range $\rho = 1 - 2$, and as will be discussed in Section 4.4.3 the mean-field theory suggests a transition takes place at $\rho_c = 1$. Although this phase quantitatively and qualitatively looks like a standard condensate, numerical analysis shows that the transition density ρ_c diverges as $\ln(L)$, in a similar way to that observed for biased hopping rates in [140]. This can be seen from Figure 4.7 where we have analysed the size of the position of the peak, n_{peak} , in the distribution of the standard condensate phase. If the fluid contains on average $N_c = L\rho_c(L)$ particles, then

$$\frac{n_{\text{peak}}(L)}{N} \simeq (\rho - \rho_c(L)) \frac{L}{N} = (1 - \rho_c(L)/\rho). \quad (4.3.4)$$

Measurements of the value of $n_{\text{peak}}(L)$ (Figure 4.7) show that $n_{\text{peak}}(L) \propto -\ln(L)$, and thus that $\rho_c \propto \ln(L)$.

4.4 Mean-Field Theory

In an attempt to learn more about the phase diagram we find numerically, we formulate a mean-field theory for the occupancy distribution $p(n, t)$ based on the dynamics of the system. The theory is ‘mean-field’ in the sense that we disregard any spatial structure in the system, but, as we will see, the spatial structure and the resulting spatial correlations are important features of the dynamics, and the theory is somewhat limited without them.

A standard procedure to learn more about a probability distribution is to define a generating function for the distribution $p(n, t)$, which can provide accessible route to the moments of the distribution, or even an expression for the distribution $p(n, t)$ itself. However, we will fail to learn anything from the generating function because we find it to be part of an infinite hierarchy of equations that we cannot solve. Nevertheless, analysis of the second moment of the mass distribution using the mean-field master equations allows us to predict a condensation transition in ρ at $\rho_c = 1$, and we are able to gain some insight into the consequences of the choice of dynamics as a result. We are also able to analyse the case where all hopping rates are equal ($b = 0$) and find that the mean-field theory still predicts $\rho_c = 1$, confirming that the choice of dynamics has direct influence on the ρ phase transition.

4.4.1 Master Equations

We begin by writing three master equations: for $p(0, t)$, $p(1, t)$ and $p(n > 1, t)$. As a consequence of the modification to the dynamic rule when the number of masses hopping is 1, each master equation has terms unique to each case. The master equations are

$$\frac{dp(0, t)}{dt} = p(1, t)u(1) - p(0, t)v , \quad (4.4.1)$$

$$\frac{dp(1, t)}{dt} = p(0, t)p(2, t)u(2) + [p(0, t)u(1) - 2u(1) - v]p(1, t) + v , \quad (4.4.2)$$

and, for $n > 1$,

$$\frac{dp(n,t)}{dt} = -[u(n)+v]p(n,t) + p(1,t)u(1)p(n-1,t) + \sum_{m=2}^{n+1} p(n-m+1,t)p(m,t)u(m) , \quad (4.4.3)$$

where we have defined

$$v = \sum_{m=1}^{\infty} p(m,t)u(m) . \quad (4.4.4)$$

The terms on the right hand side of these equations represent the flow of probability into and out of the state given in the time derivative. Contributions typically look, for example, like

$$+p(n-1,t)p(1,t)u(1) , \quad (4.4.5)$$

which represents flow into $p(n,t)$ caused by a single particle hopping with rate $u(1)$ into a site with occupancy $n-1$, or

$$-p(n,t)u(n) , \quad (4.4.6)$$

which represents flow out of $p(n,t)$ caused by particle hopping out of a site with occupancy n . In the equations above, the raw contributions of these types have been rearranged into simpler forms.

4.4.2 Failure of the Generating Function Technique

We now proceed to calculate the generating function, which we define as

$$Q(z,t) = \sum_{n=1}^{\infty} z^n p(n,t) , \quad (4.4.7)$$

in order to learn more about the probability distribution $p(n,t)$. From the master equations (4.4.2) and (4.4.3), we can write an equation for $Q(z,t)$,

$$Q(z,t) = z \frac{dp(1,t)}{dt} + \sum_{n=2}^{\infty} z^n \frac{dp(n,t)}{dt} , \quad (4.4.8)$$

which, after much algebra, can be expressed as

$$\begin{aligned} \frac{dQ(z,t)}{dt} = & -vQ(z,t) - R_1(z,t) + [v - u(1)p(1,t)]z \\ & + u(1)p(1,t)[p(0,t) + Q(z,t)]z \\ & + z^{-1}(p(0,t) + Q(z,t))(R_1(z,t) - u(1)p(1,t)z), \end{aligned} \quad (4.4.9)$$

where

$$R_i(z,t) = \sum_{n=1}^{\infty} p(n,t)[u(n)]^i z^n, \quad (4.4.10)$$

and $Q(z,t) = R_0(z,t)$.

By using the master equations again, this time to obtain an equation for $R_i(z,t)$:

$$\begin{aligned} \frac{dR_i(z,t)}{dt} = & u(1)p(1,t)z \left[p(0,t)u(1)^i + \sum_{n=1}^{\infty} p(n,t)u(n+1)^i z^n \right] \\ & + \sum_{m=2}^{\infty} \sum_{n=0}^{\infty} p(n,t)p(m,t)u(m)u(n+m-1)^i z^{n+m-1} \\ & + [v - u(1)p(1,t)]u(1)^i z - vR_i(z,t) - R_{i+1}(z,t). \end{aligned} \quad (4.4.11)$$

What we see is that $\partial R_i / \partial t$ depends on $R_{i+1}(z,t)$, and so we have an infinite hierarchy of equations, which we were unable to solve. Thus, we must take a different approach than the generating function approach in order to learn more about the observed phases.

4.4.3 Prediction of a Condensation Transition at $\rho_c = 1$

Instead of continuing with the generating function, we can study the time evolution of the moments

$$\overline{n^k} = \sum_{n=0}^{\infty} n^k p(n,t) \quad (4.4.12)$$

of the distribution $p(n, t)$. The zeroth moment \bar{n}^0 is 1, because the distribution is normalised, and the first moment $\bar{n} = \rho$, the density. Thus, the time derivative of each is zero. We instead study the second moment,

$$\bar{n}^2 = \sum_{n=0}^{\infty} n^2 p(n, t) . \quad (4.4.13)$$

Again, using our master equations (4.4.1), (4.4.2), and (4.4.3), we can write

$$\begin{aligned} \frac{d}{dt} \bar{n}^2 &= p(0, t)p(2, t)u(2) + [p(0, t)u(1) - 2u(1) - v]p(1, t) + v \\ &+ p(1, t)u(1) \sum_{n=2}^{\infty} n^2 p(n-1, t) - \sum_{n=2}^{\infty} n^2 [u(n) + v]p(n, t) \\ &+ \sum_{n=2}^{\infty} \sum_{m=2}^{n+1} n^2 p(n-m+1, t)p(m, t)u(m) . \end{aligned} \quad (4.4.14)$$

With some algebra, and by defining

$$w_i = \sum_{n=1}^{\infty} p(n, t)u(n)n^i , \quad (4.4.15)$$

where $w_0 = v$, we can simplify (4.4.14) to

$$\begin{aligned} \frac{d}{dt} \bar{n}^2 &= u(1)p(1, t)[-2 + \bar{n}^2 + 2\bar{n} + 1 - 2\bar{n} + 2 - \bar{n}^2 + 2\bar{n} - 1] \\ &+ v[1 - \bar{n}^2 + \bar{n}^2 - 2\bar{n} + 1] \\ &+ w_2 - w_2 + 2w_1(\bar{n} - 1) . \end{aligned} \quad (4.4.16)$$

Then by cancelling terms and rewriting \bar{n} as ρ we get the result

$$\frac{d}{dt} \bar{n}^2 = 2[\rho u(1)p(1, t) + (w_1 - v)(\rho - 1)] . \quad (4.4.17)$$

This equation gives us some information about the effect of ρ on the dynamics of \bar{n}^2 , and thus the variance σ^2 .

To understand what this is it is helpful to define the mean particle current

between sites as

$$J = p(1)u(1) + \sum_{n=2}^{\infty} (n-1)p(n,t)u(n) = J_1 + J_2 . \quad (4.4.18)$$

The term

$$J_1 = p(1,t)u(1) \quad (4.4.19)$$

represents the contribution to J from hops out of a site occupied by a single mass, and the term

$$J_2 = \sum_{n=2}^{\infty} (n-1)p(n,t)u(n) \quad (4.4.20)$$

represents the contribution to J from hops of $n-1$ particles out of sites occupied by n particles. J_1 and J_2 are always positive, because we have restricted the particles to move in only one direction. Now, noting that

$$w_1 - v = \sum_{n=1}^{\infty} (n-1)p(n,t)u(n) , \quad (4.4.21)$$

we can rewrite (4.4.17) as

$$\frac{d}{dt} \overline{n^2} = 2[\rho J_1 + (\rho - 1)J_2] . \quad (4.4.22)$$

When $\rho < 1$, the current of mass hopping from sites with more than one particle reduce the rate of change of $\overline{n^2}$ and when $\rho > 1$ the larger mass hops will increase the rate of change of $\overline{n^2}$. This is a direct consequence of the different dynamical rules for $n = 1$ and $n > 1$.

When a single particle hops from a site with occupancy 1 either the variance of the distribution remains the same, because there was an empty site ahead, or it increases, because the site ahead was not empty, and the mass from two sites has been concentrated onto one. In a backchip mass hops from a site with more than one unit of mass and exactly one unit is left behind. However, on the site ahead there will be on average ρ units of mass. If $\rho > 1$, this process will concentrate more of the mass onto a single site; if $\rho < 1$, then this process spreads the mass out across two sites; and if $\rho = 1$ then, on average, this process will have no effect on the variance of the mass distribution (see Figure 4.8).

By setting the time derivative in (4.4.17) to zero we can find a condition on

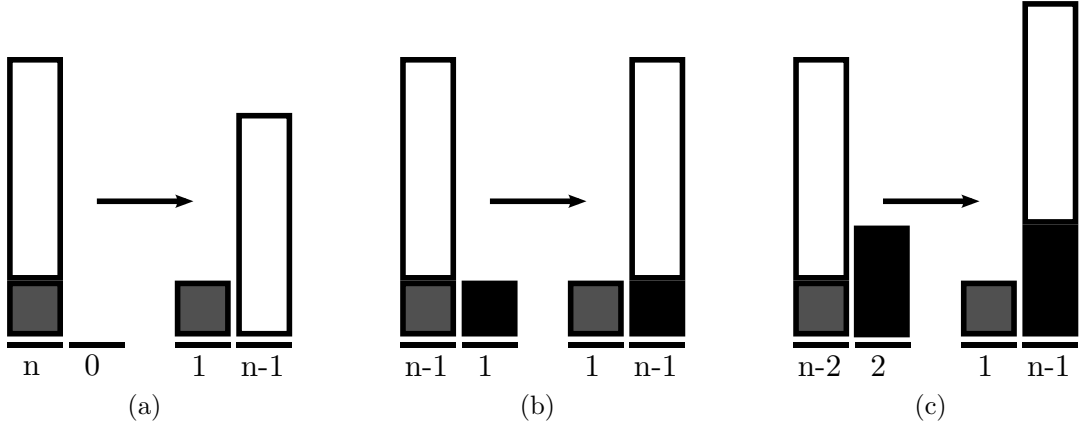


Figure 4.8: When a backchip occurs from a site with large occupancy, if the average occupancy, or density ρ , ahead is: (a) less than 1 the backchip will result in mass spreading out; (b) exactly 1 the mass distribution is unchanged; (c) greater than 1 the backchip will concentrate the mass.

the currents J_1 and J_2 , and thus the distribution, for which a steady state exists. We find

$$J_2 = \frac{\rho}{1 - \rho} J_1 , \quad (4.4.23)$$

which clearly cannot be satisfied if $\rho > 1$, because $J_2, J_1 > 0$, regardless of the choice of $u(n)$. This means that there is no steady state when $\rho > 1$ and, combined with our analysis of $\frac{d}{dt}\overline{n^2}$, tells us that in this case the mass in the system accumulates indefinitely and condenses onto a subset of the sites.

4.4.4 Special Case: $b = 0$

An interesting question is whether the condensation transition still exists when $b = 0$, where the backchips and single particle hops occur at the same rate. In this case the hop rate $u(n) = 1$ and is independent of the occupancy of the site being hopped from. If the phase transition were to exist in this case then it would be evidence that its existence is a consequence of the dynamics alone, and not the form of the hop rate.

Using the explicit form of the hop rate $u(n) = 1 + b/n$ and setting $b = 0$, we find

$$J_1 = p(1) \quad (4.4.24)$$

and

$$J_2 = \sum_{n=2}^{\infty} (np(n) - p(n)) = (\rho - 1) - (1 - p(1) - p(0)) , \quad (4.4.25)$$

where $p(n)$ is the steady state probability of an occupancy n . Using (4.4.1), the master equation for $p(0, t)$, we find that

$$v = \frac{p(1)}{p(0)} , \quad (4.4.26)$$

and, from the definition of v (4.4.4),

$$v = 1 - p(0) = S , \quad (4.4.27)$$

where S is the probability that a site is occupied, meaning that

$$p(1) = p(0)(1 - p(0)) . \quad (4.4.28)$$

Now, the steady state relationship between $J_{1,2}$ and ρ becomes

$$\begin{aligned} 0 &= p(0)(1 - p(0))\rho + (\rho - 1)(\rho - (1 - p(0))) \\ &= (1 - S)S\rho + (\rho - 1)(\rho - S)S , \end{aligned} \quad (4.4.29)$$

which can be rearranged to find

$$S^2 - \rho^{-1}S + (1 - \rho) = 0 . \quad (4.4.30)$$

We can use this equation to find solutions for S for different ranges of ρ , with the condition that S lies in the interval $[0, 1]$ because it is a probability, hoping to see evidence of a change of state in the dependence of S on ρ . To do this we define

$$r(S) = S^2 - \rho^{-1}S + (1 - \rho) \quad (4.4.31)$$

and

$$r'(S) = \frac{\partial r(S)}{\partial S} = 2S - \rho^{-1} , \quad (4.4.32)$$

and sketch this function for different values ρ to find solutions $S(\rho)$ for the various cases (see Fig. 4.9).

When $\rho < 1$: $r(0) > 0$, $r'(0) < 0$ and $r(1) < 0$, so the function goes from

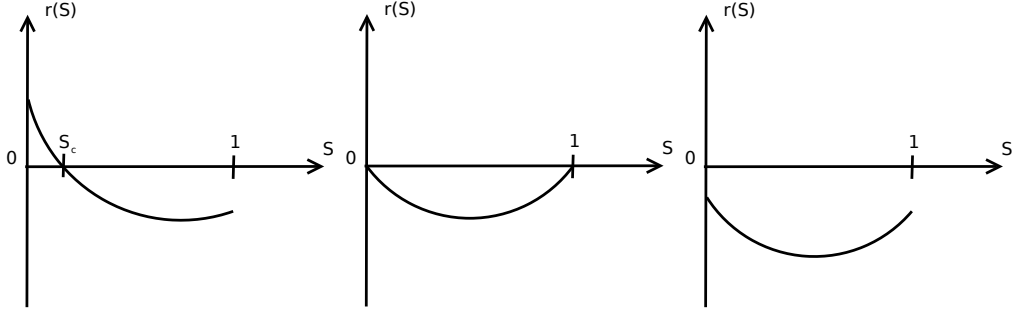


Figure 4.9: Sketches of $r(S)$ against S for: (left) $\rho < 1$; (centre) $\rho = 1$; (right) $\rho > 1$.

positive to negative, crossing the axis once. This means that $r(S)$ has a single root at $S_c(\rho)$ in the interval $(0, 1)$, and thus predicts that the occupation probability $S = S_c$ when $\rho < 1$. When $\rho = 1$, we find simply that $r(S) = S(S - 1)$, which has two roots: $S_c = 0$ or 1 . This suggests a change in the dynamics at $\rho = 1$, but it is not clear exactly what the nature of this change is. $S_c = 0$ implies that none of the sites are occupied, and could indicate that all of the mass has condensed onto a single site. However, $S_c = 1$ indicates that every site is occupied, and because the density $\rho = 1$ this would mean that all sites contain on average 1 particle, which is a very homogeneous state. When $\rho > 1$, $r(s) < 0$ at both $S = 1$ and 0 , so we see there are no solutions in the interval $[0, 1]$. This suggests a transition to a state which is no longer satisfactorily described by the mean-field equations. One could infer from this that perhaps spatial correlations perform a more important role at densities greater than 1, something not taken into account by the mean-field theory.

So, interestingly, when $b = 0$, the mean-field theory does suggest a transition as the density is increased across the critical value ρ_c . This prediction does not quite match up to the measured ρ_c , as detailed in Section 4.3.3, where the critical density $\rho_c(L)$ actually diverges weakly with the system size L , and this is likely to be because of the important role correlations play in the dynamics.

We have already seen that when $b > b_c$ the system enters into a highly ordered state with strong spatial correlations. Even when $b = 0$, one could argue that one expects the local density of particles to be ≤ 1 behind any multiply-occupied sites due to the single unit of mass that remains after a hop, which would be an

example of the kind of spatial correlation one might to expect to influence the dynamics. In the next section we present an improved theory that takes into account some of the spatial structure of the condensed phase.

4.5 Condensate Frame Mean Current Analysis

As is seen from the numerics, the system exhibits a coherent moving structure comprising of a condensate and its tail (Figure 4.5). This is evidence that the occupancies of sites near the condensate are significantly correlated and suggests that the simple Mean-Field Theory from Section 4.4 is therefore unlikely to be able to accurately describe the transition into this highly ordered state as b is increased.

We now construct an approximate theory that does take into account some of the spatial structure of the condensate phase, which we find allows us to estimate the critical value $b_c \simeq 0.62$ at which the transition to a strong condensate occurs. In doing so, we make two main assumptions. First, working in the frame of reference of the condensate by labelling sites $k = 1, 2, 3, \dots$ according to how far *behind* the condensate they are, we assume that almost all of the mass occupies site $k = 0$. In other words, we assume that a strong condensate has formed. Second, we allow the probability distribution for the number of particles n on each site k to take a *different* form, $p_k(n)$, on each site *but*, for the sake of analytical progress, we assume that the occupancies on different sites are uncorrelated.

We distinguish between the dynamics of particles in the tail, and of the condensate itself. When mass is transferred in the tail (either by a single particle hop, or by a backchip), it moves in the *negative k* direction, *towards the condensate*, from $k + 1 \rightarrow k$. This leads to a mass current J_k due to hopping from site k to $k - 1$ given by

$$J_k = u(1)p_k(1) + \sum_{n=1}^{\infty} (n-1)u(n)p_k(n) . \quad (4.5.1)$$

Meanwhile, the condensate hops with rate $\simeq 1$ since its mass is of order N and we consider the limit of large N . In the frame of reference of the condensate, this causes the whole tail to shift its position which is accounted for by relabelling the indices $k \rightarrow k + 1$. Consequently, the *total* average current *arriving at site k* in

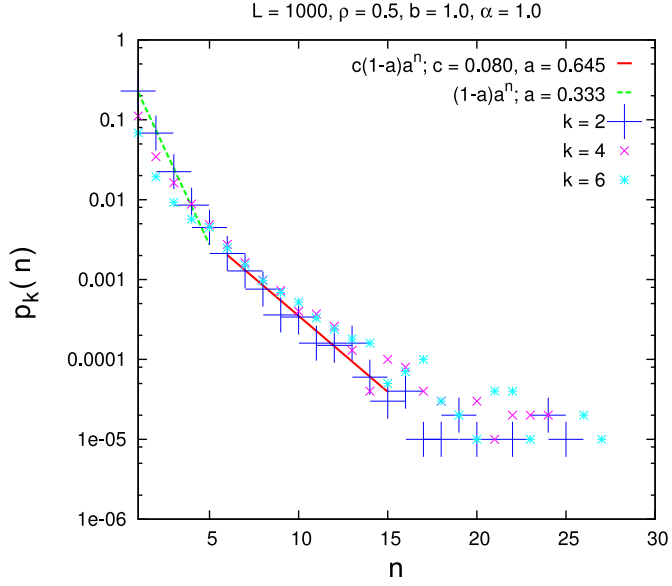


Figure 4.10: Plots of the occupancy distribution $p_k(n)$ at site k behind the condensate ($k = 1, 4, 6$). To the distribution for $k = 2$ (large blue +) we have fitted the function $c(1-a)a^n$ (red solid line) to the middle of the tail, and $(1-a)a^n$ (green dashed line) to the front of the tail. Above $n \sim 15$ the data is too noisy to be fit to reliably. ($\rho = 0.5$, $L = 1000$, $b = 1.0$, $\alpha = 1.0$.)

the *positive k direction i.e.* from site $k - 1$ to k is

$$K_{k-1} = \overline{n_{k-1}} - J_k . \quad (4.5.2)$$

By continuity, the mean occupancy of site k changes with time as

$$\frac{d}{dt} \overline{n_k} = K_{k-1} - K_k . \quad (4.5.3)$$

In the steady state $\frac{d}{dt} \overline{n_k} = 0$, so we find $K_k = K$ for all sites k , which means that (4.5.2) becomes

$$K = \overline{n_{k-1}} - J_k . \quad (4.5.4)$$

Inserting the explicit form (4.2.1) for $u(n)$ (with $\alpha = 1$) into (4.5.1) we obtain

$$\begin{aligned} J_k &= (1+b)p_k(1) + \sum_{n=1}^{\infty} (n-1)(1+bn^{-1})p_k(n) \\ &= (1+b)p_k(1) + \sum_{n=1}^{\infty} np_k(n) + (b-1) \sum_{n=1}^{\infty} p_k(n) - b \sum_{n=1}^{\infty} n^{-1}p_k(n) \\ &= (1+b)p_k(1) + \overline{n_k} + (b-1)(1-p_k(0)) - b\widehat{n_k^{-1}}. \end{aligned} \quad (4.5.5)$$

where

$$\widehat{n_k^{-1}} = \sum_{n=1}^{\infty} \frac{p_k(n)}{n}, \quad (4.5.6)$$

that is, an average of $1/n$ over the part of the distribution where $n \geq 0$. To proceed we must also determine an appropriate form for $p_k(n)$. We have performed some numerical analysis of $p_k(n)$ in the sites immediately preceding the condensate to allow us to make the appropriate choice. As shown in Figure 4.10, we find that it is not easy to fit a simple function to the distribution $p_k(n)$, but to make progress we assume

$$p_k(n) = (1-a_k)a_k^n, \quad (4.5.7)$$

a geometric distribution, which describes the mass in different parts of the tail of the condensate reasonably well (Figure 4.10). This is much easier to work with analytically than other possible assumed distributions as it has the useful property that the parameter a_k can be expressed in terms of the mean occupancy $\overline{n_k}$ at site k as $a_k = \overline{n_k}/(1+\overline{n_k})$. This allows us to express the current (4.5.5) entirely in terms of $\overline{n_k}$ and b , using

$$p_k(0) = \frac{1}{1+\overline{n_k}} \quad (4.5.8)$$

$$p_k(1) = \frac{\overline{n_k}}{(1+\overline{n_k})^2} \quad (4.5.9)$$

$$\widehat{n_k^{-1}} = \frac{\ln(1+\overline{n_k})}{1+\overline{n_k}}. \quad (4.5.10)$$

Inserting these expressions into (4.5.5), we find

$$J_k = \bar{n}_k + \frac{(1+b)\bar{n}_k}{(\bar{n}_k+1)^2} - \frac{(1-b)\bar{n}_k}{(\bar{n}_k+1)} - \frac{b \ln(\bar{n}_k+1)}{(\bar{n}_k+1)}. \quad (4.5.11)$$

Next, we make the continuum approximation $k \rightarrow x$ in (4.5.4) by Taylor expanding \bar{n}_{k-1} about $x = k$ to first order. This leads to the equation

$$\begin{aligned} \frac{\partial \bar{n}}{\partial x} &= \bar{n} - J(\bar{n}) - K \\ &= f(\bar{n}) - K \end{aligned} \quad (4.5.12)$$

where

$$f(\bar{n}) = -\frac{(1+b)\bar{n}}{(\bar{n}+1)^2} + \frac{(1-b)\bar{n}}{(\bar{n}+1)} + \frac{b \ln(\bar{n}+1)}{(\bar{n}+1)}. \quad (4.5.13)$$

The boundary condition is $n_0 = 1$ which comes from the fact that every time the condensate hops it leaves one particle behind. In the continuum limit, this boundary condition becomes $\bar{n}(0) = 1$.

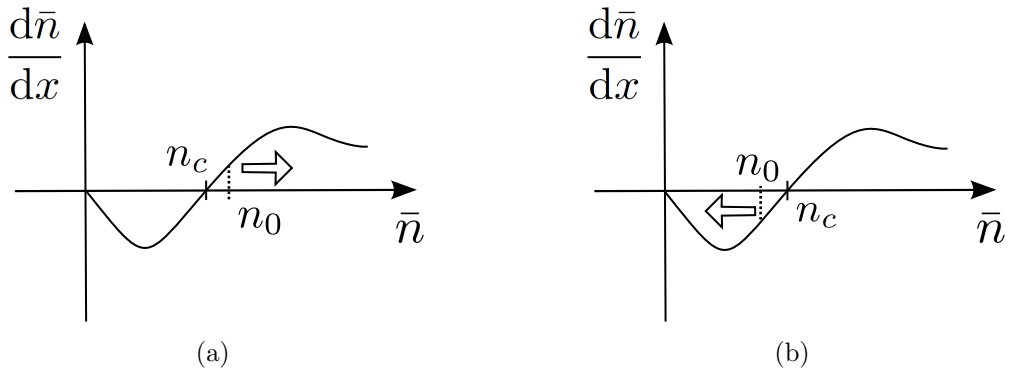


Figure 4.11: Using the boundary condition $\bar{n}(x = 0) = n_0 = 1$ we see graphically that (a) if $n_c < n_0$ then as x increases, as we move further away from the condensate, so too does \bar{n} . It does so indefinitely, resulting in an infinite mean occupancy infinitely far from the condensate. (b) If $n_c > n_0$, then we see that as x increases, $\bar{n}(x)$ decreases to 0.

For the case of the strong condensate, there is no mass at $x \rightarrow \infty$ which means that $K = 0$ and therefore that $\frac{\partial \bar{n}}{\partial x} = f(\bar{n})$. The form of $f(\bar{n})$ is illustrated in Figure 4.11. We note the limits $f(0) = 0$ and $f(\bar{n}) \rightarrow 1 - b$ for $\bar{n} \rightarrow \infty$. We also observe that there is an unstable fixed point at n_c , the non-zero root of $f(\bar{n})$, at which $\frac{d\bar{n}}{dx} = 0$. As illustrated in Figure 4.11, the value of n_c relative to

the boundary condition $n_0 = 1$ will iteratively determine the values of $\bar{n}(x)$ at successively larger x .

If $n_c < n_0$ (Figure 4.11(a)) then $\frac{d\bar{n}}{dx} > 0$ for all $\bar{n} > n_c$. This means that \bar{n} will increase indefinitely as x increases, resulting in an infinite mean occupancy far from the condensate. This contradicts the assumption that there is no mass as $x \rightarrow \infty$ and therefore we discard this solution as unphysical.

If $n_c > n_0$ (Figure 4.11(b)) then the gradient of \bar{n} is negative, and it remains negative up to the stable fixed point at $\bar{n} = 0$. This means that successively further from the condensate \bar{n} decreases continuously to 0. This is the physical solution. The consistency condition for this solution gives us a condition for the existence of the strong condensate: $n_c > n_0 = 1$. This can be translated into a condition on b by using the fact that $f(n_c) = 0$. Substituting $\bar{n} = n_0 = 1$ into (4.5.13) and setting the resulting expression to zero, we find an equation for the critical value $b = b_c$,

$$-\frac{1+b_c}{4} + \frac{1-b_c}{2} + \frac{b_c \ln 2}{2} = 0 , \quad (4.5.14)$$

such that we have a strong condensate for $b > b_c$. From this, we find

$$b_c = \frac{1}{3 - 2 \ln 2} \simeq 0.62 . \quad (4.5.15)$$

This prediction for b_c agrees fairly well with the numerical results displayed in Figure 4.15 and Figure 4.16. In that figure the sample variance $\sigma^2 = \sum_i \overline{(n_i/N - \rho)^2}$ of the occupancy per particle n/N is plotted against b and shown to increase sharply from $\sigma \simeq 0$ to $\sigma \simeq 1$ at a value of $b \simeq 0.5$. This corresponds to the transition from the fluid, in which the mass is evenly distributed and the sample variance is small, to the strong condensate phase in which the sample variance approaches 1. This transition point appears to be independent of ρ and sharpens as the system size increases.

4.5.1 Generalisation to any Real, Positive α

In the ZRP, the transition to the condensate phase was found with the generic hop rate $u(n) = 1 + b/n^\alpha$ (see (4.2.1)) only for $\alpha \leq 1$. In the model here, we find that the transition to a strong condensate phase is present for all $\alpha > 0$. We

can repeat the previous calculation, which had $\alpha = 1$, with $\alpha > 0$ to find and expression for $b_c(\alpha)$.

First, similarly to (4.5.5), we find

$$\begin{aligned} J_k &= (1+b)p_k(1) + \sum_{n=1}^{\infty} (n-1) \left(1 + \frac{b}{n^\alpha}\right) p_k(n) \\ &= (1+b)p_k(1) + \bar{n}_k - (1-p_k(0)) + b \sum_{n=1}^{\infty} n^{1-\alpha} p_k(n) - b \sum_{n=1}^{\infty} n^{-\alpha} p_k(n) \end{aligned} \quad (4.5.16)$$

Again, we assume a geometric distribution $p_k(n) = (1-a_k)a_k^n$, as given by (4.5.7), and the associated properties

$$\begin{aligned} a_k &= \frac{\bar{n}_k}{1+\bar{n}_k}, \\ p_k(0) &= \frac{1}{1+\bar{n}_k}, \\ p_k(1) &= \frac{\bar{n}_k}{(1+\bar{n}_k)^2}, \end{aligned} \quad (4.5.17)$$

to write

$$\begin{aligned} J_k &= \bar{n}_k - 1 + \frac{(1+b)\bar{n}_k}{(1+\bar{n}_k)^2} + \frac{1}{(1+\bar{n}_k)} \\ &\quad + \frac{b}{(1+\bar{n}_k)} \sum_{n=1}^{\infty} n^{1-\alpha} a_k^n - \frac{b}{1+\bar{n}_k} \sum_{n=1}^{\infty} n^{-\alpha} a_k^n. \end{aligned} \quad (4.5.18)$$

Now we use the definition of the polylogarithm function

$$\text{Li}_s(z) = \sum_{n=1}^{\infty} \frac{z^n}{n^s}, \quad (4.5.19)$$

to find

$$\begin{aligned} J_k &= \bar{n}_k - 1 + \frac{(1+b)\bar{n}_k}{(\bar{n}_k+1)^2} + \frac{1}{(\bar{n}_k+1)} \\ &\quad + \frac{b}{(\bar{n}_k+1)} \left[\text{Li}_{\alpha-1} \left(\frac{\bar{n}_k}{\bar{n}_k+1} \right) - \text{Li}_\alpha \left(\frac{\bar{n}_k}{\bar{n}_k+1} \right) \right]. \end{aligned} \quad (4.5.20)$$

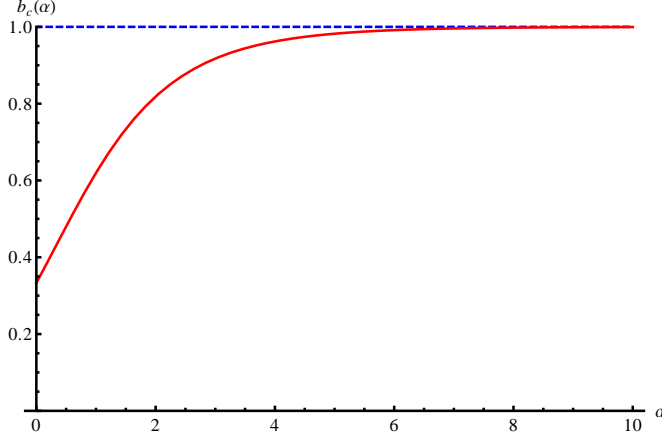


Figure 4.12: A plot of $b_c(\alpha)$ (red, solid). b_c increases monotonically from $b_c(0) = 1/3$ and asymptotically approaches $b_c = 1$ (blue, dashed).

By making the same continuum approximation as before (4.5.12) we obtain

$$\begin{aligned} f(\bar{n}) &= 1 - \frac{(2+b)}{(\bar{n}+1)} + \frac{(1+b)}{(\bar{n}+1)^2} \\ &\quad - \frac{b}{(\bar{n}+1)} \left[\text{Li}_{\alpha-1} \left(\frac{\bar{n}}{\bar{n}+1} \right) - \text{Li}_\alpha \left(\frac{\bar{n}}{\bar{n}+1} \right) \right]. \end{aligned} \quad (4.5.21)$$

Finally, using the boundary condition $\bar{n}(0) = 1$ and the constraint on the stable fixed point $n_c(b, \alpha)$, we obtain

$$b_c(\alpha) = \left[1 + 2 \left(\text{Li}_{\alpha-1} \left(\frac{1}{2} \right) - \text{Li}_\alpha \left(\frac{1}{2} \right) \right) \right]^{-1}, \quad (4.5.22)$$

which increases monotonically from $b_c(0) = \frac{1}{3}$ and is bounded from above by 1 (Figure 4.12).

It is important to note that (4.5.22) holds for $\alpha > 0$ and the point $\alpha = 0$ is singular, because for $\alpha > 0$ the condensate moves with rate 1 whereas for $\alpha = 0$ all masses, including any condensate, move with rate $1 + b$. Thus at $\alpha = 0$ the mechanism for the maintenance of a moving condensate is no longer valid, as there is no reason small masses would tend to catch up to large masses ahead. This is confirmed by the simulation results, shown in Figure 4.13(a), for $\alpha = 0$. Measuring the variance of the mass distribution we see no evidence of a condensate forming above a certain value of b .

On the other hand, we can probe the validity of (4.5.22) as $\alpha \searrow 0$ by

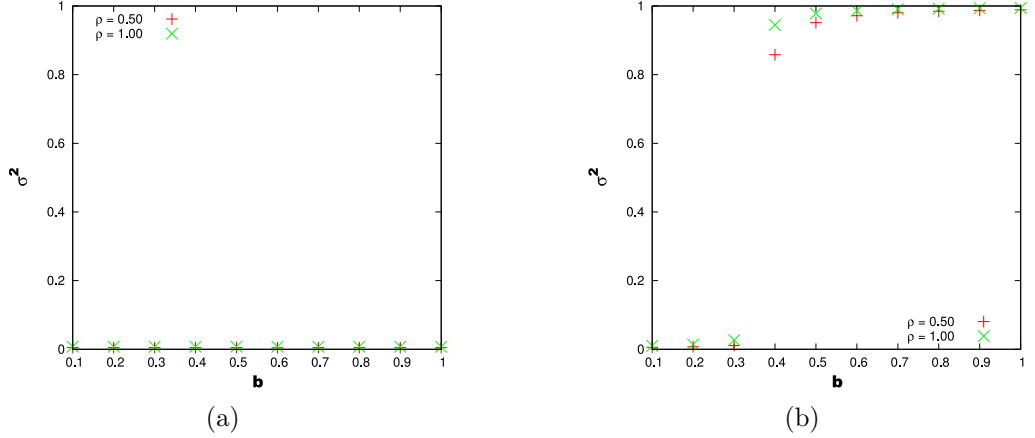


Figure 4.13: Plots of σ^2 against b ($L = 1000$). (a) With $\alpha = 0$ all masses move with the same rate and no transition is observed in b . (b) Using the modified hop rate $u_{log}(n)$ given in (4.5.23) we can probe $b_c(\alpha)$ as $\alpha \searrow 0$. A transition occurs when b is in between 0.3 and 0.4, in good agreement with the prediction $b_c(\alpha = 0) = 1/3$ from (4.5.22).

simulating the dynamics with the modified hop rate

$$u_{log}(n) = 1 + \frac{b}{\ln(n+1)}. \quad (4.5.23)$$

As $\ln n$ increases more slowly than any power of n we can consider (4.5.23) as approximating the limit of an arbitrarily small, positive choice of α . The results from the simulations with $u_{log}(n)$ presented in Figure 4.13(b) show that there is a transition to the strong condensate phase in the region $b \sim 0.3 - 0.4$, which gives us yet more confidence in the analytic result (4.5.22).

We have also performed simulations at α values larger than 1 (Figure 4.14). We find that the transition becomes more gradual for larger values of α , and occurs over a region of values of b which are larger than the value of b_c predicted by (4.5.22). By studying various system sizes (Figure 4.14(c)) we see that evidence that the gradual nature of the transition is a finite size effect, as it becomes more sharp when we increase the system size. The hop rate $u(1) = 1 + b$ for all α , but for large α the hop rate from sites with low occupancies (greater than 1) is reduced significantly. This has the effect of suppressing the existence of single occupancy sites because single units of mass always catch up with a site ahead of mass greater than one, in the same way that the condensate is maintained. We note that although the prediction for b_c seems to agree well with simulations

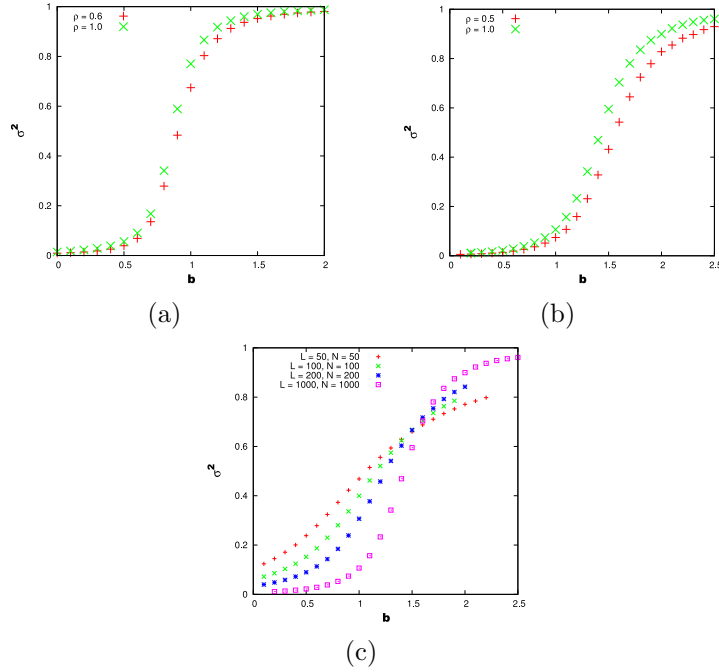


Figure 4.14: Plot of σ^2 against b for (a) $\alpha = 2$ ($L = 500$) and (b) $\alpha = 10$ ($L = 1000$). The transition becomes less sharp as α is increased, and takes place over a range of values of b which are greater than the b_c predicted by (4.5.22). The formula (4.5.22) predicts that $b_c(\alpha = 2) = 0.8185$ and $b_c(\alpha = 10) = 0.9995$. (c) At $\alpha = 10$ the transition becomes sharper as L is increased, which is evidence that its gradual nature is a finite size effect. We can estimate $b_c \sim 1.6 \pm 0.1$ from the crossover of the curves.

for $\alpha = 0$ and $\alpha = 1$, for larger α , b_c appears to overshoot the asymptote $b_c = 1$ predicted by the approximate theory.

4.6 Classification of the Strong Condensate Phase Transition

To learn more about the critical value b_c and the nature of the transition we analyse data from different system sizes L at the same density $\rho = 0.5$. First, by studying a plot of the order parameter σ against b for this data in Figure 4.15, we see the transition occurs over a similar range of b for all system sizes L . Furthermore, the transition sharpens with increasing system size and there is a stable intersection of the curves at $b = 0.5$. This strongly suggests that in the thermodynamic limit the transition would be discontinuous in σ at $b_c = 0.5$.

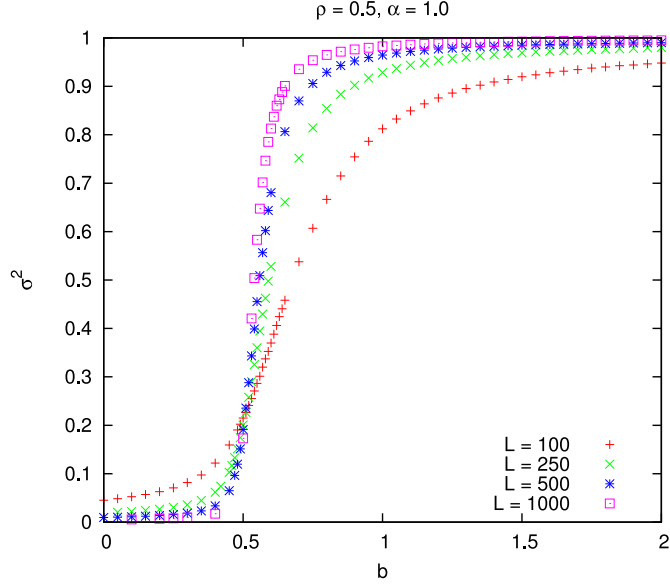


Figure 4.15: Plot of σ^2 against b , for various L with $\rho = 0.5$. A transition is seen to occur for all system sizes, with a clear crossover point in the σ^2 - b curves at $b = 0.5$, which is indicative of the critical value $b_c = 0.5$.

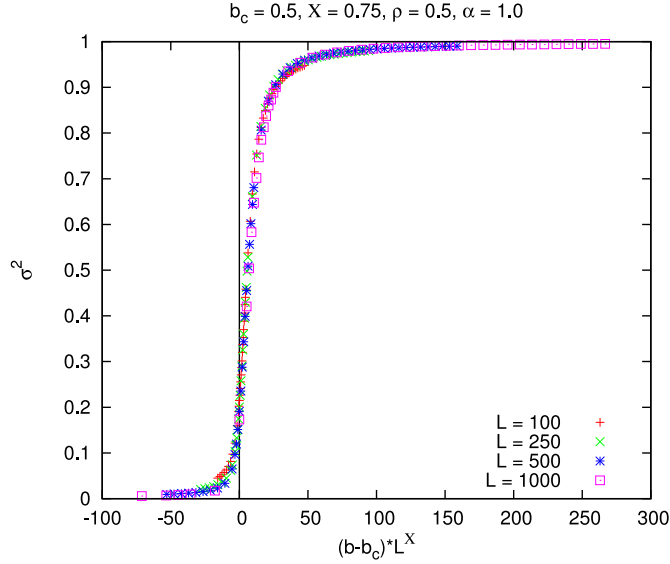


Figure 4.16: Plot of σ^2 against b , for various L with $\rho = 0.5$. We perform a finite size scaling procedure on b , rescaling it to $(b - b_c)L^X$. The choice of parameters for the best collapse of the data onto a single curve is $b_c = 0.5$ and $X = 0.75$.

Our confidence in the measurement of b_c is reinforced by the result of applying a finite size scaling procedure to the same data, as shown in Figure 4.16. We plot the order parameter σ against a rescaled hop rate parameter $b' = L^X(b - b_c)$ and,

through the choice of b_c and X , find the best data collapse when $b_c = 0.5$, and the scaling exponent $X = 0.75$.

In future we could learn try to learn more about the transition by analysing the Binder cumulant [18]

$$U_4 = 1 - \frac{\langle n^4 \rangle}{3\langle n^2 \rangle^2}, \quad (4.6.1)$$

where $\langle n^i \rangle$ is the i -th moment of the occupancy n . A more sophisticated estimate for the critical value of b_c could be obtained by measuring the crossover of U_4 plotted against b at different system sizes L .

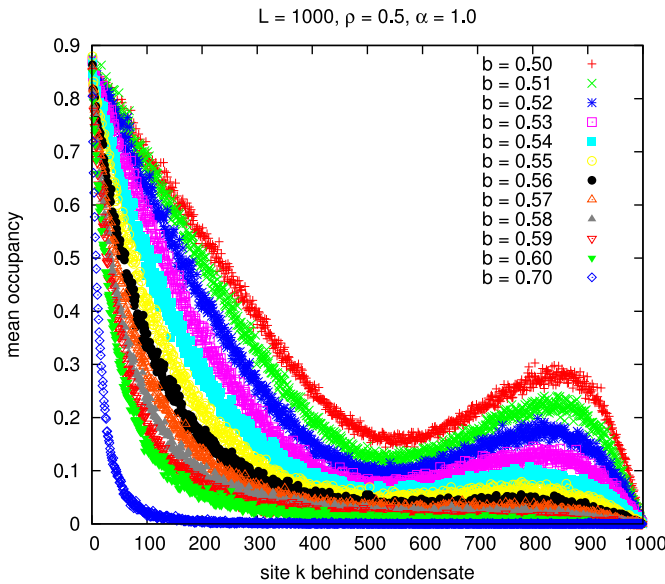


Figure 4.17: A plot of the mean occupancy at a site k behind the condensate site, measured numerically. The decay length in the region $0 < k < 500$ can be seen to slowly increase as $b \searrow 0.5$.

Looking at the distribution of mass at a site k behind the condensate (Figure 4.17) one can see that there is a decay length associated with the average shape of the tail of mass behind, which increases as $b \searrow 0.5$. To better understand how this decay length changes as the b approaches the (numerical) critical value b_c from above, we fit an exponential distribution to the tail at different values of b , and then plot the dependence of the fitted decay length λ on b .

As shown in Figure 4.18 the decay length λ appears to diverge like a power law with exponent $\nu \simeq 1.69$ as $b \searrow 0.5$ before beginning to flatten off as $b - 0.5$ becomes very small. We attribute this flattening off effect to the finite system size:

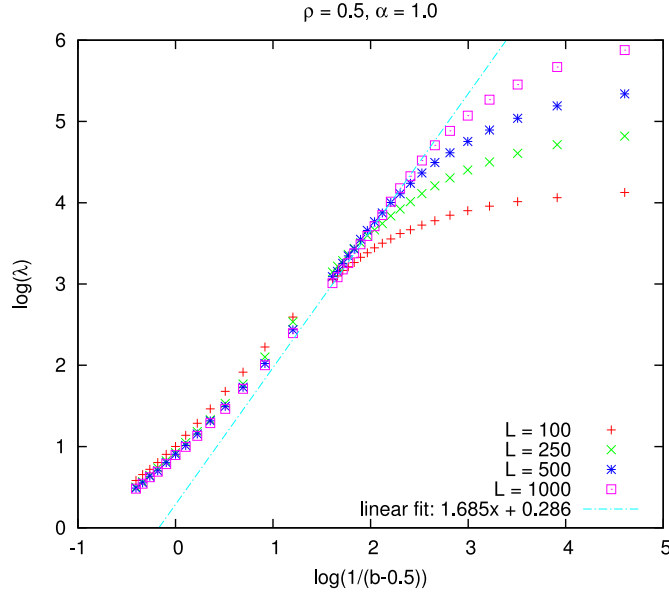


Figure 4.18: The decay length $\lambda(b)$ measured from the tails in Figure 4.17 fits a power law in the scaling regime but flattens out as $b \searrow 0.5$. Numerically, the system size only affects the b dependence of $\lambda(b)$ as b approaches 0.5. As L is increased $\lambda(b)$ becomes closer to the power law at $b \searrow 0.5$.

in Figure 4.17 it is clear that as $b \searrow 0.5$ the tails develop some additional structure far from the condensate (in the region $500 < k < 1000$), and in Figure 4.18 the data points move closer to the power law fit as the system size is increased in such a way that we expect the infinite system would show the power law divergence without the flattening out effect.

A diverging length scale of this nature is a characteristic of continuous phase transitions, seemingly at odds with the early evidence for the transition being first-order in nature. The resolution is to conclude that the phase transition here exhibits the characteristics of a *mixed order* or *hybrid* phase transition. Transitions of this nature are not unprecedented, for example, in [10, 11] mixed order transitions in long range lattice models are considered. In another example a phase transition in the size of the giant viable cluster of a multiplex network, is shown to be discontinuous in the order parameter but also to exhibit critical behaviour above the critical point [14]. This asymmetry is attributed to the specifics of the dynamics, which only provide a mechanism for critical behaviour above the critical point and not below.

I speculate that the mixed order transition in the present work may also be

attributed to the difference in mechanisms above and below the transition: from above, the transition is brought about by the divergence of a length scale in a coherent structure, namely the tail; from below we see no coherent structures until the condensate itself is formed.

4.6.1 Connection to the Driven Asymmetric Contact Process (DACP)

Another interesting observation is that the critical exponent here is measured to be approximately 1.69, which is similar to the value $\nu_{\parallel} = 1.7338$ (see (2.2.6) in Section 2.2.3) of the numerically measured critical exponent associated with the temporal correlation length in directed percolation (DP) [80]. Similarities can be seen between the dynamics of the mass in the tail in the frame of reference of the condensate and the dynamics of the driven asymmetric contact process (DACP) which exhibits a phase transition in the DP universality class, specifically with the temporal exponent measured at 1.7(2) [43].

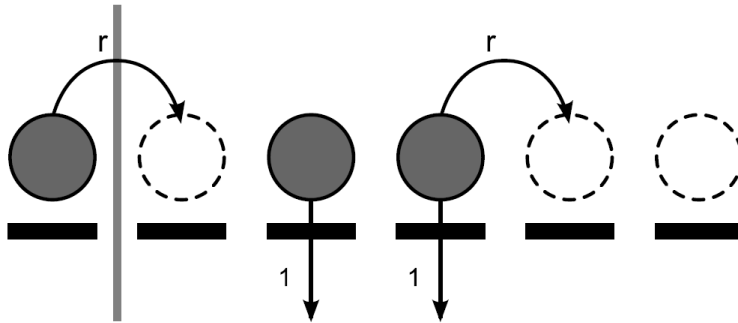


Figure 4.19: (Reproduced from [43]) A schematic diagram of the DACP. The first site is always active. Active sites become inactive with rate 1, or activate the site to their right with rate r .

Similarly to Directed Percolation, described in Section 2.2.3, the DACP is a one-dimensional lattice model of active and inactive sites, as shown in Figure 4.19. The first site, at the left end of the lattice, is kept active throughout. Active sites can either become inactive with rate 1, or they can activate the site to their right with rate r .

If one considers the dynamics of the system in the frame of the strong condensate, one can identify dynamical similarities. The condensate is similar

to the always-active boundary site, ‘activating’ the next site along, by putting some mass that itself can hop on it, at a constant rate. Sites further and further away become activated as the condensate makes successive moves. The backchip process generates new singly-occupied sites which themselves can become ‘inactive’ by recombining with other occupied sites, leaving a vacant site behind.

Interestingly the mapping between the two is not exact, even though there is some similarity in the temporal exponent. It may be of interest to investigate the similarities and differences between the models and the consequences for the exponents in greater depth in the future.

4.6.2 Divergence in the approximate theory

To see whether the approximate theory of section Section 4.5 also captures the existence of a mixed order transition I numerically integrated (4.5.13) in order to measure how a length scale in the profile of the solution for $n(x)$ changes as $b \searrow b_c$. To do this, I measured the distance from $x = 0$ to the point at which the gradient $d\bar{n}(x)/dx$ had the greatest magnitude, as this was the most prominent, well-defined feature of $n(x)$.

In contrast to the results from simulation (Figure 4.18), we find (Figure 4.21) that according to the theory the length scale $\lambda(b)$ of the tail diverges as

$$\lambda(b) \sim \log \left(\frac{1}{b - b_c} \right). \quad (4.6.2)$$

The divergence is still indicative of a mixed-order transition, but it points to one which has a weakly diverging length scale.

This can also be seen in the approximate theory by studying the mass in the tail very close to the condensate. By considering $\epsilon = b - b_c \ll 1$ and $\eta = n_0 - \bar{n} = 1 - \bar{n} \ll 1$ we can make a Taylor expansion of $f(\bar{n}, b)$ given in (4.5.13), to find

$$f(1 - \eta, b_c + \epsilon) = f(1, b_c) - A\epsilon - B\eta + \mathcal{O}(\eta^2, \epsilon^2, \epsilon\eta), \quad (4.6.3)$$

where

$$A = \frac{1}{4b_c}, \quad B = \frac{1 - b_c \ln 2}{4}, \quad \text{and} \quad f(1, b_c) = 0. \quad (4.6.4)$$

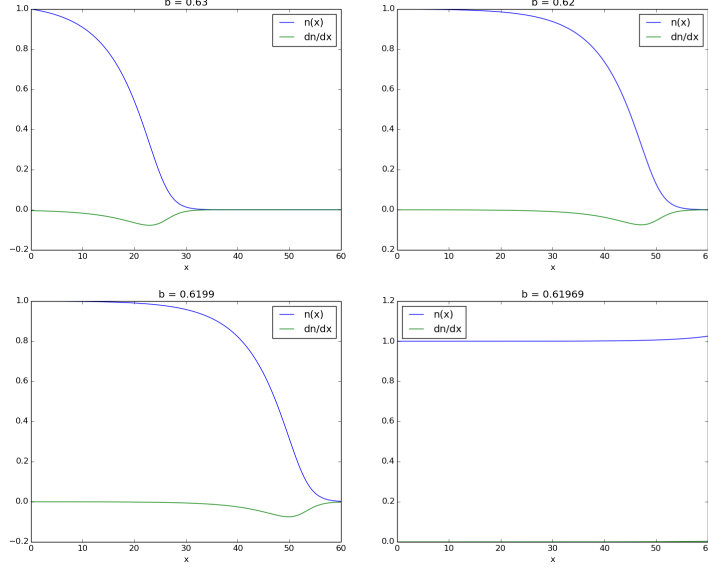


Figure 4.20: Plots of $\bar{n}(x)$, and its gradient, from the mean-field theory of Section 4.5 at different values of b . To see if it predicts a diverging length scale, I measured the distance from the origin at which the gradient of $\bar{n}(x)$ had the largest magnitude. We can see that this distance continually increases as $b \searrow b_c \simeq 0.619692$, and the function diverges when $b < b_c$.

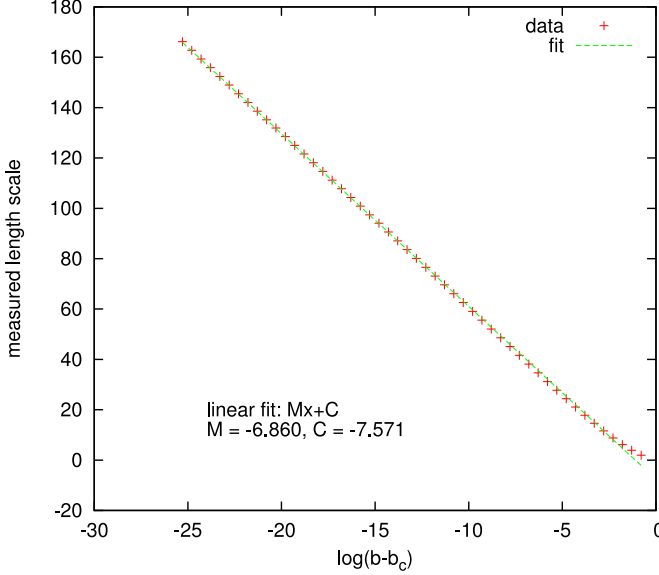


Figure 4.21: By numerically integrating (4.5.13) we measure a length scale in the tail to diverge logarithmically as $b \searrow b_c$.

Using the relationship $f(\bar{n}, b) = d\bar{n}(x)/dx$ we can then write

$$\frac{d\eta}{dx} = A\epsilon + B\eta \quad (4.6.5)$$

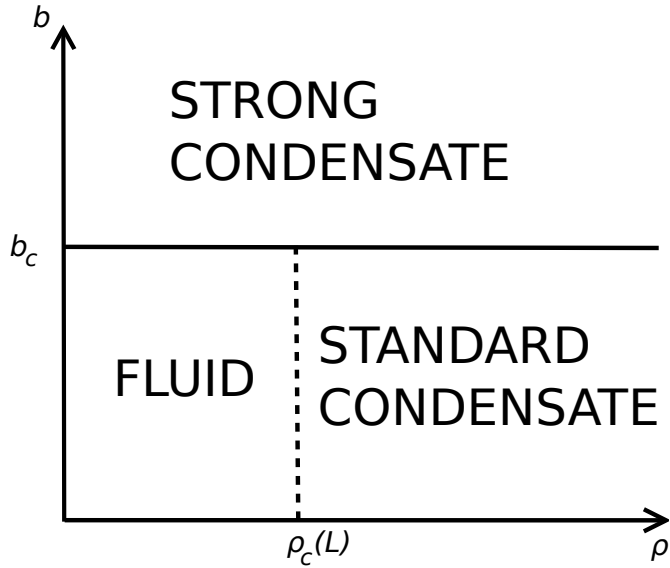


Figure 4.22: A sketch of the phase diagram for our system. Above the value b_c , the system exhibits a strong condensate phase. Below b_c and for low densities the system exists in a fluid phase. Above a certain value ρ_c , the system exhibits the characteristics of a standard condensate phase, but this critical density diverges as $L \rightarrow \infty$.

and integrate to find

$$\eta(x) = \frac{A}{B} \epsilon (e^{Bx} - 1). \quad (4.6.6)$$

A characteristic length scale λ can then be defined by the value of x at which η reaches some arbitrary finite value, yielding $\frac{A}{B} \epsilon e^{B\lambda} = \text{constant}$. Thus

$$\lambda(\epsilon) = \frac{|\ln \epsilon|}{B} + \text{constant} \quad (4.6.7)$$

So we see that as $\epsilon \searrow \frac{B\eta}{A}$, the characteristic length scale λ diverges slowly as a logarithm.

4.7 Discussion and Conclusions

The hopping dynamics with the ‘backchip’ processes that I have studied in this chapter give rise to a system with an interesting phase diagram in terms of the hop rate b and the particle density ρ , which is shown in Figure 4.22. For hop rates greater than a critical value $b_c \simeq 0.62$, and at *all* densities ρ , one sees a

strong condensate phase. Below b_c , there is a fluid phase. When the density is higher than a critical value ρ_c , evidence of a condensate phase, similar to that seen in the ZRP, is observed. However, I show that the critical density ρ_c actually diverges with the system size L , and so in the infinite system, one would see only the two phases: strong condensate and fluid.

The key feature is a strong condensate phase in which the condensate and its short tail of trailing particles move together through the system. This phase is present at all densities ρ when the parameter b in the hopping rate $u(n) = 1 + b/n^\alpha$ is greater than a critical value b_c , which appears to be independent of the density. Numerically I have measured $b_c = 0.5$ for the case $\alpha = 1$, which is in fairly good agreement with the value $b_c \simeq 0.62$ found using the condensate frame analysis of section 4. I classify the transition as being mixed order as it exhibits a discontinuity in the order parameter σ^2 , which is indicative of a 1st order phase transition, as well as a diverging length scale, in this case the decay length of the tail of the condensate, which is a characteristic of a 2nd order transition.

The results also show a number of additional interesting features of the condensate phase. First, the condensate and its tail comprise a coherent object that moves throughout the system, and the stability of the condensate lies in the dynamics of the vanishingly small fraction of particles in the tail. Once a few particles are left behind through backchipping they quickly rejoin the condensate. This picture is substantiated by the theory of section 4 which demonstrates that the tail of a moving strong condensate necessarily decays quickly to zero for b greater than a critical value b_c . Second, by extending the analysis to values of $\alpha \neq 1$ in (4.2.1), I find that the strong condensation phenomenon is generically present for any $\alpha > 0$. As illustrated in Figure 4.12 the function $b_c(\alpha)$ increases monotonically from $b_c(0) = 1/3$ and asymptotically approaches 1 as $\alpha \rightarrow \infty$. We recall that in the standard ZRP, condensation is present only for $\alpha < 1$. Simulation results confirm the existence of the strong condensate for $\alpha > 1$, although the approximate theory appears to underestimate the transition point.

Below the critical b_c , we see behaviour more reminiscent of the standard ZRP, in which there is an apparent transition from a fluid phase at low density, to a standard condensate phase above a critical value of ρ . However we see numerically that this critical value $\rho_c \sim \ln(L)$ as $L \rightarrow \infty$, in a similar way to that observed

in [140]. Here, the condensate is not a true feature of the system in the large L limit, but rather a finite size effect. This suggests that systems in which aggregates diffuse and chip, the most relevant quantity in determining whether condensation occurs is the rate of decay of the chip rate with the aggregate size.

Interestingly, I also find that a simple mean-field theory, which neglects spatial structure, predicts that the dynamical rules (a single particle hops from a singly occupied site and all but one of the particles hop from a multiply occupied site) alone are enough to induce a transition between a homogeneous and inhomogeneous state, as the density is increased. In fact, the upper bound of 1 on the critical density in this case is entirely a consequence of the fact that a single unit of mass is left behind, when a large mass hops. The importance of the amount of mass left behind also plays an important role in the condensate frame analysis of currents in the tail. The boundary condition $\overline{n(0)} = 1$ is a direct consequence of the fact that a single unit remains after a hop, which in turn is directly determines the value of b_c .

To understand the role of the mass left behind and the interaction between these dynamical processes better, it would be interesting to study a generalisation of this model where $n - a$ particles hop in unison for $n > a$ and a single particle hops for $n \leq a$. We have shown here that in the case $a = 1$ a strong condensate forms and travels through the system, with its structure maintained by the effects of hops from its tail. On the other hand the case $a = N$ yields the ZRP, where only one particle may hop at a time and a condensation occurs for sufficiently large choice of b , but with a static condensate. It would then be interesting to ask how a should scale with N for one to observe a moving, as opposed to static, condensate and at what speed it would travel.

Chapter 5

A Membrane-Interface Model for Lamellipodia Growth

5.1 Introduction

Directional motility is a fundamental and ubiquitous cellular process, the origin of which can be dated to more than 1 billion years ago [139]. The *lamellipodium* is a cytoskeletal network of filaments of polymeric actin, a multifunctional protein molecule found in almost all eukaryotic cells, which plays a crucial role in cell motility. Polymerisation at the ‘front’ and depolymerisation at the rear of the filament causes it to ‘treadmill’ in the forward direction, and as many of these filaments treadmill towards the cell membrane their leading edge pushes it forwards and as such the whole cell can move.

It has been found that this kind of motility is actually an autonomous property of the leading lamellipodium [51, 170] and in this chapter I present a simple membrane-interface (MI) model for this motile structure without any cellular details. The model, which will be described in detail in Section 5.2, essentially consists of a rigid wall, representing the cell membrane or boundary, which diffuses in one-dimension in the presence of a one-dimensional growing interface, representing the edge of the lamellipodium.

From the point of view of statistical physics, my primary interest is how the characteristics of the growing interface are modified through the interaction with a diffusing wall. The characteristic I give most attention to is the scaling of the interface width, which one can compare with the EW and KPZ universality

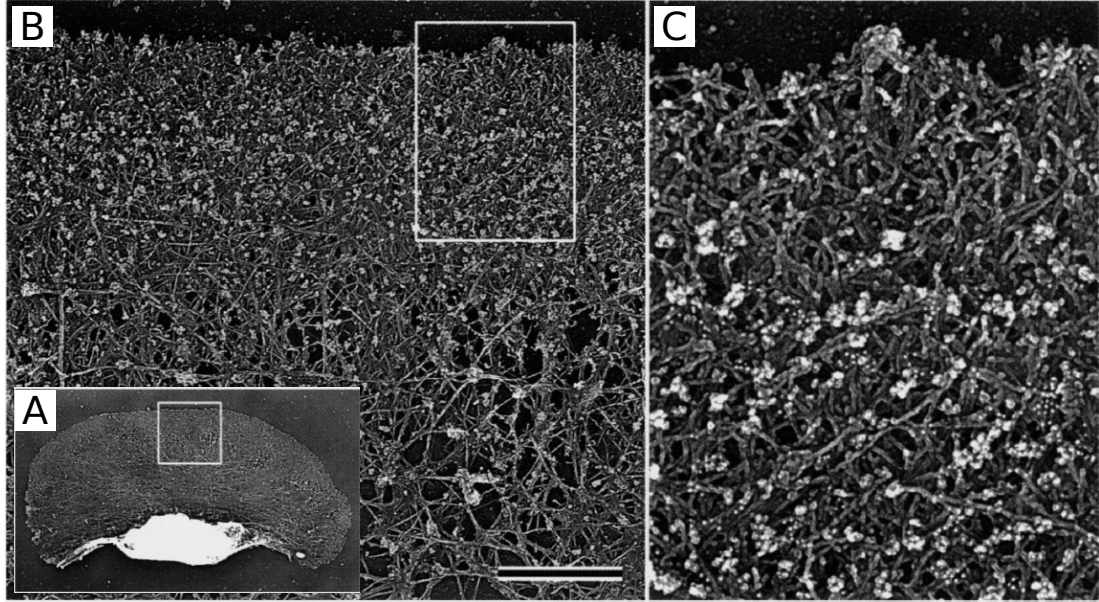


Figure 5.1: (Reproduced from [161]) **A:** A *Xenopus* keratocyte cell, moving in the upwards direction. The box highlights a section of the leading lamellipodium, which is expanded and shown in B. **B:** An image of the actin filaments in the leading lamellipodium. The top surface of the filamentous region has some rough structure. The arrangement of the filaments in the bulk appears disordered and shows different characteristics at different distances from the surface. **C:** An enlarged view of the box in B. At the surface the arrangement of filament tips appears to lack order.

classes described in Section 2.6. In particular I investigate how its properties are affected by different biases in the diffusion of the wall, which are directly comparable to the effect of forces at the cell membrane. A bias in the diffusion of the cell membrane towards the interface represents a load force, for example a surface tension, on the membrane which is of particular interest in studies of cell motility. I also look at bias *away* from the membrane. This is comparable to the effect of pulling the cell membrane away from the body of the cell, which is a less well studied phenomenon. From a biophysical perspective I am interested to learn how the applied force, or the bias in this model, affects the velocity of the membrane.

The construction of the MI model is motivated by observations and measurements of the physical structure of the lamellipodium itself (see Figure 5.1). The lamellipodium in motile cells is a thin, flat protrusion, 0.1-0.2 μm deep,

consisting of a high density of filaments of polymeric actin, with $100/\mu\text{m}$ of the leading edge [1]. Actin itself is the most abundant protein in most eukaryotic cells, and in the lamellipodium the filaments it forms are double helical and, importantly, molecularly polarised. The globular actin subunits have what are known as their ‘barbed’ and ‘pointed’ ends, from which polymerisation and growth is favoured at the barbed end and depolymerisation is favoured at the pointed end [139]. In the cell, these polymeric actin filaments are found to orient themselves with the barbed ends pointed outwards, towards the cell membrane [158]. In the lamellipodium the filaments form a dense array of short, branched filaments [161, 162] that are not uniformly perpendicular to the cell membrane but instead are distributed over a range of angles, typically around 35° to the normal of the leading edge [118]. This dense structure with cross-linking between different filaments gives the lamellipodium sufficient mechanical strength such that polymerisation pushes the leading edge forward rather than the filament backwards.

These are the structural properties of the lamellipodium that provide the basis for the core features of the model. The lamellipodium is essentially flat and grows in one dimension and so I construct a one-dimensional model. The asymmetry in the filaments and their polymerisation properties forms the basis for directional growth in the interface, and surface tension at the membrane, an important factor in lamellipodium motility [142], combined with thermal fluctuations leads us model it as wall which undergoes a biased random walk.

I choose to model the growth of the lamellipodium with just an interface rather than trying to represent its internal structure because of the wide array of complicated features of its interior (see Figure 5.2). For instance, a new filament can branch off from an existing filament starting from some way down its length [130, 162] and capping proteins bind to the barbed ends, preventing further association or dissociation of subunits [40] (with a half time of about 1 s [152]). Also further away from the leading edge are filaments which are observed to be longer and unbranched, as opposed to the short branched filaments seen nearer [158]. As the cell moves, existing short branched filaments which are left behind are ‘remodelled’ to be longer and unbranched, and the dissociated monomers recycled for further growth [139]. My view is that all of this complex internal structure only becomes relevant for cell motility in the effect it has on the

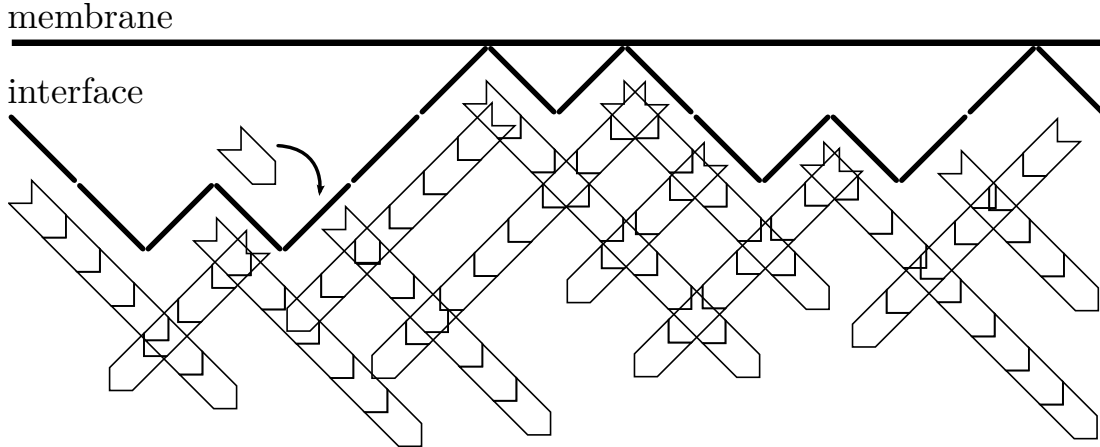


Figure 5.2: The leading edge of the messy network of actin filaments in the lamellipodium is modelled using an interface, which grows up against a diffusing, infinite, solid wall, which represents the cell membrane. Absorption of an actin monomer by a filament is represented by the growth of a single point on the interface towards the membrane.

structure of the leading edge of the lamellipodium, which is the part that *ratchets* the membrane to cause motility, and so I assume that the structure of the edge can be described by a generic interface of the type discussed in Section 2.6. As an aside, to my knowledge no one has yet measured the structural properties of the leading edge of the lamellipodium, as shown in Figure 5.1, and it would be of great interest to learn whether it shares properties with the KPZ or DP universality classes, or with a different or new class altogether.

The ratcheting mechanism for motility was first proposed by Peskin *et al.* in an effective model for the mechanism by which a single actin filament can push against a membrane, known as the *Brownian Ratchet* [136] (Figure 5.3). In this model the filament polymerises towards the membrane, but once it comes closer than the length of a single monomer, no further polymerisation can occur until the membrane diffuses far enough away that there is enough space for another monomer to join on. Importantly, it also showed that the ratcheting effect exists when there is a load force on the membrane against the direction of motion, the sort of which is caused by the surface tension at the membrane of the cell.

This model, the first to show how Brownian motion could be ‘rectified’ to generate unidirectional, propulsive forces, spawned a great deal of further research

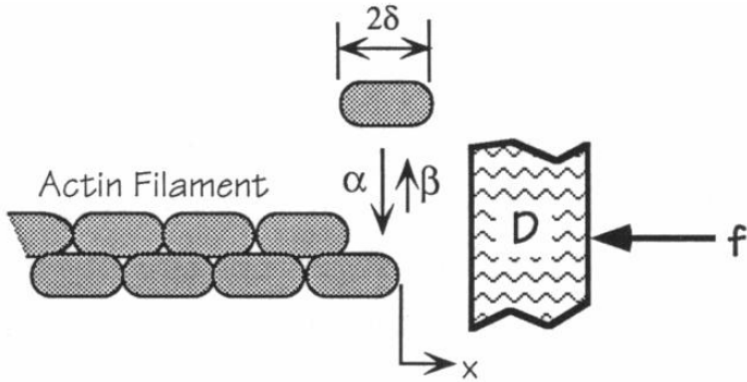


Figure 5.3: (Reproduced from [136]) A schematic diagram of the Brownian Ratchet, as presented in Ref [136]. A particle diffuses in one-dimension with diffusion constant D , under the influence of an external load force f . If the particle diffuses a distance δ or greater away from the tip of the actin filament, there is space for an actin monomer to be adsorbed, which occurs with rate α . With rate β an actin monomer can desorb from the tip, which can occur regardless of the position of the particle.

into Brownian Ratchet models for propulsive forces. The model has subsequently been built upon to include thermal fluctuations in the filament itself, to try to better account for experimental measurements of cell motility [122, 123], and also to include effect of attachment or ‘tethering’ between the filament and the diffusive object it ratchets [123, 179].

As discussed above, in the specific case of lamellipodia the cell membrane is not pushed by a single filament of actin, but by many. The ratcheting properties of many filaments pushing against a single diffusing obstacle has been studied by Hohlfeld and Geissler [88]. In this study the authors numerically measure the ratcheting velocity of a varied number of filaments against a biased diffusive membrane. They find that the ratcheting velocity is increased by having a larger number of pushing filaments and from their analytic theories show that the effect of correlations between filaments near the lead filament play an important part in the dynamics.

The MI model is not the first to study the dynamics of an interface in the presence of a solid wall. In the context of studies of non-equilibrium wetting the dynamics of a growing KPZ type interface against a flat infinite surface, often referred to as the ‘substrate’, have been studied [82–84]. These models show

transitions between pinned and growing phases, where in the former the interface on average stays close to the substrate and in the latter it moves away from it. In a non-equilibrium wetting model with long range interactions it is found that for a certain choice of the long range interaction the transition between the phases actually belongs to the DP universality class [72, 74]. These studies and Ref [73] also feature non-equilibrium wetting in the presence of a *moving substrate*. This substrate moves towards the interface with a constant velocity, and there is no exclusion. Instead of being impeded by the interface, the wall pushes any local parts of the interface it meets upwards and away from it. By decreasing the velocity of the substrate they see a phase transition from a pinned to depinned phase, as long as the substrate attraction parameter is small enough. The unique features of the MI model are first that the substrate, or membrane, undergoes a random walk moving it closer to *or further from* the interface, and second that the interaction between the substrate and the interface is an exclusion interaction, meaning that the motion of either can be impeded by the presence of the other.

The control parameter I focus on is the measure of bias u of the random walk of the membrane, which can take values between 0 and 1 inclusive. The membrane is totally biased towards the interface when $u = 0$, meaning it can only move towards it. When $u = 1$, the opposite is true and the membrane can only move away from the interface. There is no bias in the motion of the interface when $u = 0.5$, which is equivalent to the scenario where there is no load force. The results of the numerical simulations show three distinct phases in the structure of the interface and the velocity of the membrane. The first phase, which I call the *smooth phase*, occurs when the bias $u < u_1 \simeq 0.62$. In this phase, the interface is narrow (hence ‘smooth’) and essentially bound to the membrane across its width. The interface pushes the membrane at a velocity which is approximately linear in the bias u : as u increases, so too does the membrane velocity. In the *rough phase*, where $u_1 < u < u_2 = 3/4$, the interface is rough, with the same roughness exponent $1/2$ as the KPZ class of interfaces. In this phase, the membrane and the interface are bound over a very small region, independent of the interface size. The interface still pushes the membrane, but in this regime the interface has reached its maximum velocity so increasing u has no effect on the velocity of the membrane. Finally, when $u > 3/4$ the membrane’s

natural drift velocity becomes greater than the velocity of the interface, and the two structures decouple. I call this the *unbound phase*, in which the interface behaves like a normal KPZ interface.

The research presented in this section was conducted in collaboration with Martin Evans and Richard Blythe, but has not yet been published. In particular, I performed the numerical analysis and developed the two random walker model of Section 5.6.1, and we worked collaboratively on the remainder of the analysis.

5.2 Membrane-Interface (MI) Model

The MI model consists of two key components, the membrane and the interface, which move independently in a discretised 2 dimensional space, and neither component can pass through the other. The x direction is parallel to the length of the membrane and perpendicular to its direction of motion, and conversely the y direction is parallel to the direction of motion of the membrane and perpendicular to its length.

The membrane is a solid wall which spans the entire width of the space in the x direction. It undergoes a random walk, in steps of 1 unit, in the y direction, where with probability u it takes a step *away from* the interface, and with probability $1 - u$ it takes a step *towards* it. The membrane and the interface are allowed to touch, but no part of the interface is allowed to pass through the membrane. A step by the membrane towards the interface which would cause this to occur is forbidden.

The interface is composed of L individual segments, connected to each other at their ends, which extend 1 unit in the x direction and 1 unit *up or down* in the y direction. The interface is periodic, so the plane in which it moves has a total width L in the x direction. There are L points which lie in between the segments, and the i -th point is found at a distance y_i from the membrane. The mutual exclusion of the membrane and interface means that all values of $y_i \geq 0$; negative values could only exist if the interface had passed through the membrane, and so are forbidden. When $y_i = 0$, the membrane and interface are in contact at point i .

As shown in Figure 5.4, the segments of the interface can be represented by

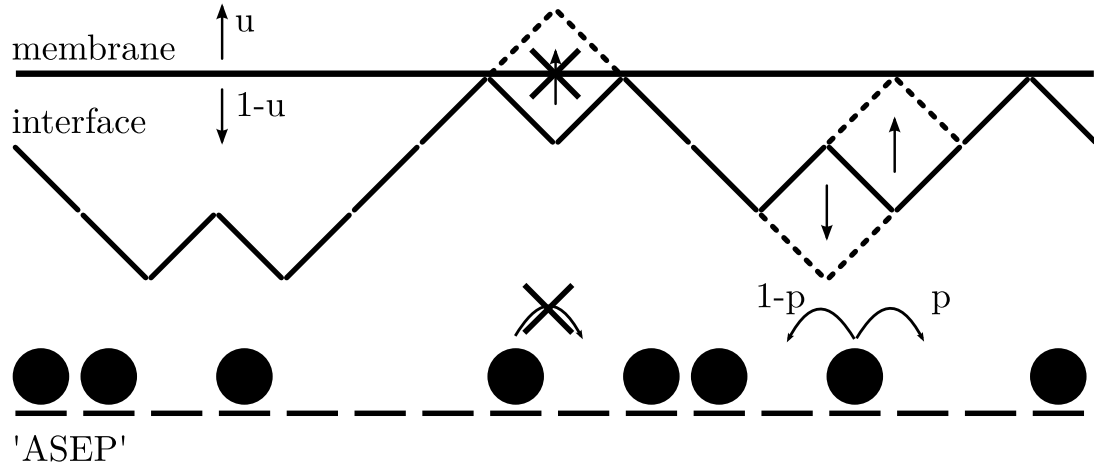


Figure 5.4: A diagram illustrating the MI model I study in this chapter. The membrane steps away (towards) the interface with rate u ($1 - u$). Particles in the ASEP, representing the slopes in the interface, hop to the right (left) with rate p ($1 - p$). Any move that would cause the interface to pass through the membrane is forbidden.

an asymmetric exclusion process (ASEP): each segment corresponds to a site in the ASEP; a segment which, ‘reading’ in the positive x direction, goes towards the membrane is represented by a vacant site in the underlying ASEP, and a segment which goes away from the membrane is represented by a site occupied by a particle. Particles in the underlying ASEP can hop to a vacant adjacent site with probability p in the positive x direction and with probability $1 - p$ in the negative x direction. Adsorption and desorption of monomers at the interface is represented by particle hops: when a particle hops in the positive x direction, a ‘down-up’ pair of segments become an ‘up-down’ pair of segments, and the point on the interface at which the two segments has moved 2 units towards the membrane. Such hops which would make y_i negative are forbidden by the exclusion rule. Similarly, when a particle hops in the negative x direction, an ‘up-down’ pair of segments becomes a ‘down-up’ pair, and the point connecting the two has moved two steps away from the membrane.

5.3 Numerical Methods

To investigate the properties of the MI model, I performed Monte Carlo simulations of the dynamics. I set $p = 1$, which means that the interface can only

grow towards the membrane, and cannot pull away from it of its own accord. I simulated an ASEP with the additional constraints on the particle movement which comes from the exclusion between the membrane and interface, from which I made measurements of the quantities of interest at different values of u , the membrane bias.

Practically this was done using an array of integers with values 0 or 1, representing vacant or occupied ASEP sites respectively, and by tracking a single separation distance, y_0 , which is the separation between the membrane and the interface at the first point of the interface. To allow periodic boundaries to be implemented, the lengths L of interfaces simulated must be multiples of 2, because it takes at least two steps for a section of the interface to return to its original height. For this reason I simulated interfaces of size 2^λ , and I chose the values of λ to be the integers from 8 to 13 inclusive, giving us a data from system sizes ranging from 256 to 8192.

In total there are $N = L/2$ particles being simulated. With probability $1/(N+1)$ an event in which the membrane attempts a move was generated, and with probability $N/(N+1)$ an event in which a particle attempts a move was generated. This is done to model the scenario where the rate of diffusion of the interface is equivalent to the rate of absorption of monomers at the interface. One Monte Carlo time step was defined as having elapsed after the occurrence of $N + 1$ attempted events.

I simulated the dynamics on a number of copies of a configuration which was initially flat with the membrane and interface in contact, and with the same parameter values. These simulations were allowed to equilibrate, after which the measured variables were averaged across the simulations and over time. This was done over a range of system sizes, and for values of u regularly incremented from 0 to 1 in steps $\Delta u = 0.01$.

5.3.1 Quantities of Interest

When quantifying the behaviour and properties of the interface over the range of u we are interested in measuring a number of different quantities.

The first of these is the mean separation \bar{y} between the interface and the

membrane. This is simply defined as

$$\bar{y} = \frac{1}{L} \sum_{i=1}^L y_i . \quad (5.3.1)$$

The sum over i is a sum across every point on the interface, which must be done each time we wish to take a measurement of \bar{y} . In general, this quantity is time dependent, but we assume that the interface equilibrates and reaches a steady state, within which \bar{y} should remain constant. The measurement of \bar{y} is important because the membrane and interface can move independently, so there is reason to expect that the steady state value may depend in some way on the membrane bias u .

In the context of interfaces, it is always of interest to measure the width, W , of the interface, defined here as

$$W = \sqrt{\frac{1}{L} \sum_{i=1}^L (y_i^2 - \bar{y}^2)} . \quad (5.3.2)$$

Aside from the mean interface position or height, the width is one of the simplest and most revealing measures of the spatial structure of the interface, which can give us information about whether the interface is smooth or rough. Furthermore, by measuring the width in relation to the system size L , we can quantify just how rough or smooth the interface is. For a normal KPZ interface, the width scales with $L^{1/2}$ in the steady state. It is interesting to measure what effect a diffusive obstacle, which would obstruct the growth of the interface, would have on the steady-state width in this case.

Another interesting quantity to measure is the number of contacts, C , which is measured directly from simulations. This quantity is interesting as a measure of binding between the membrane and the interface, and bears some relation to the width of the interface too. For instance, if all points of the interface are in contact with the membrane, then the interface will have the minimum width possible. However, it is not so easy to draw any conclusions about the width, or the structure, of the interface when C is small or zero.

Perhaps of most relevance to cell motility is the velocity v_m of the membrane itself. The membrane represents the cell membrane, and the average velocity at

which it moves is a good proxy for the velocity of the cell itself, so long as the membrane moves with the lamellipodium. In the simulations, the velocity of the membrane is measured directly from the number of steps taken by the membrane in the positive and negative y directions, and again averaged over the systems and time.

Finally, we also measure the current in the underlying ASEP, which allows us to quantify the growth rate of the interface. By defining the indicator function

$$\tau_i = \begin{cases} 0, & \text{if site vacant} \\ 1, & \text{if site occupied} \end{cases}, \quad (5.3.3)$$

then the ASEP current J is defined as

$$J = \left\langle \frac{1}{L} \sum_{i=1}^L \tau_i (1 - \tau_{i+1}) \right\rangle. \quad (5.3.4)$$

where $\langle . \rangle$ signifies an average over ensembles [52]. The quantity $\tau_i(1 - \tau_{i+1})$ measures the existence of a particle which has a vacant site ahead it can hop into, which is the only local configuration of two sites which will contribute to the current of particles. However, to measure the current in the interface here correctly, we must make the additional modification that we ignore contributions to the current from particles that would normally be able to hop, but are actually impeded by the exclusion interaction with the membrane.

5.4 Numerical Results and Discussion

The numerical measurements of the quantities of interest show 3 distinct phases of the MI model across the range of the membrane bias parameter u . The first of these phases occurs when $u \lesssim 0.62$. This is a smooth phase, where the interface is tightly bound to the membrane, and its width is small and independent of the system size. The second phase occurs in the region $0.62 \lesssim u \leq 3/4$. This is a rough phase, where the width of the interface scales with $L^{1/2}$ just as for a ZRP interface free from any obstacles, but the interface is still bound to the membrane. What is particularly interesting about this phase is that the current of adsorption of monomers in the interface, the ASEP current, has saturated at its maximal

value, and no longer increases with u . However, the velocity of the membrane also saturates; the interface and membrane move together as a coherent object with a velocity that is no longer dependent on u because the interface is pushing at its maximal velocity. Finally, when $u > 3/4$ the system enters the unbound phase. In this phase, the natural average velocity of the membrane, $2u - 1$, is great enough that it escapes from the interface and moves ballistically away. The interface is left behind on its own and is, in this case, simply the standard KPZ interface that is free to grow without any obstacles.

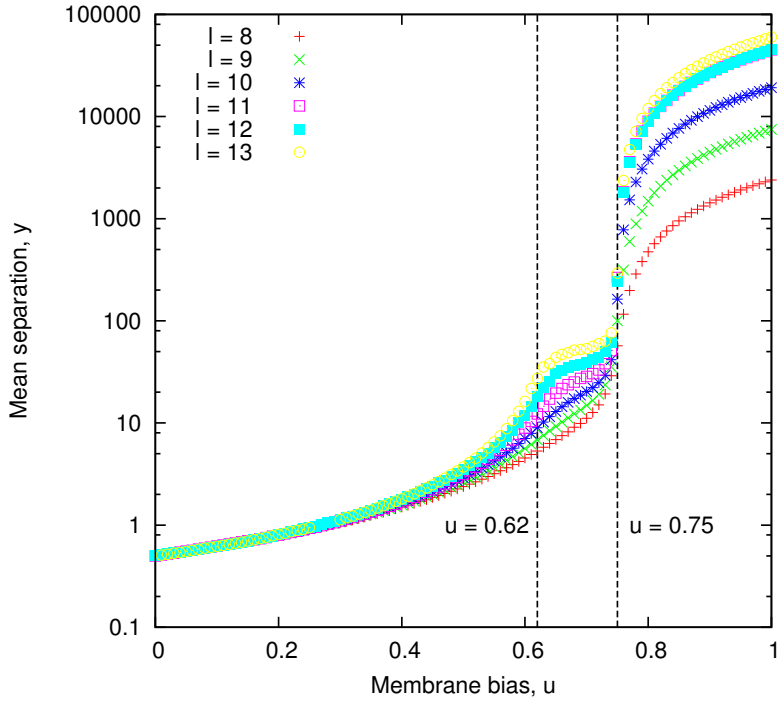


Figure 5.5: A plot of \bar{y} against u . Below $u_1 \simeq 0.62$, one sees that \bar{y} is small and independent of the system size. In the rough phase, between $u_1 \simeq 0.62$ and $u_2 = 3/4$ one sees that \bar{y} depends on the system size. One also sees additional structure becoming apparent at larger system sizes. When $u > u_2$, \bar{y} does not reach a steady state value as the membrane ‘escapes’ from the interface.

5.4.1 Smooth Phase

In the smooth phase, the interface stays very close to the membrane, as can be seen in Figure 5.5. Over a wide range of u , the mean separation \bar{y} between the interface and the membrane is of order 1, independent of the system size. Even approaching the rough phase, the mean separation only reaches sizes of order

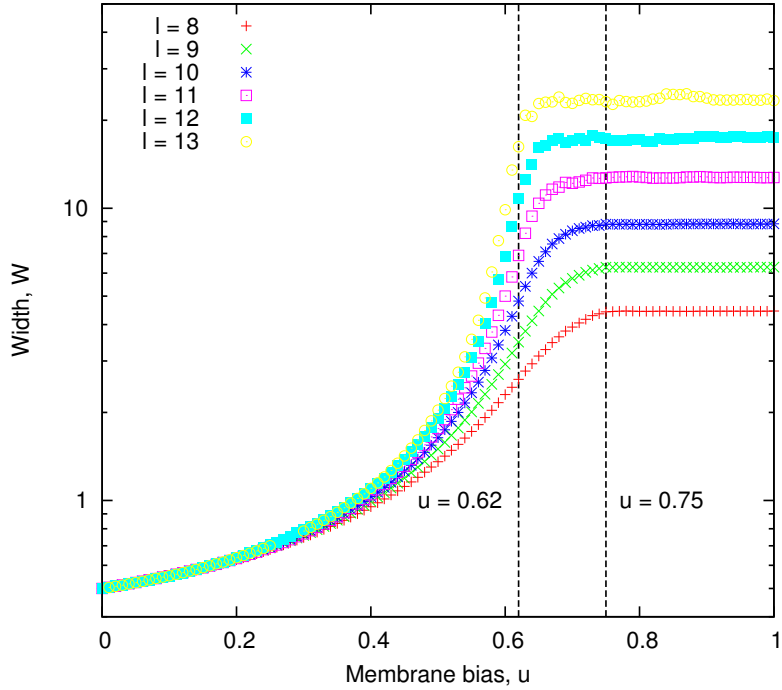


Figure 5.6: A plot of W against u . Far below $u_1 \simeq 0.62$, the width is very narrow and independent of L , which indicates a smooth interface. As we approach the rough phase, $u_1 < u < u_2$, the width develops a dependence on L , and within the rough phase itself it enters the KPZ scaling regime, with $W \sim L^{1/2}$. As expected, this scaling is maintained above $u_2 = 3/4$, where the interface is an unobstructed KPZ interface as the membrane drifts away.

10 for the largest systems measured. From measurements of W and C we can see that it is not just the mean position of the interface that stays close to the membrane, but the whole interface. From Figure 5.7 we see that in the smooth phase the interface has approximately $L/2$ points of contact with the membrane, and from Figure 5.6 we see that the width W is of order 1 throughout the phase.

Because $p = 1$, the interface always wants to grow towards the membrane, and thus the flow of current is inhibited only by the membrane blocking growth at the interface. When $u = 0$ the system is jammed and the current is 0, as the membrane can never move away from the interface to create space for it to grow. For very small u however, current can flow, albeit very slowly. In contrast to the spatial properties W , C and \bar{y} which remain approximately the same order of magnitude throughout the phase, the current J (Figure 5.8) and membrane velocity v_m (Figure 5.9) are seen to increase by 1 to 2 orders of magnitude across the smooth phase, until the maximal current is reached. What we are seeing is

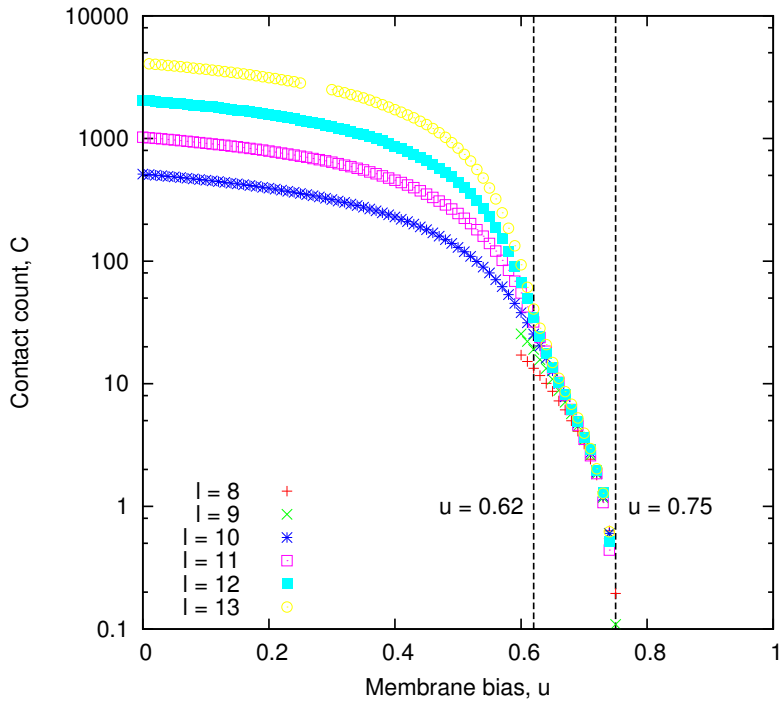


Figure 5.7: A plot C against u . In the smooth phase, $u < u_1$, C scales linearly with L , and so the density of contacts scales independently of L . This is indicative of a smooth interface pushing up against the membrane. In the rough phase $C \sim L^0$, and so the density of contacts scales as $1/L$. In this case, the interface still pushes up against the membrane, but with a vanishing density of contacts. In the rough phase, $u > u_2 = 3/4$, the membrane escapes and there are no contacts at all.

that the interface is having to push the membrane, which is impossible for $u = 0$, but gets easier as the membrane bias u away from the interface is increased. This keeps the interface close to the membrane, and its width narrow. The longer the interface has to wait for the membrane to move away, the more time there is for the trailing interface sites to ‘catch-up’.

The maximal current J_{max} reached at the upper limit of the smooth phase is simply the maximal current of the ASEP (see e.g. Ref [22] and Section 2.4):

$$J_{max} = \rho(1 - \rho) . \quad (5.4.1)$$

For an interface with periodic boundaries, what goes up must come down, and so there must be an equal number of upward slopes and downwards slopes. In the underlying ASEP, this corresponds to a particle density of exactly $1/2$. Thus, we

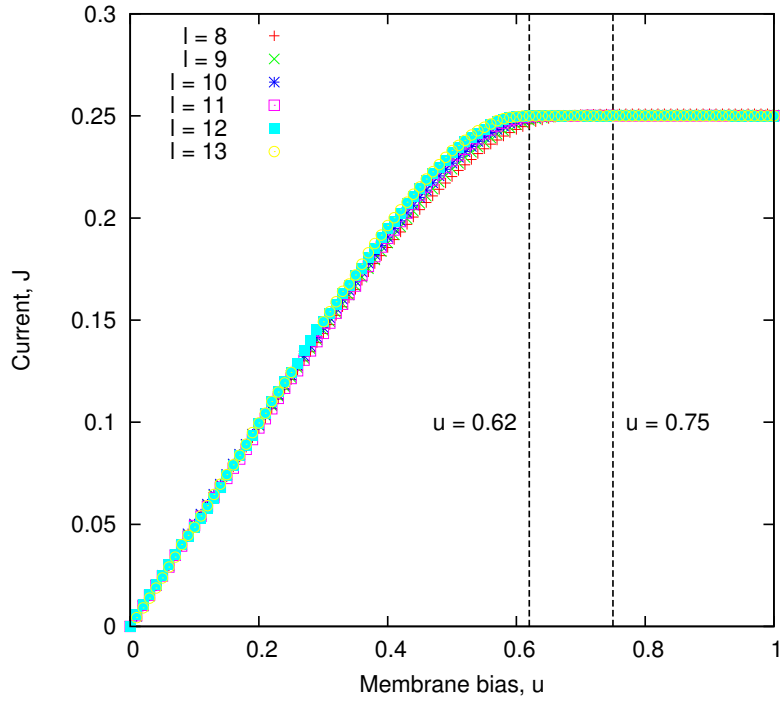


Figure 5.8: A plot of J against u . In the smooth phase, the current increases almost linearly with u until it approaches u_1 . At u_1 itself the current saturates to its maximal value, $1/4$. When $u > u_1$, in both the rough and unbound phases, the current does not change with u as it is no longer reduced by interactions with the membrane, but also can increase no further.

expect to find

$$J_{max} = \frac{1}{4}, \quad (5.4.2)$$

which is confirmed by Figure 5.8.

5.4.2 Rough Phase

As J saturates to J_{max} we enter the rough phase. Here we see that further increases in u no longer increase the membrane velocity. This is because the interface cannot grow any faster than it is doing in this phase, and so is pushing the membrane as fast as is possible. Further increases in u will have no effect until the membrane's natural average velocity $2u - 1$ becomes greater than the velocity of the interface.

The value of u at which the current saturates is a good indicator for the critical value u_1 of the transition between the rough and smooth phases. However, we

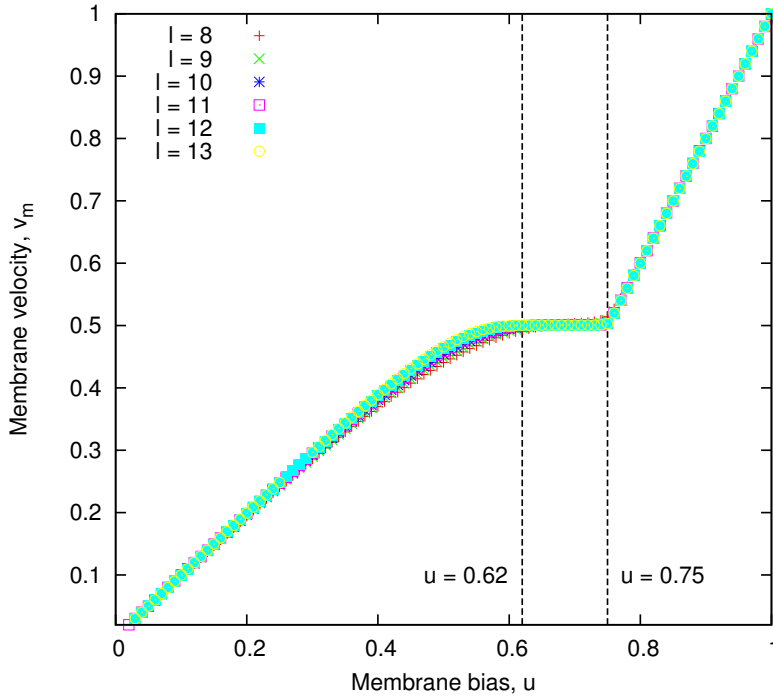


Figure 5.9: A plot of v_m against u . In the smooth phase and rough phases it has the same functional form as the current, because the velocity of the membrane is determined by the speed at which the interface can push it forwards. The membrane velocity is measured to be $v_m = 2J$. The upper transition at $u_2 = 3/4$ occurs when the natural mean drift velocity of the membrane $2u - 1$ becomes greater than the velocity $1/2$ of the interface that is pushing it, and the two parts decouple as the membrane drifts away.

can see from Figure 5.8 that it is significantly influenced by the system size. Nevertheless, a value of $u_1 \simeq 0.62$ is a reasonable estimate based on the J data, and agrees well with the prediction drawn from analysis of the width, as we will discuss in Section 5.4.3.

From the spatial measurements, we see a very significant change in the structural properties of the interface in the rough phase. First, we call it the rough phase because the width of the interface now scales with system size, specifically as $L^{1/2}$ (see Figure 5.6 and Figure 5.10). This exponent $1/2$ is the same roughness exponent found in the KPZ interface universality class. We also see that in this phase the number of contacts with the interface, C , becomes independent of the system size L , and thus as $L \rightarrow \infty$ is a vanishing fraction of L .

What we see then is that in the rough phase we have a KPZ interface with an infinitesimal fraction of points of contact with the membrane, which pushes the

membrane at its maximal growth velocity.

5.4.3 Transition Between the Smooth and Rough Phases

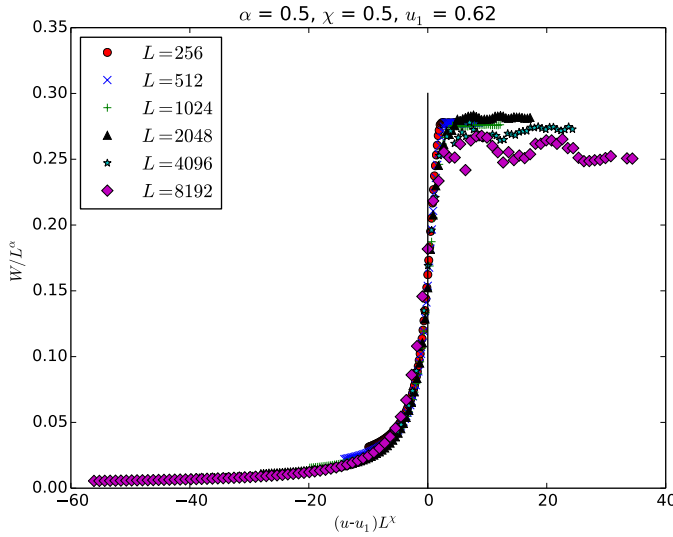


Figure 5.10: We perform a finite-size scaling procedure on the width W , plotting W/L^α against $(u - u_1)L^\chi$. The best data collapse was found for the parameters: $\alpha = 0.5$, $u_1 = 0.62$, and $\chi = 0.5$.

The nature and critical value of the transition from the smooth phase to the rough phase are not immediately obvious from the plots of the numerical measures. Certainly we can see that there is a change in the scaling behaviours of the spatial properties W , \bar{y} and C from one to the other, but any quantitative statements about the transition are difficult to make just by eye. To obtain an estimate $u_1 \simeq 0.62$ and $\alpha \simeq 0.5$ I analysed the width with a simple finite-size scaling procedure, but further analysis of how the exponent α varies with u revealed a weakness in this estimate and points to the need for some further numerical analysis.

To analyse the phase transition I used a finite-size scaling procedure (see e.g. [67, 90–92, 128, 129]), in the same way as was performed in Section 4.6, on the width data measured from simulation (Figure 5.10). This procedure tells us that the transition is discontinuous in the width, as it provides evidence that as

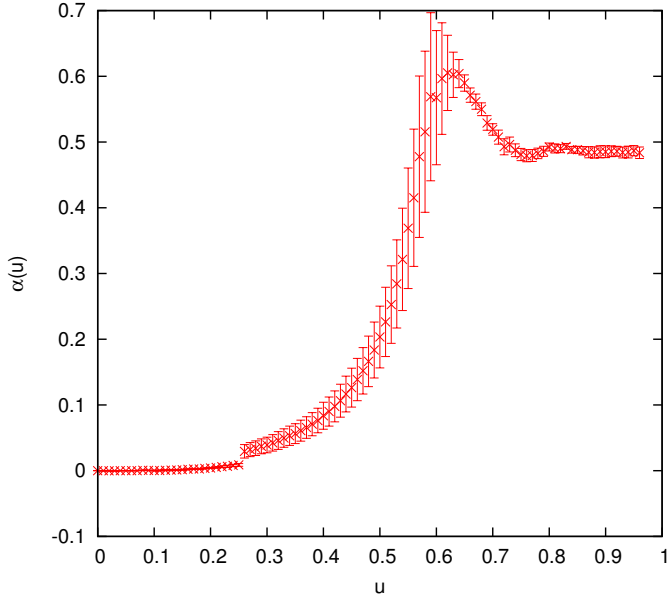


Figure 5.11: Numerical measurements of the roughness exponent α as a function of u show the expected behaviour at $u \geq 3/4$ and at small u , but unexpected behaviour around where I estimate the phase transition between the smooth and rough phases to be, $u_1 \simeq 0.62$.

$L \rightarrow \infty$ it exhibits a discontinuity, and that at the transition the width has the functional form

$$W \sim L^\alpha f((u - u_1)L^\chi) . \quad (5.4.3)$$

The best collapse was obtained for parameters

$$\alpha \simeq 0.5 , \quad \chi \simeq 0.5 , \quad u_1 \simeq 0.62 . \quad (5.4.4)$$

The result $\alpha \simeq 0.5$ is significant because it puts the rough phase interface in the same universality class as the KPZ interface. This procedure has also allowed us to measure $u_1 \simeq 0.62$.

Actually, the scaling at the u_1 transition is not so straightforward. Although a reasonable fit was found for the parameters in (5.4.4), by using a more sophisticated fitting algorithm [90, 121] I found that fits could be obtained at some other parameter values which were quantitatively just as reasonable, for instance with $\alpha \simeq 0.3$ and $u_1 \simeq 0.58$.

To investigate this further I performed a linear regression on the data for

$\ln(W(u, L))$ against $\ln(L)$, to investigate the proposition that actually near the transition that there is some u dependence in the roughness exponent α , such that

$$W \sim L^{\alpha(u)}. \quad (5.4.5)$$

What I find, as shown in Figure 5.11, is that close to and inside the rough phase there is an interesting dependence of the roughness exponent α on u . When $u > u_2 = 3/4$ we see $\alpha \simeq 1/2$, independently of the value of u , as is expected of a KPZ interface. At small u we see that $\alpha \simeq 0$ independently of u , also as we expect in the smooth phase. In between however α shows a strong functional dependence on u . From $u \simeq 0.3$ it increases super-linearly from 0 to approximately 0.6 at $u \simeq 0.60 - 0.64$, and then it decreases down to 1/2 at $u = 3/4$. The peak in this plot does suggest a significant change in the phase behaviour at $u \simeq 0.60 - 0.64$, which at least corroborates the initial identification of a phase transition in this region. What the implications of this are for whether this is a first-order transition or not are as of yet unclear.

The analysis of this observation has not yet progressed any further than as presented here, but it is certainly an interesting avenue to pursue. Speculatively, one might suggest that there are sub-phases of the rough phase that require further analysis. What is also clear from this plot is that more numerical analysis would be useful. A greater range of system sizes simulated would help the analysis, but also more careful simulation of the rough phase, which has significant error bars in Figure 5.11, would help to improve our understanding of the nature of this phase.

The finite size scaling procedure used to analyse the width would indicate the the transition in the width between the rough and smooth phases is first-order, but the difficulty in performing that procedure makes it difficult to be confident in drawing this conclusion. In the current the transition between the two phases is continuous, with a possible discontinuity in one of its derivatives. It may actually be possible then that the transition is of mixed order, as is seen in Ref [10, 11], but further analysis is required.

5.4.4 Unbound Phase

The unbound phase is relatively straightforward to understand, as it exhibits a decoupling between the (biased) diffusive membrane and the growing KPZ interface. The transition to the the unbound phase occurs at a value u_2 where the natural drift velocity of the membrane becomes greater than the maximal interface velocity.

The interface velocity v_i is simply

$$v_i = \text{monomer size} * \text{current} = 2J , \quad (5.4.6)$$

and (with the result (5.4.2)) its maximal value is

$$v_{i,max} = 2J_{max} = 2 * \frac{1}{4} = \frac{1}{2} . \quad (5.4.7)$$

The natural average membrane velocity is simply

$$v_n = u - (1 - u) = 2u - 1 . \quad (5.4.8)$$

The membrane will be able to escape from the interface when $v_n > v_{i,max}$ which can be used to find a condition on u :

$$\begin{aligned} 2u - 1 &> \frac{1}{2} \\ u &> \frac{3}{4} , \end{aligned} \quad (5.4.9)$$

and thus we have found the upper critical value, $u_2 = 3/4$.

This is exactly what we see in the simulations. When $u > 3/4$ the contact count C becomes exactly zero, and the membrane velocity switches to the functional form $v_m = 2u - 1$, the membrane's natural average velocity. The mean separation \bar{y} between the membrane and the interface does not reach a steady state, as the membrane continually gets further and further away from the interface. The width is now simply the width of the KPZ interface, which scales as $L^{1/2}$

5.5 Simple Mean-Field Theory

To try to learn more about the three phases observed in the simulations, and to try and estimate the critical values of u , we developed a simple mean-field theory to describe the probability that a piece of the interface chosen at random lies at a distance y from the membrane. This theory does predict three phases in u , and provides estimates for the critical values u_1 and u_2 , but incorrectly predicts a scaling of the width in the rough phase of $W \sim L^1$, which is significantly different to $W \sim L^{1/2}$ which we measure, and which is normally seen in random walk and diffusive processes (see Chapter 2).

5.5.1 Master Equation and Generating Function

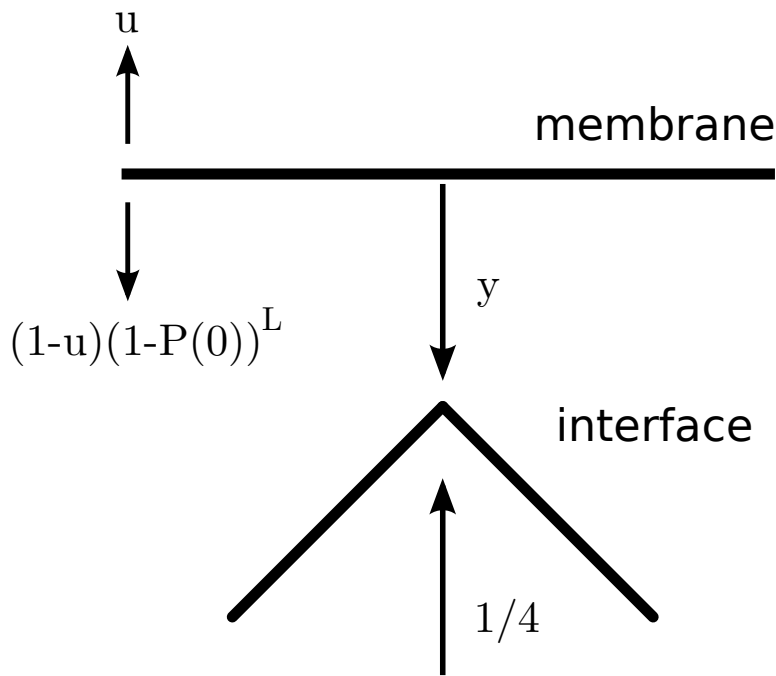


Figure 5.12: A schematic diagram of the processes which occur in the simple mean-field theory. A point on the interface lies a distance y from the membrane. With rate $1/4$ the interface grows *two steps* towards the membrane, reducing y by 2. With rate u the membrane steps away from the interface, increasing y by 1. With rate $(1 - u)(1 - P(0))^L$ the membrane steps towards the interface, reducing y by 1. Any process which would make y negative is prohibited.

The mean-field theory describes the probability $P(y)$ that a point on the interface is a distance y from the membrane, and is described by the master

equation

$$\begin{aligned} \frac{\partial P(y)}{\partial t} = & uP(y-1)1_{y>0} + \frac{1}{4}P(y+2) + (1-u)[1-P(0)]^L P(y+1) \\ & - uP(y) - \frac{1}{4}P(y)1_{y>1} - (1-u)[1-P(0)]^L P(y)1_{y>0}. \end{aligned} \quad (5.5.1)$$

On the top row, we have the gain terms, and on the bottom the loss. The function $1_X = 1$ if the condition X is met, or 0 otherwise. The first and fourth terms, preceded by a factor u , represent the effect of the membrane moving away from the interface. In the first term the indicator $1_{y>0}$ accounts for the fact that after the membrane moves upwards, this point of the interface cannot be a distance $y = 0$ away, because it would previously have had to have distance $y = -1$, which is impossible. The second and fifth term are preceded by a factor $1/4$. This is the maximal current of the ASEP, and these terms represent individual monomer growth events in the interface. In the fifth term, the factor $1_{y>1}$ accounts for the fact that if $y \leq 1$ then a growth event in the interface at this point would make y negative, and is prohibited. Finally the third and sixth terms represent the effect of the membrane moving downwards towards the interface. The factor $[1-P(0)]^L$ represents the influence of the remainder of the interface: the membrane cannot move down towards the interface if any other part of the interface is touching the membrane. The sixth term also contains a factor $1_{y>0}$, which prevents the membrane from moving downwards if $y = 0$.

Now, we define the generating function

$$G(z) = \sum_{y=0}^{\infty} z^y P(y), \quad (5.5.2)$$

and in the steady state, with $\partial P(y)/\partial t = 0$ we find that the master equation (5.5.1) becomes

$$\begin{aligned} 0 = & zaG(z) + \frac{G(z)}{z^2} - \frac{P(1)}{z} - \frac{P(0)}{z^2} + \frac{bG(z)}{z} - \frac{bP(0)}{z} \\ & - (a+b+1)G(z) + P(0) + bP(0) + zP(1), \end{aligned} \quad (5.5.3)$$

where we have defined

$$a = 4u, \quad b = 4(1-u). \quad (5.5.4)$$

This can be rearranged to give

$$G(z)[az^3 - (a+b+1)z^2 + bz + 1] = (z-z^3)P(1) + (1+bz-z^2-bz^2)P(0), \quad (5.5.5)$$

from which one can factorise out $(1-z)$, and then rearrange to obtain

$$G(z) = \frac{P(1)(1+z)z + P(0)(1+(1+b)z)}{1+(b+1)z-az^2}. \quad (5.5.6)$$

We require that the distribution $P(y)$ is normalised, meaning

$$G(1) = \sum_{y=0}^{\infty} P(y) = 1, \quad (5.5.7)$$

from which we find an equation relating $P(0)$ and $P(1)$:

$$2P(1) + (1+b)P(0) = 2 + b - a. \quad (5.5.8)$$

5.5.2 Predictions of Critical Values

The normalisation condition allows us to make simple predictions for the critical values of u , u_1 and u_2 . First, notice that for the distribution to be normalised the condition

$$2 + b - a > 0 \quad (5.5.9)$$

must be satisfied. If it is not satisfied for some set of parameter values, then there is no steady state at those values.

Now we first consider the case where $P(0)$ is finite and greater than $\mathcal{O}(\frac{1}{L})$. In this case, remembering that $b = 4(1-u)(1-P(0))^L$, $b \rightarrow 0$ as $L \rightarrow \infty$ and so the condition (5.5.9) becomes

$$\begin{aligned} a &< 2, \\ u &< \frac{1}{2}. \end{aligned} \quad (5.5.10)$$

This tells us that a steady state where $P(0) > \mathcal{O}(\frac{1}{L})$, which is what we see in the smooth phase, exists only when $u < 1/2$. Thus we have predicted the lower critical value $u_1 = 1/2$.

Next we can ask what happens when $u \geq 1/2$. In this case b must be finite

and so, to leading order in L , we require $P(0) \leq \mathcal{O}(\frac{1}{L})$ for this to be true. In the infinite system size limit, $L \rightarrow \infty$, $P(0) \rightarrow 0$ and we find $b \rightarrow 4(1 - u)$. In this case the condition (5.5.9) becomes

$$\begin{aligned} 2 + 4 - 4u - 4u &> 0, \\ u &< 3/4. \end{aligned} \quad (5.5.11)$$

This means that, for $u \geq 3/4$ no steady steady state is possible, and thus we have an estimate for the upper critical exponent $u_2 = 3/4$, which is in agreement with the simulations and the result (5.4.9).

In general, for a finite system, we see that for finite b we require

$$P(0) = -\frac{\ln c}{L}, \quad (5.5.12)$$

where c is independent of L , but not u . This scaling of $P(0)$ is what we see in Figure 5.7 for the measured contact count C . The average contact count C is related to $P(0)$ by

$$P(0) = \frac{C}{L}. \quad (5.5.13)$$

In Figure 5.7 we see in the rough phase that $C \sim L^0$, and so $P(0) \sim L^{-1}$.

5.5.3 Prediction for the Scaling of the Width

Now, we proceed to see what this theory predicts for the width of the interface, by analysing the generating function $G(z)$. To begin, we notice that the denominator of $G(z)$ is quadratic in z , and thus $G(z)$ can be written as

$$G(z) = \frac{P(1)z^2 + (P(1) + (1+b)P(0))z + P(0)}{-a(z - z_-)(z - z_+)}. \quad (5.5.14)$$

Because

$$|z_-| < |z_+| \quad (5.5.15)$$

the pole at z_- is nearer the origin, and will dominate the integral

$$P(n) = \oint \frac{dz}{2\pi i} \frac{G(z)}{z^n} \quad (5.5.16)$$

at large n , but because

$$z_- < 0 \quad (5.5.17)$$

this means that the distribution would oscillate between positive and negative values as n is increased. Negative values are obviously unphysical, so the term $(z - z_-)$ in the denominator must be cancelled by the numerator. Thus,

$$P(1)(1 + z)z + P(0)(1 + (1 + b)z) = -a(Az + B)(z - z_-) , \quad (5.5.18)$$

and we obtain another condition which relates $P(0)$ and $P(1)$:

$$P(1)(1 + z_-)z_- + P(0)(1 + (1 + b)z_-) = 0 . \quad (5.5.19)$$

$G(z)$ can now be written as

$$G(z) = \frac{(Az + B)}{(z - z_+)} . \quad (5.5.20)$$

Comparing the numerator of this equation with that of (5.5.14), we find

$$P(1)z^2 + (P(1) + (1 + b)P(0))z + P(0) = -aAz^2 + (az_-A - aB)z + az_-B . \quad (5.5.21)$$

We can then read off

$$P(0) = -aA , \quad A = -\frac{1}{a}P(0) = z_+z_-P(0) , \quad (5.5.22)$$

$$P(1) = -\frac{B}{z_+} , \quad B = -z_+P(0) , \quad (5.5.23)$$

and another condition for $P(0)$ and $P(1)$:

$$-a(B - Az_-) = P(1) + (1 + b)P(0) . \quad (5.5.24)$$

The generating function can be written

$$\begin{aligned}
 G(z) &= -\frac{Az + B}{z_+} \frac{1}{1 - z/z_+} \\
 &= -\frac{Az + B}{z_+} \sum_{y=0}^{\infty} \left(\frac{z}{z_+} \right)^y \\
 &= -\frac{B}{z_+} - \left(A + \frac{B}{z_+} \right) \sum_{y=1}^{\infty} \left(\frac{z}{z_+} \right)^y
 \end{aligned} \tag{5.5.25}$$

Substituting in from (5.5.22) and (5.5.23) we find

$$G(z) = P(0) + [P(0) - z_+ z_- P(1)] \sum_{y=1}^{\infty} \left(\frac{z}{z_+} \right)^y. \tag{5.5.26}$$

Thus, using the definition of $G(z)$ we can read off

$$P(y) = \frac{P(0) - z_+ z_- P(1)}{z_+^y}, \tag{5.5.27}$$

for $y > 0$. Self-consistently,

$$P(1) = \frac{P(0) - z_+ z_- P(1)}{z_+}, \tag{5.5.28}$$

and so

$$P(1) = \frac{P(0)}{z_+(1 + z_-)}. \tag{5.5.29}$$

Substituting back into (5.5.27) we find that $P(y)$ is

$$P(y) = \frac{1}{1 + z_-} \frac{P(0)}{z_+^y}, \quad y > 0, \tag{5.5.30}$$

and the generating function

$$G(z) = P(0) \left[1 + \left(\frac{1}{1 + z_-} \right) \sum_{y=1}^{\infty} \left(\frac{z}{z_+} \right)^y \right]. \tag{5.5.31}$$

We can now use this generating function to calculate the mean separation, \bar{y} , and then the width, W , and use the resulting expressions to analyse the scaling

with the system size L . First,

$$\bar{y} = \left. \frac{dG}{dz} \right|_{z=1} = \sum_{y=1}^{\infty} y P(y) . \quad (5.5.32)$$

From (5.5.31)

$$\frac{dG}{dz} = \frac{P(0)}{1 + z_-} \sum_{y=1}^{\infty} y \frac{z^{y-1}}{z_+^y} , \quad (5.5.33)$$

which is used to find

$$\bar{y} = \frac{P(0)}{1 + z_-} \sum_{y=1}^{\infty} y \frac{1}{z_+^y} = \frac{P(0)}{1 + z_-} \frac{z_+}{(z_+ - 1)^2} . \quad (5.5.34)$$

From the second derivative of the generating function

$$\frac{d^2G}{dz^2} = \sum_{y=1}^{\infty} y(y-1) z^{y-2} P(y) = \frac{P(0)}{1 + z_-} \sum_{y=1}^{\infty} y(y-1) \frac{z^{y-2}}{z_+^y} , \quad (5.5.35)$$

we see that

$$\left. \frac{d^2G}{dz^2} \right|_{z=1} = \overline{y^2} - \bar{y} , \quad (5.5.36)$$

and so

$$W^2 = \left. \frac{d^2G}{dz^2} \right|_{z=1} + \bar{y} - \overline{y^2} . \quad (5.5.37)$$

With $z = 1$ we find

$$\begin{aligned} \left. \frac{d^2G}{dz^2} \right|_{z=1} &= \frac{P(0)}{1 + z_-} \sum_{y=1}^{\infty} y(y-1) z_+^{-y} \\ &= \frac{2\bar{y}}{(z_+ - 1)} , \end{aligned} \quad (5.5.38)$$

and so

$$W^2 = \bar{y} \left(\frac{z_+ + 1}{z_+ - 1} - \overline{y} \right) . \quad (5.5.39)$$

The L dependence of this expression comes from the L dependence of $P(0)$. In the bound phase, for b to be finite we require $P(0) \sim \mathcal{O}\left(\frac{1}{L}\right) = \frac{-\ln c}{L}$, where c is a constant. To calculate the L scaling of W , we must first find the leading order L scaling of z_{\pm} and \bar{y} . The calculation of the leading order dependence on

L of all of these quantities involves a long sequence of Taylor expansions, which is outlined in Appendix C.1. For brevity, we skip to the result

$$W \sim L , \quad (5.5.40)$$

and so this theory predicts that the width W scales *linearly* with the system size L . This result, although not accurate according to the simulations, is not surprising. In the mean-field theory, adjacent sites on the interface may only differ in height by one unit; a condition known as “restricted solid-on-solid” (RSOS) [12, 103]. This mean-field theory contains no such condition, and so it allows large fluctuations in the width across its length, which would explain the prediction for the width to scale as linearly with L , rather than with \sqrt{L} as we might expect.

In the next section I present another theoretical approach which has given us some insight into the mechanisms behind the phase behaviour observed numerically, but has not yielded any predictions for critical values or scaling exponents.

5.6 The Importance of Jammed Regions of the Interface

An interesting feature of this system which is difficult to see from the properties I measured numerically is the occurrence of contiguous regions of the interface which are jammed, or pinned, against the membrane. The existence of this phenomenon is made clear by visualisations of the state of the ASEP which underlies the interface at successive time steps (Figure 5.13). Furthermore, these visualisations reveal that there are strong temporal correlations between where in the interface these jammed regions occur. This indicates another reason why the simple mean-field theory failed to fully describe the key features of the system: it did not capture the effects of these strong temporal and spatial correlations.

The difference in the nature of these jammed region of interface seem to be a key distinguishing feature of the three phases we see. In the unbound phase we expect no restrictions on the growth of the interface and indeed we see no regions of interface which are stuck against the membrane. In the smooth phase, most if not all points of the interface are jammed against the interface, and the length of

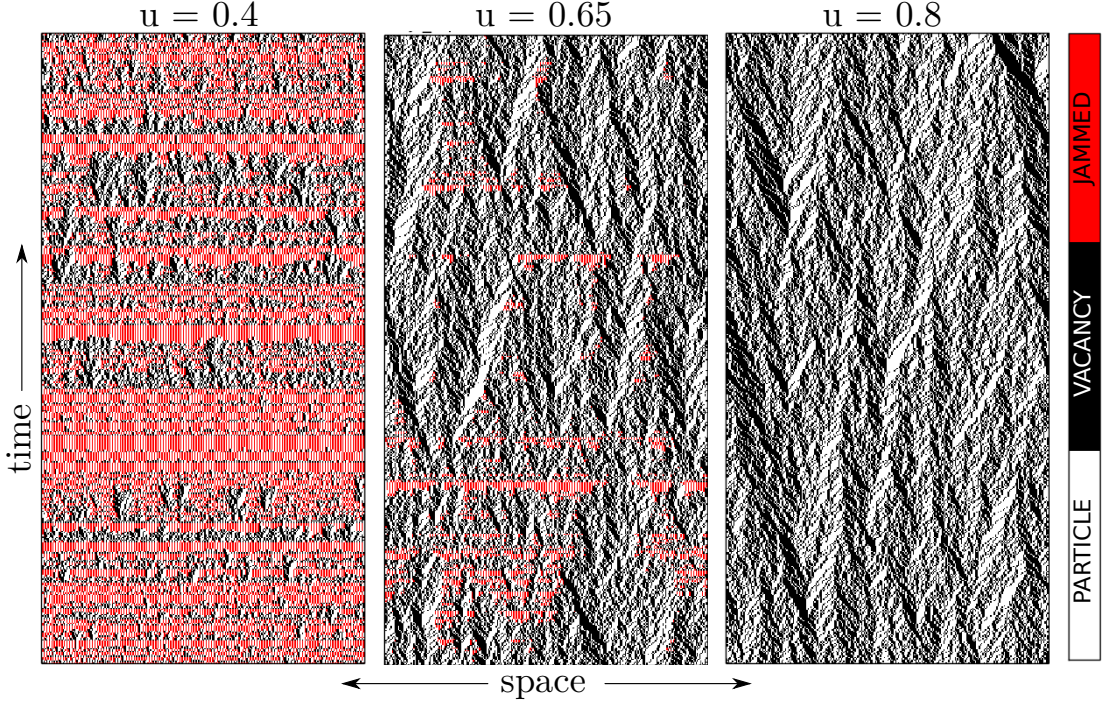


Figure 5.13: A visualisation of the underlying ASEP array for $L = 256$ over 500 time steps. Each row shows state of the ASEP at a single time step with vacant sites in white, occupied sites in black, and occupied sites where the particle cannot jump forward due to the effect of the membrane in red. **Left:** $u = 0.4$. This is the smooth phase. Regions of interface that are pinned to the membrane span the entire system. **Centre:** $u = 0.65$. In the rough phase, there are contiguous regions of interface pinned to the membrane that do not span the entire length. Jammed regions are likely to reoccur in the same or similar regions of the interface where they did previously. **Right:** $u = 0.8$. In the unbound phase there is no interaction between the membrane and interface.

the jammed regions are of order system size L . Finally, in the rough phase, the jammed regions seen are finite in length, but do not span the entire system.

Based on these observations, I have developed a simple model describing the length of a jammed region of the interface in order to try and understand the existence of the phases in the MI model. This model has been successful in demonstrating that three phases similar to those observed in the simulations can be described through the simple dynamics of a jammed region of interface alone. Unfortunately I have not been able to use this model to extract predictions for the critical values or the nature of the phase transition.

5.6.1 A Simple Two-Random-Walker Model

The model is motivated as follows. When the interface comes into contact with the membrane, there will be one or more jammed interface points resulting in a vacant-occupied site pair in the ASEP, where the particle is stuck regardless of whether the site ahead is free. Subsequent particle hops either side of this pair of sites create new interface sites which are pinned against the membrane, and so a region of jammed sites grows outwards from the original contact point. The growth of a jammed region in this way can only happen if there are any contact points at all, and so as soon as the membrane steps away the interface is free to grow again in these regions.

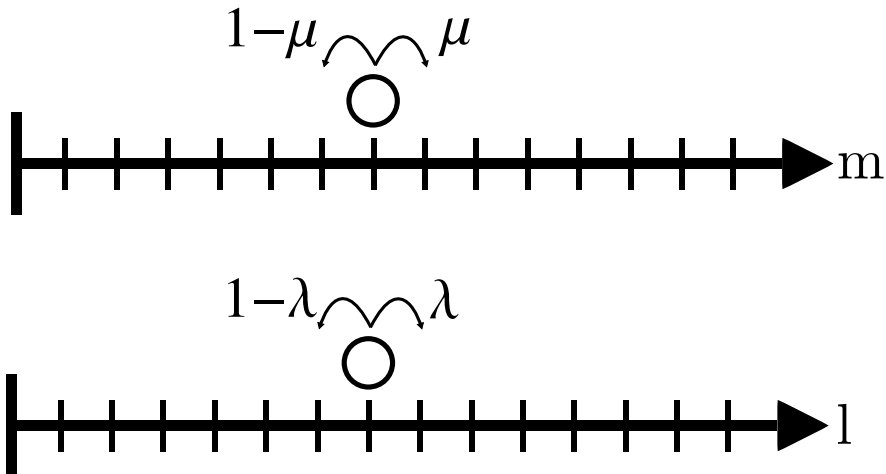


Figure 5.14: Diagram of the Two Random Walker model. l can only increase in size if $m = 0$, and can only decrease in size if $m > 0$. In the ‘annealed’ case: l increases by 1 with probability $\lambda P^*(0)$ and decreases by 1 with probability $(1 - \lambda)(1 - P^*(0))$, where $P^*(0)$ is the steady state probability that $m = 0$.

To capture this behaviour we define the model such that it consists of two random walkers, each on a half-infinite lattice of sites, as shown in Figure 5.14. One represents the distance of the membrane from the interface, and has position m . When $m = 0$, the membrane and the interface are in contact. The other walker represents the length of a region of jammed sites, and has position l . The particle m hops to the right, increasing in value, with rate μ , and hops to the left, decreasing in value, with rate $1 - \mu$. Similarly, the particle l hops to the right, increasing in value, with rate λ , and hops to the left, decreasing in value, with rate $1 - \lambda$. Neither particle can reach negative sites. The coupling between the

membrane-interface separation, m , and the length of a jammed region l , exists in the following rule: l can only increase when $m = 0$, and can only decrease when $m > 0$. To simplify the analysis we weaken this condition: l increases with probability $\lambda P^*(0)$ and decreases with probability $(1 - \lambda)(1 - P^*(0))$, where $P^*(0)$ is the steady state probability that $m = 0$.

A particularly appealing feature of this model is that when the membrane moves away from the interface, when $m > 0$, the length of the jammed region is not immediately forgotten, and l is not immediately reset to 0. This allows the model to capture an element of the memory of the length of the jammed interface region seen in the MI simulations.

5.6.2 Prediction of Phases in the Mean Length \bar{l}

By defining $P(m, t)$ as the probability that the distance from the membrane to the interface is m at time t , and $Q(l, t)$ as the probability that the jammed region of interface has length l at time t , we can write down master equations for both. For $m > 0$

$$\frac{\partial P(m, t)}{\partial t} = \mu P(m - 1, t) - [\mu + (1 - \mu)]P(m, t) + (1 - \mu)P(m + 1, t), \quad (5.6.1)$$

and for $m = 0$

$$\frac{\partial P(0, t)}{\partial t} = (1 - \mu)P(1, t) - \mu(0)P(0, t). \quad (5.6.2)$$

For $l > 0$

$$\begin{aligned} \frac{\partial Q(l, t)}{\partial t} &= \lambda P^*(0)Q(l - 1, t) \\ &- [\lambda P^*(0) + (1 - \lambda)(1 - P^*(0))]Q(l, t) \\ &+ (1 - \lambda)(1 - P^*(0))Q(l + 1, t), \end{aligned} \quad (5.6.3)$$

and for $l = 0$:

$$\frac{\partial Q(0, t)}{\partial t} = (1 - \lambda)(1 - P^*(0))Q(1, t) - \lambda P^*(0)Q(0, t). \quad (5.6.4)$$

We can then define the steady state probabilities $P^*(m)$, $Q^*(l)$ such that

$$\frac{\partial P^*(m)}{\partial t} = 0, \quad \frac{\partial Q^*(l)}{\partial t} = 0. \quad (5.6.5)$$

We first consider the dynamics of the distance m , which is independent of the dynamics of the length l . In the steady state, the master equations give us the relationships

$$P^*(1) = \frac{\mu}{1-\mu} P^*(0) \quad (5.6.6)$$

and

$$P^*(m+1) = \frac{1}{1-\mu} P^*(m) - \frac{\mu}{1-\mu} P^*(m-1) . \quad (5.6.7)$$

Using these, one can then prove by induction that

$$P^*(m) = \left(\frac{\mu}{1-\mu} \right)^m P^*(0) . \quad (5.6.8)$$

We fix $P^*(0)$ by requiring that the probability distribution is normalised.

$$\begin{aligned} 1 &= \sum_{m=0}^{\infty} P^*(m) \\ &= \sum_{m=0}^{\infty} \left(\frac{\mu}{1-\mu} \right)^m P^*(0) \\ &= P^*(0) \sum_{m=0}^{\infty} r^m , \end{aligned} \quad (5.6.9)$$

where

$$r = \frac{\mu}{1-\mu} . \quad (5.6.10)$$

For $0 \leq r < 1$:

$$P^*(0) = 1 - r , \quad (5.6.11)$$

and for $r \geq 1$ there is *no steady state* $P^*(m)$. $P^*(0)$ can be written

$$P^*(0) = \frac{1-2\mu}{1-\mu} , \quad (5.6.12)$$

and from the steady state condition

$$0 < P^*(0) \leq 1 , \quad (5.6.13)$$

we find that

$$0 \leq \mu < \frac{1}{2} . \quad (5.6.14)$$

Unsurprisingly, when $\mu \geq 1/2$, m drifts to away to infinity and there is no steady state.

Now that we have found an expression for $P^*(0)$ in terms of m , we can analyse the jammed length l . By substituting $\lambda P^*(0)$ for μ and $(1 - \lambda)(1 - P^*(0))$ for $(1 - \mu)$ we see that the solution for $Q^*(l)$ has the same form as that for $P^*(0)$:

$$Q^*(l) = \left(\frac{\lambda P^*(0)}{(1 - \lambda)(1 - P^*(0))} \right)^l Q^*(0). \quad (5.6.15)$$

Just as with $P^*(0)$, we can fix $Q^*(0)$ by requiring $P^*(m)$ to be normalised. This gives us

$$Q^*(0) = 1 - \rho, \quad (5.6.16)$$

where

$$\rho = \frac{\lambda P^*(0)}{(1 - \lambda)(1 - P^*(0))}, \quad (5.6.17)$$

for $0 \leq \rho < 1$. When $\rho \geq 1$ there is *no steady state* $Q^*(l)$. We can also rewrite the expression for ρ in terms of μ by using the expression for $P^*(0)$, which gives

$$\rho = \frac{\lambda(1 - 2\mu)}{(1 - \lambda)\mu}. \quad (5.6.18)$$

To see if we can gain some insight into the phases observed in the simulations, we calculate the steady state mean jammed length

$$\begin{aligned} \bar{l} &= \sum_{l=0}^{\infty} l Q^*(l) \\ &= (1 - \rho) \sum_{l=0}^{\infty} l \rho^l \\ &= \frac{\rho}{1 - \rho}. \end{aligned} \quad (5.6.19)$$

It is clear that $\rho < 1$ is required for \bar{l} to be finite, and $\rho > 1$ is unphysical.

Already, we can see that when $P^*(0) = 0$, and $\lambda \neq 0$, then $\rho = 0$ regardless of the value of λ . This occurs when $\mu \geq 1/2$ and describes the situation where the membrane drifts away, and $\bar{l} = 0$ in the steady state.

To understand what happens when $\mu < 1/2$, we make the substitution for ρ

to and find that

$$\bar{l} = \frac{\lambda(1 - 2\mu)}{\mu(1 - \lambda) - \lambda(1 - 2\mu)} . \quad (5.6.20)$$

For a steady state in \bar{l} to exist, the following relationship must be satisfied:

$$0 \leq \rho < 1 , \quad (5.6.21)$$

which leads to the condition

$$0 \leq \frac{\lambda}{1 + \lambda} < \mu . \quad (5.6.22)$$

This tells us that when $\mu < 1/2$ there are two cases. The first, in the region where this condition is satisfied, describes the situation where m stays close enough to 0 for \bar{l} to reach a finite steady state value $\rho/(1 - \rho)$. When this condition is not satisfied, $Q^*(0)$ has no steady state value, and therefore neither does $Q^*(l)$, and \bar{l} diverges as the jammed region increases in size indefinitely.

These three phases are shown in the phase diagram Figure 5.15. The steady state with $\bar{l} = 0$ is region A; the steady state with $\bar{l} = \rho/(1 - \rho)$ is region B; and the regime with no steady state for \bar{l} is region C.

This result has as nice correspondence to the numerical results. We can identify the parameter μ with the interface bias u , and λ is, in some way which we have not been able to make clear, related to the interface growth probability, p . For a fixed value of p , and thus a fixed value of λ , we see that as μ , or u , is increased from 0, the system passes through 3 phases (Figure 5.15). The first (C) is one with a jammed region of interface which spans its entire length; the smooth phase. The second (B) is a region with a jammed length of interface which is finite in size, similar to the jammed regions seen in the rough phase. Finally, increasing μ further, we cross into a phase (A) where the membrane escapes and there are no jammed regions in the interface.

Although we have not been able to use this model to predict the critical values of u or to categorise the nature of the transitions, we have managed to gain some useful insight into the behaviour we observe. The rate at which the interface grows, related to λ , and the rate at which the membrane moves away from the interface are competing processes which determine how much time the interface spends in contact with the membrane. More importantly they determine how

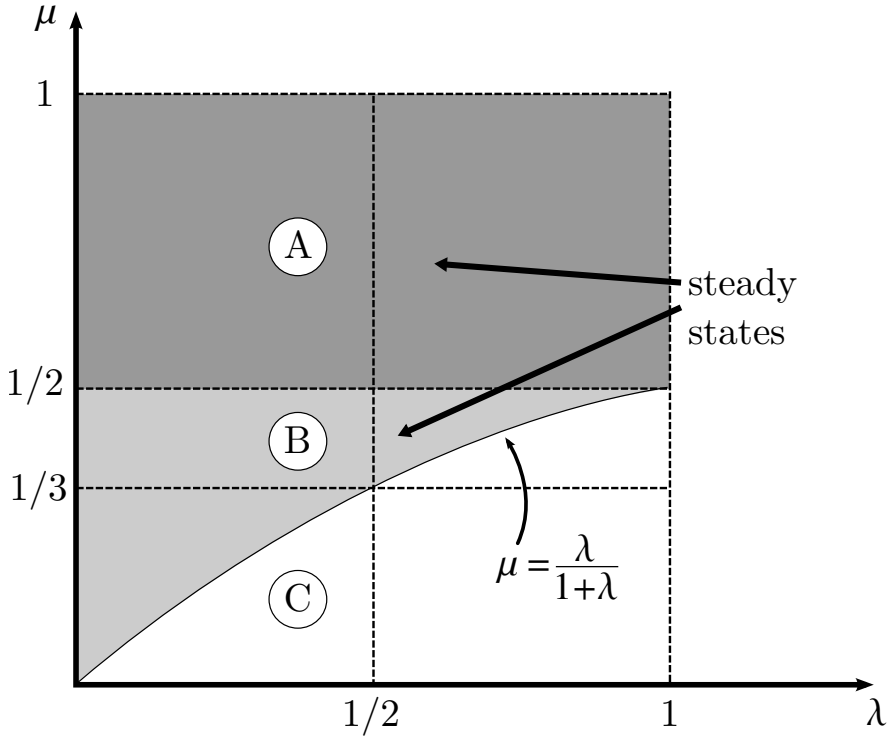


Figure 5.15: **(A)** There is no $P^*(0)$, so $m \rightarrow \infty$. Thus a steady state with $Q^*(0) = 1$ and $\bar{l} = 1$ is reached. **(B)** A steady state is reached with $\bar{l} = \rho(1-\rho)^{-1}$, with $0 < \rho < 1$. $\rho = \lambda(1 - 2\mu)/(\mu(1 - \lambda))$. This phase is bounded by $\mu = 1/2$ from above and by $\mu = \lambda/(1 + \lambda)$ from below. **(C)** There is no steady state for $Q^*(0)$, $Q^*(m)$, and thus $\bar{l} \rightarrow \infty$.

much a contiguous region of contacts between the interface and the membrane can grow before the membrane moves away, and how likely that structure will persist until contact with the membrane returns. We have observed such a structure in the simulations (Figure 5.13), and this model highlights the importance of the dynamics of this structure in characterising the phase of the system.

5.7 Discussion and Conclusions

In summary, the MI model of an interface growing towards a diffusing wall, the membrane, has revealed an interesting set of phases observed as the bias of the diffusion of the wall is varied. I have shown that when $u < u_1 \simeq 0.62$ the system is in the smooth phase, where the interface has a very narrow width and is in contact with the membrane at a number of points proportional to the size of

the interface. In this phase, the velocity of the membrane is determined by the velocity at which the interface grows due to the effect of the interface pushing the membrane.

This continues on into the rough phase, when $u_1 < u < u_2 = 3/4$, where the membrane velocity is still determined by the speed at which the interface pushes it at. Interestingly, the interface has reached its maximal velocity in this phase, which is greater than the natural drift velocity $2u - 1$ of the membrane, so increasing u has no effect on the velocity of the membrane. We also see that the interface in this regime is rough, its width having roughness exponent $1/2$, and has a subextensive number of contacts with the membrane. We have seen from visualisations of the underlying ASEP array that in this phase the parts of the interface in contact with the membrane are typically localised and contiguous, indicating that there are strong correlations in the distances from the membrane of the interface points closest to it.

As u is increased further, the drift velocity of the membrane becomes greater than the velocity of the interface once $u > u_2 = 3/4$. At this point the membrane ‘escapes’: the membrane and the interface decouple, with the membrane drifting away and the interface evolving as an unobstructed KPZ interface.

It is clear that the fluctuations in the height, the width, play an important role in the phases observed, alongside the dynamics of the membrane. When the membrane is in contact with a smooth interface, it inhibits growth of large portions of the interface. Then, when the membrane makes an excursion away from the interface, the interface can grow unhindered and its width can increase. Once the membrane returns to a wide interface, it can only inhibit further growth of the highest interface points, and so with an increased width growth within the interface is inhibited less by the membrane. The membrane bias parameter u then controls how often the membrane inhibits the roughening of the interface by controlling how much time the two are in contact with each other.

The simple mean-field theory has given predictions of $u_1 = 0.5$ and $u_2 = 3/4$ which compare well with the numerical results. These predictions rely on observations of how much of the interface is in contact with the membrane, which tells us that this property of the system, namely C , plays an important role in the phase behaviour. The failure of this theory to correctly predict the right roughness of the interface in the rough phase tells us that the correlations between sites play

an important role, similarly to [88], and are crucial to understanding the phase behaviour of the system.

The importance of these correlations was revealed by the visualisations of which regions of the interface were jammed against the membrane (Figure 5.13). We developed a simple model based on two random walkers which describes how these jammed regions may grow or shrink when their growth is stochastically switched on and off by the effect of the diffusing membrane. The fact that this model showed three phases tells us that the amount by which these jammed regions are allowed to grow, determined by the interaction with the membrane, may be the key dynamical process influencing the structure of the observed smooth and rough bound phases.

An interesting result of the research in the context of Brownian ratchets is velocity profile that I have measured numerically. Just like in previous ratcheting models [88, 136], we have seen that there is a steady ratcheting velocity under the equivalent of a constant load force ($u < 1/2$), but more interesting is the velocity we see in the rough phase. In the rough phase, the ratcheting velocity, the velocity v_m of the membrane, no longer depends on the load force (membrane bias). Furthermore, we see that a steady state ratcheting velocity can be achieved under a pulling force ($u > 1/2$). To my knowledge, neither of these effects have been reported in the literature so far, and it may be that experimentally measuring the motility of a cell under a pulling force would yield some interesting results.

My view that the leading edge of the lamellipodium can be described by a KPZ interface is purely speculative. It would be very interesting to see whether the experimentally measured characteristics of the leading edge of the lamellipodium do indeed correspond to those of a KPZ interface or a different class altogether.

There are still questions addressed in this research that remain unanswered, particularly around the nature of the smooth and rough phase, possibly rough *phases*, and the associated phase transitions. Moving forwards in this research there are two clear avenues that can be taken.

The first is to obtain more numerical data, and data of a higher quality, particularly in and around the rough phase. Certainly with more sophisticated algorithms, and more system sizes, one could learn more about the roughness

exponent α and its dependence on u , as shown in Figure 5.11. Also, as made clear in Section 5.6, there seems to be an important role for the localised regions of contacts between the interface and the membrane. It would be useful to make more varied measurements of the spatial properties of these jammed regions, such as their lengths and how many of these regions there are, as well as giving some consideration to measuring the temporal properties of these regions, in particular their persistence and recurrence times.

The second avenue to explore would be to develop a more sophisticated theory to describe the dynamics. The natural next step is to try and introduce the RSOS constraint into the existing mean-field theory, to try and predict the correct scaling properties of the width. One way to do this, would be to use the transfer matrix formalism in a similar way as has been done in Ref [82–84, 109]. This is an approach that we have attempted, but have found problematic so far. By using the form for $P(y)$, given in (5.5.30), as the statistical weight for height y above the membrane at each point on the interface, one can use the transfer matrix to select only interfacial configurations with height differences of 1 between adjacent sites. In attempting this procedure we noticed that, upon including the full array of L sites in the theory described in Section 5.5, the simple ‘single-site’ mean-field master equation (5.5.1) is no longer correct, and requires modification in order to be consistent and physical. As of yet, we have not been able to solve the generating function which satisfies this master equation.

It is also worth noting previous theoretical approaches to analysing ratcheting dynamics, that may provide inspiration for possible theoretical descriptions of the MI model. In the original study of the Brownian ratchet a diffusion equation with non-local moves, similar to the ‘resetting’ in the model presented in Chapter 3, was solved to find the ratcheting velocity [136]. Also, in the study of the many-filament ratchet in Ref [88] it was found that specification of the statistics of the leading filament separately from the bulk filaments was necessary to obtain analytic predictions that agreed well with simulations.

In future work it may be of interest to consider in detail the effect that reducing the value of p less than 1 would have on the dynamics. This is easy to motivate from a biophysics point of view: in the lamellipodium both adsorption *and* desorption occur at the barbed ends of filaments, meaning they can shrink

as well as grow [139]. One could then ask questions about how the velocity of the membrane is effected, and perhaps whether there is an optimal pair of values for p and u which maximise the velocity of the bound interface and membrane.

One could also take further steps towards trying to compare more accurately how the growth in the MI model compares with growth seen in the lamellipodium. Appropriate values for the parameters p and u could be estimated to match the monomer adsorption and desorption rates of the actin monomers and the load forces or surface tensions measured in experiment. Furthermore, one would have to adapt the relative probabilities at which membrane and interface events are selected. In the implementation of the MI model a membrane event happened with probability $1/(N + 1)$ and an interface event happened with probability $N/(N + 1)$, which represents the case where the adsorption rate similar to the rate of diffusion. Experimental measurements for actin polymerisation rates [138] combined with reasonable estimates for the diffusion constant of the membrane [136] suggest that at the leading edge of the lamellipodium the membrane diffusion rate is much greater than that of actin adsorption. The appropriate modification to the event selection probabilities would be to select a membrane event with probability $\gamma/(\gamma + N)$ and an interface event with probability $N/(\gamma + N)$, with $\gamma \sim \mathcal{O}(N)$ or greater.

Chapter 6

Conclusions

In this thesis I have studied three distinct non-equilibrium mass transport models, with a view to understanding the role that stochasticity and fluctuations play in the dynamics of each. Despite the significant differences in the model definitions, for instance whether they are defined in discrete or continuous time and space, or whether they describe the dynamics of a single agent, many agents, or both, there are deep connections at the fundamental level between the processes seen in each. The studies of these different models have yielded sometime surprising results and given us some interesting insights.

The study of the effect of partial absorption (Chapter 3) at the target of a diffusive searcher which stochastically resets its position has shown this effect to be quite intuitive. The Mean Time to absorption (MTA) of the searcher increases with the amount of imperfection of the absorption and the temporal decay rate of the survival probability decreases with the amount of imperfection. Both of these results are fully consistent with our expectation that imperfect absorption at the target will increase the duration of the search. The results also showed that the consequence of partial absorption was an *additive* increase to the MTA with perfect absorption in such away that it is clear that the MTA is simply the sum of the mean time taken to the first incidence of the target's and searcher's positions and the mean time taken to be absorbed after this occurs.

The study of the Zero-Range Process (ZRP)-like mass transport model (Chapter 4) revealed the existence of a very interesting strong condensate phase. Above a critical hopping parameter $b_c \simeq 0.62$, which is independent of the mass density, a moving strong condensate exists at all densities. This condensate is

‘strong’ in that it contains a fraction of the total system mass that tends to 1 in the limit of infinite system size. What is particularly interesting about the mechanism that maintains this moving condensate is that it is a consequence of the dynamics of the subextensive fraction of mass that follows the condensate around in its ‘tail’. As long as these small units of mass hop fast enough relative to the condensate they can keep replenishing it while it sheds mass as it moves. From the mean-field analysis of the mass current in the tail of the condensate we found that the boundary condition that plays a crucial role in determining the value of b_c is actually directly related to the hopping mechanism we employ through the single unit of mass left behind. This leads us to speculate that the amount of mass left behind in the ‘backchip’ moves is the key feature influencing the dynamics and the value of b_c . Another interesting insight gained from the analysis of the tail currents was that, in the frame of the condensate, there seems to be a similarity between the tail dynamics and the dynamics of the Driven Asymmetric Contact Process (DACP) and thus the Directed Percolation (DP) universality class. Further evidence for this connection was seen from the divergence of the decay length in the tail. This decay length was measured to diverge with exponent $\simeq 1.69$, not much different to the temporal exponent measured at 1.7(2) in the DACP and the DP exponent $\nu_{\parallel} = 1.7338$. The divergence of this decay length at the transition is also interesting because we also measure a discontinuity in the order parameter at the transition, indicating that the transition is actually mixed-order, rather than first-order or continuous.

From the membrane-interface (MI) model (Chapter 5) we have found that the presence of the diffusing wall, the ‘membrane’, has had some surprising consequences for the growing interface. We see that, upon varying the bias in the random walk of the membrane, there are three distinct phases that the system is found in. When the bias $u > u_2 = 3/4$ we see that the membrane and interface decouple and in this unbound phase the interface grows like a Kardar-Parisi-Zhang (KPZ) interface. This transition value of $u_2 = 3/4$ was confirmed by the simple mean-field theory, as well as being easy to predict from simple physical arguments: once $u \geq 3/4$ the membrane’s average velocity is greater than that of the interface, and they separate. The smooth phase, seen when u is small is conceptually easy to understand. The bias in the membrane keeps it pressed up against the interface, and the interface pushes it along against its

preferred direction of motion. All parts of the interface push up close to the membrane, and so its width is smooth. In the rough phase, between the smooth and unbound phases the dynamics are very interesting, but difficult to analyse. In this phase we see that the number of contacts between the membrane and interface scales as $1/L$ and the roughness exponent of the width is approximately $1/2$. The numerical analysis of the transition value $u_1 \simeq 0.62$ has been difficult. Finite-size scaling has not been as reliable as in Chapter 4 and we have actually found numerically that the roughness exponent has an unexpected functional dependence on u . The theoretical analysis of this transition has also been difficult due to the important role played by spatial *and* temporal correlations across the interface and in the regions in contact with the membrane. Possibly the best indicator for the transition into the rough phase is the saturation of the interface current J and the membrane velocity v_m at $u \simeq 0.6$. There is still evidence of system size dependence of this value however, and it may be possible that in the $L \rightarrow \infty$ limit that the saturation occurs somewhere closer to $u = 0.5$. The saturation of the velocity in the rough phase however is one of the most interesting properties of this system. In this phase the interface cannot push any faster, but upon increasing u the velocity of the membrane is not great enough for it to escape the influence of the interface until $u = u_2 = 3/4$.

The research into the MI model is clearly not concluded. There are still unanswered questions surrounding the smooth to rough transition. More sophisticated numerical simulation would hopefully allow us to identify the critical value u_1 conclusively, but also give us an understanding of the nature of the phase transition. There is some indication from the analysis of the width that it is discontinuous between the smooth and rough phases, which would indicate the existence of a first-order transition. However, the current and membrane velocity change continuously from an increasing function of u to a constant saturation value and it is possible that the gradient of the current is discontinuous at this point, which would indicate a continuous transition. There is also some evidence of a diverging length scale in the length of the contiguous, ‘jammed’, regions of contacts between the membrane and interface. It would be useful in future to obtain numerical data specifically for analysing the properties of this feature, as well as to perform a more detailed numerical analysis of the dependence on u of the roughness exponent.

An avenue that has not been explored as fully as I would have liked is how well the MI model performs as a Brownian ratchet, and as a model specifically for motility of the lamellipodium. Although I have measured the membrane velocity, I have not yet been able to perform a detailed comparison between what I measure and what is seen in earlier Brownian ratchet models. One seemingly unique feature we have is the presence of a region of velocity which is independent of the applied force. Furthermore, a significant difference between the ratchet here and the many filament ratchet of Ref [88] is that we see little or no dependence of the membrane velocity on the system size.

Another speculative observation from the MI model is that the dynamics of the so-called jammed regions of the interface which are in contact with the membrane could be thought of as having behaviour similar to that of a contact process, and maybe points to the smooth-to-rough transition being part of the DP universality class. While the membrane is touching the interface, interface points that are adjacent to points of contact with the membrane can be ‘activated’ and become contact points themselves. This could be viewed as a contact process where active sites, the contact points, activate adjacent sites and make them contact points too. This kind of idea lends itself naturally to the continuous phase transition that I speculate that we see between the rough and smooth phases, although it may just as likely be that this phase transition belongs to a class unrelated to the DP class.

This is of course highly speculative, but the analogy to a contact process that can be made in both the moving condensate phase transition and the smooth-to-rough MI transition does at least highlight some phenomenological connections between the two models. It may also be that there is a connection between the MI model and the search process with resetting that was studied in Chapter 3. With a change of frame of reference, the steps taken by the membrane could instead be seen as the interface ‘resetting’ its position one unit backwards or forwards, while preserving its shape. Although this may not be quite the same thing as resetting, the features common to both are a diffusive process combined with a non-local move, or jump. The resetting of an interface has been studied in Ref [78], but in that case the profile was reset to a smooth, flat configuration. It may be of interest to analyse how the height of a growing interface is affected by local moves which preserve its shape.

In terms of general understanding that I have gained from the research presented here, there are two things that stand out. The first is the potentially important effects that a subextensive part of the system can have on the whole. For instance, in Chapter 4 it was the effect of the vanishing fraction of total mass that was found in the tail of the moving condensate that was responsible for its maintenance. Also, in the rough phase of the MI model the number of contacts between the membrane and the interface scales as $1/L$, but it is only these few contacts which are interacting with the membrane, while the rest of the interface grows seemingly unaware of it.

The second is the difference ways that boundary conditions play a role in the dynamics of these transport processes. In Chapter 3, the boundary condition specified the level of interaction between the target and the searcher, whereas in Chapter 5 the boundary condition in the analysis of the condensate tail was responsible for determining the value of the critical value b_c . These boundary conditions were also used to model two very different properties of the system. In the search process, the boundary condition specified a special property of a single point in the search space, whereas in the condensate analysis the boundary condition described a property of the behaviour of all the mass units in the system.

Finally, I think there are some interesting questions that arise as a follow on to all three models I have presented here. From the search process, it would be interesting to see how partial absorption affects a search strategy when the *location of the target* is less well defined. It is certainly true that normally a searcher at best only knows where a target is likely to be. One might guess that if the interaction between searcher and target is imperfect in some way, then a good search strategy would require the searcher to sample certain locations from the target distribution more often, whereas if the interaction is perfect, a single pass of each possible target location would suffice.

From the considerations of the effect of the boundary condition on the predicted value of b_c , it is natural to ask what happens when the boundary condition is different. This would correspond to a ‘backchip’ which leaves more than one unit of mass behind. So, generally one could ask what happens in

a system where single mass units hop when $n \leq a$, and $n - a$ particles hop when $n > a$. Furthermore, if a is increased to the *total particle number* N , then this model is equivalent to the ZRP again. Given that the ZRP exhibits a static condensate whereas our backchip model exhibits a moving condensate, what happens in between?

The last of the models, the MI model, actually provides a rare opportunity to ask some experimental questions. To a statistical physicist, perhaps the most interesting question would be whether the interfacial properties of the lamellipodium could actually be measured. If so, would it be part of the KPZ class? Or perhaps the DP class, which has historically lacked experimental realisation [81], only gaining such as recently as 2007 [165, 166]. Another possible experimental question to ask would be how the motility of cells and their leading lamellipodia are affected by a *pulling* force. This type of force corresponds to $u > 1/2$ in our model and it may be interesting to see whether a force independent velocity is observed.

Appendix A

Concepts, Methods and Models

A.1 Relationship Between the Occupancy Distribution and the First-Passage Probability

As discussed in Section 2.3.3, the explicit connection between the first-passage probability $F(x, t|x_0)$ and the occupation probability $P(x, t|x_0)$ for a random walker or diffusive particle is not obvious. In the following I outline a simple derivation of this connection.

First, we can say that for a random walk originating at x_0 to be at x at time step t , it must have reached x for the first time at an earlier time t' , and then returned to x after $t - t'$ additional steps. Although initially this may not seem to correctly correspond to how me imagine this process to occur, if one considers the case $t' = t$ then this describes the case where the walk first reaches x at t , which may be the the process one had in mind. We can express this as

$$P(x, t|x_0) = \delta_{x,x_0}\delta_{t,0} + \sum_{t' \leq t} F(x, t'|x_0)P(x, t - t'|x) , \quad (\text{A.1.1})$$

where the term of Kronecker deltas, $\delta_{x,x_0}\delta_{t,0}$, accounts for the initial condition $x = x_0$. In the second term, the factor $P(x, t - t'|x)$ represents the probability that, after reaching x at t' , the random walk will be found at this position again after a further $t - t'$ steps. A factor $F(x, t - t'|x)$ is not used because the walk is allowed to return any number of times in the intervening period. To solve this

equation, we define the generating functions

$$P(x, z|x_0) = \sum_{t=0}^{\infty} z^t P(x, t|x_0) , \quad F(x, z|x_0) = \sum_{t=0}^{\infty} z^t F(x, t|x_0) , \quad (\text{A.1.2})$$

before multiplying (A.1.1) by z^t and summing over all t . We can use the convolution relation

$$\sum_{t=0}^{\infty} z^t \sum_{t'=0}^t G(t') H(t-t') = \sum_{t'=0}^{\infty} \sum_{\tau=0}^{\infty} z^{t'} G(t') z^{\tau} H(\tau) = G(z) H(z) , \quad (\text{A.1.3})$$

and rearrange to find

$$P(x, z|x_0) = \delta_{x,0} + F(x, z|x_0) P(0, z|x_0) . \quad (\text{A.1.4})$$

From this, we see that

$$F(z, t|x_0) = \begin{cases} \frac{P(x, z|x_0)}{P(x_0, z|x_0)} , & x \neq 0 \\ 1 - \frac{1}{P(x_0, z|x_0)} , & x = 0 \end{cases} . \quad (\text{A.1.5})$$

From this expression, one could in theory perform the inverse transform to find $F(x, t|x_0)$, or simply use it directly to calculate the moments of the first-passage time (see e.g. [66, 127]).

A.2 Bose-Einstein Condensation

Condensation in the Zero-Range Process, as discussed in Section 2.5.1, has some similarities to the phenomenon of Bose-Einstein (BE) condensation (see e.g. [8, 42, 56, 137]), a phase transition seen at low temperatures in a Bose gas. A Bose gas is defined to be a gas of non-interacting, indistinguishable, bosonic particles, which we couple to a reservoir of particles and energy. Here we present a brief review of BE condensation and draw attention to connections between it and ZRP condensation.

A key property of the Bose gas is that the grand canonical partition \mathcal{Z} function

can be written as a product of single particle partition functions \mathcal{Z}_i of the quantum states i with energies ϵ_i :

$$\mathcal{Z} = \prod_i \mathcal{Z}_i . \quad (\text{A.2.1})$$

Now, for bosons

$$\mathcal{Z}_i = \frac{1}{1 - z \exp(-\epsilon_i/k_B T)} , \quad (\text{A.2.2})$$

where T is the temperature, k_B is Boltzmann's constant, and z is the fugacity, which controls the mean number of particles, and is related to the chemical potential by $z = \exp(\mu/k_B T)$. From \mathcal{Z}_i we can find the Bose-Einstein distribution for the mean occupancy \bar{n}_i of the single particle state i :

$$\bar{n}_i = z \frac{\partial \ln \mathcal{Z}_i}{\partial z} = \frac{1}{z^{-1} \exp(\epsilon_i/k_B T)} . \quad (\text{A.2.3})$$

On average, the bose gas contains $N(z)$ particles, which is related to \mathcal{Z} by

$$N(z) = z \frac{\partial \ln \mathcal{Z}}{\partial z} . \quad (\text{A.2.4})$$

The value of N is fixed by our choice of the fugacity z , which is a feature that plays a key role in the condensation transition in the ZRP. Also central to the ZRP condensation transition is the product form of \mathcal{Z} , described in (A.2.1), which we can exploit to write

$$N = \sum_i z \frac{\partial \ln \mathcal{Z}_i}{\partial z} = \sum_i \bar{n}_i , \quad (\text{A.2.5})$$

allowing us to express the mean number of particles N in the gas as the sum of the mean occupancies \bar{n}_i of the single particle states. Now, N can be approximated by the integral

$$N = \int_0^\infty \frac{g(\epsilon)}{z^{-1} \exp(\epsilon/k_B T) - 1} d\epsilon , \quad (\text{A.2.6})$$

using the density of states $g(\epsilon)$ (in 3D), which at low T can be written

$$g(\epsilon) \sim \epsilon^{1/2} = D\epsilon^{1/2} , \quad (\text{A.2.7})$$

where D is some constant, the details of which are unimportant. By solving (A.2.6) we can find $\mu(N, T)$ or $z(N, t)$ which gives the average number of particle

N at temperature T .

For low energy states, the average occupancy must still be positive, and so $z^{-1} - 1 > 0$, which is satisfied only if $\mu < 0$. Now, as one lowers T , to keep N fixed, $\mu \nearrow 0$. At some temperature, T_c , $\mu = 0$. By evaluating the integral (A.2.6) at $\mu = 0$, one finds

$$N = D(k_B T_c)^{3/2} I_0 , \quad (\text{A.2.8})$$

where

$$I_0 = \int_0^\infty \frac{x^{1/2}}{e^x - 1} dx \quad (\text{A.2.9})$$

is a constant¹. At temperatures below T_c however, we cannot solve (A.2.6) to find $\mu(N, T) \leq 0$ which would give us the right N . The resolution is to consider the occupancy of the ground state \bar{n}_0 with energy $\epsilon_0 = 0$. In the integral (A.2.6) $g(0) = 0$ and so when $T > T_c$ this state is not occupied and contributes nothing to N . When $T < T_c$, there is a maximum number of particles $N_c = D(k_B T_c)^{3/2} I_0$ that the energy states above the ground state can support, and so the remaining particles must go into the ground state. This is the phenomenon that we describe as “condensation”, which happens in a very similar way in the ZRP.

For completeness, one can calculate the occupancy of the ground state. When $T < T_c$,

$$N = \bar{n}_0 + \int_0^\infty \frac{g(\epsilon)}{\exp(\epsilon/k_B T) - 1} d\epsilon , \quad (\text{A.2.10})$$

which, using (A.2.8), can be written as

$$N = \bar{n}_0 + N \left(\frac{T}{T_c} \right)^{3/2} , \quad (\text{A.2.11})$$

and so

$$\bar{n}_0 = N \left(1 - \left(\frac{T}{T_c} \right)^{3/2} \right) . \quad (\text{A.2.12})$$

¹Explicitly, $I_0 = \zeta(3/2)\Gamma(3/2) \approx 2.31516$, where $\zeta(s)$ is the Riemann zeta function and $\Gamma(s)$ is the gamma function.

Appendix B

Partial Absorption in a Diffusive Search Process

B.1 Equivalence of the Radiation Boundary Condition and the Sink term.

In Section 3.2.3 we state without proof that the so-called radiation boundary condition [144, 147], given by

$$\left. \frac{\partial p(x, t)}{\partial x} \right|_{x=x_B} = \frac{a}{D} p(x_B, t) , \quad (\text{B.1.1})$$

is equivalent to the sink term

$$-a\delta(x - x_B)p(x, t) \quad (\text{B.1.2})$$

in the master equation

$$\frac{\partial p(x, t|z)}{\partial t} = D \frac{\partial^2 p(x, t|z)}{\partial x^2} - rp(x, t|z) + r\delta(x - x_0) - ap(0, t)\delta(x) , \quad (\text{B.1.3})$$

which is given in (3.2.15). We now proceed to show this equivalence, using a procedure which closely follows that in [176].

We begin by considering an absorbing region of width $2x_B$ centered at the origin of the real line, at the *boundaries* of which an incident diffusive particle

is absorbed with rate a . The master equation for the probability density of the particle in this system reads

$$\frac{\partial p(x, t)}{\partial t} = \frac{\partial^2 p(x, t)}{\partial x^2} - a\delta(x_B - |x|)p(x, t). \quad (\text{B.1.4})$$

We define the survival probability of the particle at time t as the integral over all space

$$n(t) = \int_{-\infty}^{+\infty} p(x, t)dx \quad (\text{B.1.5})$$

and probability that the particle is at a position $|x| > x_B + \epsilon$ as

$$m(t) = \int_{-\infty}^{-(x_B + \epsilon)} p(x, t)dx + \int_{x_B + \epsilon}^{\infty} p(x, t)dx. \quad (\text{B.1.6})$$

We assume that, far away from the absorbing region,

$$\left. \frac{\partial p(x, t)}{\partial x} \right|_{x \rightarrow \pm\infty} = 0 \quad (\text{B.1.7})$$

and perform the necessary integrals on (B.1.4) to obtain

$$\frac{\partial n(t)}{\partial t} = -a[p(-x_B, t) + p(x_B, t)] \quad (\text{B.1.8})$$

from (B.1.5), and

$$\frac{\partial m(t)}{\partial t} = D \left[\left. \frac{\partial p}{\partial x} \right|_{x=-x_B} - \left. \frac{\partial p}{\partial x} \right|_{x=x_B} \right] \quad (\text{B.1.9})$$

from (B.1.6). Now we demand that

$$\lim_{\epsilon \rightarrow 0} \frac{\partial m}{\partial t} = \frac{\partial n}{\partial t} \quad (\text{B.1.10})$$

to find

$$\left. \frac{\partial p}{\partial x} \right|_{x=\pm x_B} = \pm \frac{a}{D} p(\pm x_B, t), \quad (\text{B.1.11})$$

which is as the radiation boundary condition quoted above. Thus we have shown that a sink term of the form

$$-a\delta(x - x_B)p(x, t) \quad (\text{B.1.12})$$

in a master equation of the form of (3.2.15) is equivalent to the boundary condition (3.2.16).

B.2 MTA with a resetting position distribution $\mathcal{P}(x)$

Here we present the calculation of the MTA in the case where the searcher is reset to a position drawn from the general distribution $\mathcal{P}(x)$, which was discussed in Section 3.4.

In this case, the particle resets with rate r to a random position drawn from the distribution $\mathcal{P}(x)$. The resetting term $rq(x_0, t)$ in the backward master equation (3.2.18) becomes $r \int dx \mathcal{P}(x)q(x, t)$ and so, for the survival probability $q(z, t)$, the master equation itself reads

$$\frac{\partial q(z, t)}{\partial t} = D \frac{\partial^2 q(z, t)}{\partial z^2} - rq(z, t) + r \int \mathcal{P}(x)q(x, t)dx - aq(0, t)\delta(z). \quad (\text{B.2.1})$$

The calculation of the MTA is a straightforward generalisation of that presented in Section 3.4 with resetting to a single position x_0 . The Laplace transformation of the master equation yields

$$D \frac{\partial^2 \tilde{q}(z, s)}{\partial z^2} - (r + s)\tilde{q}(z, s) = -1 - r \int \mathcal{P}(x)\tilde{q}(x, s)dx + a\tilde{q}(0, s)\delta(z). \quad (\text{B.2.2})$$

Comparing this with

$$D \frac{\partial^2 \tilde{q}(z, s)}{\partial z^2} - (r + s)\tilde{q}(z, s) = -1 - r\tilde{q}(x_0, s) + a\tilde{q}(0, s)\delta(z). \quad (\text{B.2.3})$$

as given in (3.3.2) we see that the expression is the same, except in the second term $\tilde{q}(x_0, s)$ has been replaced with an integral over a dummy variable x . Therefore we can make a direct substitution into the previous solution to find

$$\tilde{q}(z, s) = -\frac{a\tilde{q}(0, s)}{2\alpha D} e^{-\alpha|z|} + \frac{1 + r \int \mathcal{P}(x)\tilde{q}(x, s)dx}{r + s} \quad (\text{B.2.4})$$

and, by setting $s = 0$,

$$T(z) = -\frac{aT(0)}{2\alpha_0 D} e^{-\alpha_0|z|} + \frac{1}{r} + \int \mathcal{P}(x)T(x)dx . \quad (\text{B.2.5})$$

A self consistent solution

$$T(0) = \left(1 + \frac{a}{2\alpha_0 D}\right)^{-1} \left(\frac{1}{r} + F\right) , \quad (\text{B.2.6})$$

where

$$F = \int \mathcal{P}(x)T(x)dx , \quad (\text{B.2.7})$$

is found by setting $z = 0$. Now we can write

$$T(z) = \left(\frac{1}{r} + F\right) \left(1 - \left(\frac{2\alpha_0 D}{a} + 1\right)^{-1} e^{-\alpha_0|z|}\right) , \quad (\text{B.2.8})$$

which we can multiply on both sides by $\mathcal{P}(x)$ and integrate with respect to x to find

$$F = \left(\frac{1}{r} + F\right) \left(1 - \int dz \mathcal{P}(z) \left(\frac{2\alpha_0 D}{a} + 1\right)^{-1} e^{-\alpha_0|z|}\right) , \quad (\text{B.2.9})$$

and thus

$$F = \frac{1 - I}{rI} , \quad (\text{B.2.10})$$

where

$$I = \int dz \mathcal{P}(z) e^{-\alpha_0|z|} \left(\frac{2\alpha_0 D}{a} + 1\right)^{-1} . \quad (\text{B.2.11})$$

The stationary distribution $p^*(x)$ of the diffusive process with resetting but without any absorption [57], is given by the integral

$$p^*(x) = \frac{\alpha_0}{2} \int dx' \mathcal{P}(x') e^{-\alpha_0|x-x'|} , \quad (\text{B.2.12})$$

which we use to write

$$I = \left(\frac{2\alpha_0 D}{a} + 1\right)^{-1} \frac{2}{\alpha_0} p^*(0) \quad (\text{B.2.13})$$

Now we can use (B.2.13) to find F , given by (B.2.10), and then F and (B.2.8) to

find

$$T(z) = \frac{1}{2\sqrt{rD}p^*(0)} \left(1 - e^{-\alpha_0|z|}\right) + \frac{\phi_0}{\sqrt{rD}} \frac{1}{p^*(0)}, \quad (\text{B.2.14})$$

the result quoted in (3.4.13).

Appendix C

Membrane-Interface Model

C.1 Width Scaling

In Section 5.5.3 we presented the finding that the width W scaled linearly with system size L , i.e. $W \sim L$. In this section we present the calculation that shows this, which is essentially just a sequence of Taylor expansions.

The calculation begins with the expression

$$W^2 = \bar{y} \left(\frac{z_+ + 1}{z_+ - 1} - \bar{y} \right) . \quad (\text{C.1.1})$$

for the width from (5.5.39). To learn what scaling the width has, to leading order in L , we must first find the leading order L scaling of z_{\pm} and \bar{y} . In the bound phase, for b to be finite we require $P(0) \sim \mathcal{O}\left(\frac{1}{L}\right) = \frac{-\ln c}{L}$. The expression (5.5.29)

$$P(1) = \frac{P(0)}{z_+(1 + z_-)} . \quad (\text{C.1.2})$$

tells us that $P(1) \propto P(0)$ and so, using the result from (5.5.8) that

$$2P(1) + (1 + b)P(0) = 2 + b - a , \quad (\text{C.1.3})$$

we find that

$$2 + b - a \propto P(0) \propto \frac{1}{L} . \quad (\text{C.1.4})$$

Using this and $a = 4u$ we can then write

$$1 + b = 4u - 1 + \frac{d}{L}, \quad (\text{C.1.5})$$

where $d = -\ln c$ is a constant. To proceed we will first calculate the scaling of z_{\pm} and then \bar{y} before combining these results to find W .

Using (C.1.5) we find

$$\begin{aligned} z_{\pm} &= \frac{(1+b) \pm [(1+b)^2 + 4a]^{1/2}}{2a} \\ z_{\pm} &= \frac{(4u-1) + \frac{d}{L} \pm [(4u-1)^2 + 2(4u-1)\frac{d}{L} + 16u + \mathcal{O}(\frac{1}{L^2})]^{1/2}}{8u} \\ z_{\pm} &= \frac{(4u-1) + \frac{d}{L} \pm [(4u+1)^2 + 2(4u-1)\frac{d}{L} + \mathcal{O}(\frac{1}{L^2})]^{1/2}}{8u} \\ z_{\pm} &= \frac{(4u-1) + \frac{d}{L} \pm (4u+1) \left[1 + 2\frac{(4u-1)}{(4u+1)^2} \frac{d}{L} + \mathcal{O}(\frac{1}{L^2}) \right]^{1/2}}{8u} \\ z_{\pm} &= \frac{(4u-1) + \frac{d}{L} \pm (4u+1) \left[1 + \frac{(4u-1)}{(4u+1)^2} \frac{d}{L} + \mathcal{O}(\frac{1}{L^2}) \right]}{8u}. \end{aligned} \quad (\text{C.1.6})$$

Then, considering z_+ and z_- explicitly, we find

$$\begin{aligned} z_+ &= \frac{8u}{8u} + \frac{1}{8u} \left[1 + \frac{(4u-1)}{(4u+1)} \right] \frac{d}{L} \\ &= 1 + \frac{1}{(4u+1)} \frac{d}{L}, \end{aligned} \quad (\text{C.1.7})$$

and

$$\begin{aligned} z_- &= -\frac{2}{8u} + \frac{1}{8u} \left[1 - \frac{(4u-1)}{(4u+1)} \right] \frac{d}{L} \\ &= -\frac{2}{8u} + \frac{2}{8u} \left[\frac{1}{(4u+1)} \right] \frac{d}{L} \\ &= -\frac{1}{4u} \left[1 - \frac{1}{(4u+1)} \frac{d}{L} \right]. \end{aligned} \quad (\text{C.1.8})$$

For convenience, we define

$$D = \frac{d}{4u+1} = \frac{-\ln c}{4u+1}. \quad (\text{C.1.9})$$

We can then write

$$z_+ \simeq 1 + \frac{D}{L}, \quad (\text{C.1.10})$$

$$1 + z_- \simeq \frac{(4u-1)}{4u} \left(1 + \frac{1}{(4u-1)} \frac{D}{L} \right), \quad (\text{C.1.11})$$

and

$$z_+ - 1 \simeq \frac{D}{L} \left(1 + \frac{\kappa}{D} \frac{1}{L} \right), \quad (\text{C.1.12})$$

where κ is the coefficient of the order L^{-2} term in the expansion of z_+ , which we have not calculated explicitly.

We can now substitute these into the expression (5.5.34) for \bar{y} to find

$$\begin{aligned} \bar{y} &= \left(\frac{-\ln c}{L} \right) \left(1 + \frac{D}{L} \right) \left(\frac{4u}{4u-1} \right) \left(1 + \frac{1}{4u-1} \frac{D}{L} \right)^{-1} \left(\frac{L}{D} \right)^2 \left(1 + \frac{\kappa}{D} \frac{1}{L} \right)^{-2} \\ &= (-\ln c) \frac{4u}{4u-1} \frac{L}{D^2} \left(1 + \frac{D}{L} \right) \left(1 - \frac{1}{4u-1} \frac{D}{L} \right) \left(1 - \frac{2\kappa}{D} \frac{1}{L} \right), \end{aligned} \quad (\text{C.1.13})$$

or, neglecting terms $\mathcal{O}(1/L)$ and smaller,

$$\begin{aligned} \frac{\bar{y}}{L} &= (-\ln c) \frac{4u}{4u-1} \frac{1}{D^2} \left(1 + \frac{4u-2}{4u-1} \frac{D}{L} - \frac{2\kappa}{D} \frac{1}{L} + \mathcal{O}\left(\frac{1}{L^2}\right) \right) \\ &= \frac{(-\ln c)}{D^2} \frac{4u}{4u-1} \left(1 + \left[\frac{4u-2}{4u-1} D - \frac{2\kappa}{D} \right] \frac{1}{L} + \mathcal{O}\left(\frac{1}{L^2}\right) \right). \end{aligned} \quad (\text{C.1.14})$$

We see that, to leading order in L ,

$$\bar{y} = \frac{(-\ln c)}{D^2} \frac{4u}{4u-1} L, \quad (\text{C.1.15})$$

and so \bar{y} scales *linearly* with L .

We now proceed to calculate the scaling of the width W , which as defined in (C.1.1). To simplify the calculation, discarding $\mathcal{O}(1/L^2)$ terms from (C.1.14), we

write

$$\bar{y} = Y(L + \gamma) , \quad (\text{C.1.16})$$

where

$$Y = \frac{(-\ln c)}{D^2} \frac{4u}{4u - 1} \quad (\text{C.1.17})$$

and

$$\gamma = \frac{4u - 2}{4u - 1} D - \frac{2\kappa}{D} . \quad (\text{C.1.18})$$

Also, from (C.1.7), we can write

$$z_+ + 1 \simeq 2 + \frac{D}{L} , \quad (\text{C.1.19})$$

using (C.1.9). As given in (C.1.12), we already have an expression for $z_+ - 1$ up to order L^{-2} . Thus we can write

$$\begin{aligned} W^2 &= Y(L + \gamma) \left[\left(2 + \frac{D}{L} \right) \frac{L}{D} \left(1 - \frac{\kappa}{D} \frac{1}{L} \right) - Y(L + \gamma) \right] \\ &= Y(L + \gamma) \left[\frac{L}{D} \left(2 + \frac{D}{L} - \frac{2\kappa}{D} \frac{1}{L} \right) - YL - Y\gamma + \mathcal{O}\left(\frac{1}{L}\right) \right] \\ &= Y(L + \gamma) \left[\frac{2L}{D} + 1 - \frac{2\kappa}{D^2} - YL - Y\gamma + \mathcal{O}\left(\frac{1}{L}\right) \right] \\ &= Y(L + \gamma) \left[\left(\frac{2}{D} - Y \right) L + \left(1 - \frac{2\kappa}{D^2} - Y\gamma \right) + \mathcal{O}\left(\frac{1}{L}\right) \right] \\ &= Y \left[\left(\frac{2}{D} - Y \right) L^2 + \left(\gamma \left(\frac{2}{D} - Y \right) + \left(1 - \frac{2\kappa}{D^2} - Y\gamma \right) \right) L + \mathcal{O}\left(\frac{1}{L}\right) \right] , \end{aligned} \quad (\text{C.1.20})$$

and then dividing through by L^2 we find

$$\begin{aligned} \frac{W^2}{L^2} &= Y \left[\frac{2 - YD}{D} + \left(\gamma \left(\frac{2 - DY}{D} \right) + \left(\frac{D^2(1 - Y\gamma) - 2\kappa}{D^2} \right) \right) \frac{1}{L} + \mathcal{O}\left(\frac{1}{L^2}\right) \right] \\ &= \frac{Y}{D^2} \left[D(2 - YD) + \left(\gamma D(2 - DY) + D^2(1 - Y\gamma) - 2\kappa \right) \frac{1}{L} + \mathcal{O}\left(\frac{1}{L^2}\right) \right] \\ &= \frac{Y}{D^2} \left[D(2 - YD) + \left((1 - 2\gamma Y)D^2 + 2\gamma D - 2\kappa \right) \frac{1}{L} + \mathcal{O}\left(\frac{1}{L^2}\right) \right] . \end{aligned} \quad (\text{C.1.21})$$

So, to leading order in L ,

$$W \simeq \sqrt{\frac{Y(2 - YD)}{D}} L . \quad (\text{C.1.22})$$

Thus, we have found that this model predicts that W scales linearly with L .

For completeness, we can calculate the prefactor using earlier definitions. From the definition (C.1.17) of Y we have

$$\frac{Y(2 - YD)}{D} = \frac{(-\ln c)}{D^3} \left(\frac{4u}{4u - 1} \right) \left[2 + \frac{(\ln c)}{D} \left(\frac{4u}{4u - 1} \right) \right] . \quad (\text{C.1.23})$$

Next, by simplifying using (C.1.9), we find

$$\frac{Y(2 - YD)}{D} = \frac{8u}{D^2} (1 - 2u) , \quad (\text{C.1.24})$$

and by substituting D in explicitly we find that this prefactor

$$\frac{Y(2 - YD)}{D} = \frac{8u(4u - 1)^2(1 - 2u)}{(\ln c)^2} . \quad (\text{C.1.25})$$

Appendix A. Membrane-Interface Model

Bibliography

- [1] ABRAHAM, V. C., KRISHNAMURTHI, V., TAYLOR, D. L., and LANNI, F. The Actin-Based Nanomachine at the Leading Edge of Migrating Cells . *Biophysical Journal* **77** (1999) pp. 1721 .
- [2] ABRAMSON, G. and WIO, H. S. Time behaviour for diffusion in the presence of static imperfect traps. *Chaos, Solitons & Fractals* **6** (1995) pp. 1 . Complex Systems in Computational Physics.
- [3] ALA-NISSILA, T., HJELT, T., KOSTERLITZ, J. M., and VENLINEN, O. Scaling exponents for kinetic roughening in higher dimensions. *Journal of Statistical Physics* **72** (1993) pp. 207.
- [4] ALBERTS, B., BRAY, D., HOPKINS, K., JOHNSON, A., LEWIS, J., RAFF, M., ROBERTS, K., , and WALTER, P. *Essential Cell Biology. (3 ed.)*. Garland Press: New York, 2009.
- [5] ANGEL, A. G., EVANS, M. R., LEVINE, E., and MUKAMEL, D. Critical phase in nonconserving zero-range processes and rewiring networks. *Phys. Rev. E* **72** (2005) p. 046132.
- [6] ARNDT, P. F., HEINZEL, T., and RITTENBERG, V. Spontaneous breaking of translational invariance in one-dimensional stationary states on a ring. *Journal of Physics A: Mathematical and General* **31** (1998) p. L45.
- [7] ARNDT, P. F., HEINZEL, T., and RITTENBERG, V. Spontaneous Breaking of Translational Invariance and Spatial Condensation in Stationary States on a Ring. I. The Neutral System. *Journal of Statistical Physics* **97** (1999) pp. 1.
- [8] BAIERLEIN, R. *Thermal physics*. Cambridge University Press, 1999.
- [9] BAIOD, R., KESSLER, D., RAMANLAL, P., SANDER, L., and SAVIT, R. Dynamical scaling of the surface of finite-density ballistic aggregation. *Phys. Rev. A* **38** (1988) pp. 3672.
- [10] BAR, A. and MUKAMEL, D. Mixed-Order Phase Transition in a One-Dimensional Model. *Phys. Rev. Lett.* **112** (2014) p. 015701.
- [11] BAR, A. and MUKAMEL, D. Mixed order transition and condensation in an exactly soluble one dimensional spin model. *Journal of Statistical Mechanics: Theory and Experiment* **2014** (2014) p. P11001.

BIBLIOGRAPHY

- [12] BARABÁSI, A.-L. and STANLEY, H. E. *Fractal concepts in surface growth.* Cambridge university press, 1995.
- [13] BARTUMEUS, F. and CATALAN, J. Optimal search behavior and classic foraging theory. *J. Phys. A: Math. Theor.* **42** (2009) p. 434002.
- [14] BAXTER, G. J., DOROGOVTSEV, S. N., GOLTSEV, A. V., and MENDES, J. F. F. Avalanche Collapse of Interdependent Networks. *Phys. Rev. Lett.* **109** (2012) p. 248701.
- [15] BEN-NAIM, E. and KRAPIVSKY, P. L. Cluster approximation for the contact process. *Journal of Physics A: Mathematical and General* **27** (1994) p. L481.
- [16] BEN-NAIM, E., REDNER, S., and WEISS, G. H. Partial absorption and virtual traps. *J. Stat. Phys.* **71** (1993) pp. 75.
- [17] BÉNICHOU, O., KAFRI, Y., SHEINMAN, M., and VOITURIEZ, R. Searching Fast for a Target on DNA without Falling to Traps. *Phys. Rev. Lett.* **103** (2009) p. 138102.
- [18] BINDER, K. Finite size scaling analysis of ising model block distribution functions. *Zeitschrift fr Physik B Condensed Matter* **43** (1981) pp. 119.
- [19] BINNEY, J. J., DOWRICK, N. J., FISHER, A. J., and NEWMAN, M. *The theory of critical phenomena: an introduction to the renormalization group.* Oxford University Press, Inc., 1992.
- [20] BLUMEN, A., ZUMOFEN, G., and KLAFTER, J. Target annihilation by random walkers. *Phys. Rev. B* **30** (1984) pp. 5379.
- [21] BLYTHE, R. A. and BRAY, A. J. Survival probability of a diffusing particle in the presence of Poisson-distributed mobile traps. *Phys. Rev. E* **67** (2003) p. 041101.
- [22] BLYTHE, R. A. and EVANS, M. R. Nonequilibrium steady states of matrix-product form: a solver's guide. *Journal of Physics A: Mathematical and Theoretical* **40** (2007) p. R333.
- [23] BLYTHE, R. A., EVANS, M. R., COLAIORI, F., and ESSLER, F. H. L. Exact solution of a partially asymmetric exclusion model using a deformed oscillator algebra. *Journal of Physics A: Mathematical and General* **33** (2000) p. 2313.
- [24] BOAS, M. L. *Mathematical methods in the physical sciences.* Wiley, 2006.
- [25] BORTZ, A., KALOS, M., and LEBOWITZ, J. A new algorithm for Monte Carlo simulation of Ising spin systems. *Journal of Computational Physics* **17** (1975) pp. 10 .
- [26] BOUCHAUD, J. P. and CATES, M. E. Self-consistent approach to the Kardar-Parisi-Zhang equation. *Phys. Rev. E* **47** (1993) pp. R1455.

- [27] BRACKLEY, C. A., CATES, M. E., and MARENDOZZO, D. Intracellular Facilitated Diffusion: Searchers, Crowders, and Blockers. *Phys. Rev. Lett.* **111** (2013) p. 108101.
- [28] BRAMSON, M. and LEBOWITZ, J. L. Asymptotic Behavior of Densities in Diffusion-Dominated Annihilation Reactions. *Phys. Rev. Lett.* **61** (1988) pp. 2397.
- [29] BRAMSON, M. and LEBOWITZ, J. L. Asymptotic Behavior of Densities in Diffusion-Dominated Annihilation Reactions. *Phys. Rev. Lett.* **62** (1989) pp. 694.
- [30] BRAMSON, M. and LEBOWITZ, J. L. Asymptotic behavior of densities for two-particle annihilating random walks. *Journal of Statistical Physics* **62** (1991) pp. 297.
- [31] BRAY, A. J. and BLYTHE, R. A. Exact Asymptotics for One-Dimensional Diffusion with Mobile Traps. *Phys. Rev. Lett.* **89** (2002) p. 150601.
- [32] BRAY, D. *Cell movements: from molecules to motility*. Garland Science, 2001.
- [33] BROADBENT, S. R. and HAMMERSLEY, J. M. Percolation processes. *Mathematical Proceedings of the Cambridge Philosophical Society* **53** (1957) pp. 629.
- [34] BURDA, Z., JOHNSTON, D., JURKIEWICZ, J., KAMIŃSKI, M., NOWAK, M. A., PAPP, G., and ZAHED, I. Wealth condensation in Pareto macroeconomies. *Phys. Rev. E* **65** (2002) p. 026102.
- [35] BURGERS, J. M. *Statistical problems connected with asymptotic solutions of the one-dimensional nonlinear diffusion equation*. Springer, 1972.
- [36] CHAIKIN, P. M. and LUBENSKY, T. C. *Principles of condensed matter physics*. Cambridge University Press, 2000.
- [37] CHOWDHURY, D., SANTEN, L., and SCHADSCHNEIDER, A. Statistical physics of vehicular traffic and some related systems. *Physics Reports* **329** (2000) pp. 199 .
- [38] CHOWDHURY, D., SCHADSCHNEIDER, A., and NISHINARI, K. Physics of transport and traffic phenomena in biology: from molecular motors and cells to organisms. *Physics of Life Reviews* **2** (2005) pp. 318 .
- [39] CONCANNON, R. J. and BLYTHE, R. A. Spatiotemporally Complete Condensation in a Non-Poissonian Exclusion Process. *Phys. Rev. Lett.* **112** (2014) p. 050603.
- [40] COOPER, J. A. and SCHAFER, D. A. Control of actin assembly and disassembly at filament ends. *Current Opinion in Cell Biology* **12** (2000) pp. 97 .
- [41] CORWIN, I. The Kardar-Parisi-Zhang Equation and Universality Class. *Random Matrices: Theory and Applications* **01** (2012) p. 1130001.

BIBLIOGRAPHY

- [42] COSTA, A. *Phase Transitions in Low Dimensional Driven Systems*. Ph.D. thesis, The University of Edinburgh, 2012.
- [43] COSTA, A., BLYTHE, R. A., and EVANS, M. R. Discontinuous transition in a boundary driven contact process. *Journal of Statistical Mechanics: Theory and Experiment* **2010** (2010) p. P09008.
- [44] DERRIDA, B., DOMANY, E., and MUKAMEL, D. An exact solution of a one-dimensional asymmetric exclusion model with open boundaries. *Journal of Statistical Physics* **69** (1992) pp. 667. 10.1007/BF01050430.
- [45] DERRIDA, B. and EVANS, M. R. Bethe ansatz solution for a defect particle in the asymmetric exclusion process. *Journal of Physics A: Mathematical and General* **32** (1999) p. 4833.
- [46] DERRIDA, B., EVANS, M. R., HAKIM, V., and PASQUIER, V. Exact solution of a 1D asymmetric exclusion model using a matrix formulation. *Journal of Physics A: Mathematical and General* **26** (1993) p. 1493.
- [47] DERRIDA, B., EVANS, M. R., and MUKAMEL, D. Exact diffusion constant for one-dimensional asymmetric exclusion models. *Journal of Physics A: Mathematical and General* **26** (1993) p. 4911.
- [48] DERRIDA, B., JANOWSKY, S., LEBOWITZ, J., and SPEER, E. Exact solution of the totally asymmetric simple exclusion process: Shock profiles. *Journal of Statistical Physics* **73** (1993) pp. 813.
- [49] DURANG, X., HENKEL, M., and PARK, H. The statistical mechanics of the coagulation-diffusion process with a stochastic reset. *Journal of Physics A: Mathematical and Theoretical* **47** (2014) p. 045002.
- [50] EDWARDS, S. F. and WILKINSON, D. R. The Surface Statistics of a Granular Aggregate. *Proceedings of the Royal Society of London. A. Mathematical and Physical Sciences* **381** (1982) pp. 17.
- [51] EUTENEUER, U. and SCHLIWA, M. Persistent, directional motility of cells and cytoplasmic fragments in the absence of microtubules. *Nature* **310** (1984) pp. 58.
- [52] EVANS, M. and BLYTHE, R. Nonequilibrium dynamics in low-dimensional systems. *Physica A: Statistical Mechanics and its Applications* **313** (2002) pp. 110 . Fundamental Problems in Statistical Physics.
- [53] EVANS, M., LEVINE, E., MOHANTY, P., and MUKAMEL, D. Modelling one-dimensional driven diffusive systems by the Zero-Range Process. *The European Physical Journal B - Condensed Matter and Complex Systems* **41** (2004) pp. 223.
- [54] EVANS, M. and SUGDEN, K. An exclusion process for modelling fungal hyphal growth. *Physica A: Statistical Mechanics and its Applications* **384** (2007) pp. 53
- .

- [55] EVANS, M. R. Phase transitions in one-dimensional nonequilibrium systems. *Brazilian Journal of Physics* **30** (2000) pp. 42 .
- [56] EVANS, M. R. and HANNEY, T. Nonequilibrium statistical mechanics of the zero-range process and related models. *Journal of Physics A: Mathematical and General* **38** (2005) p. R195.
- [57] EVANS, M. R. and MAJUMDAR, S. N. Diffusion with optimal resetting. *J. Phys. A: Math. Theor.* **44** (2011) p. 435001.
- [58] EVANS, M. R. and MAJUMDAR, S. N. Diffusion with Stochastic Resetting. *Phys. Rev. Lett.* **106** (2011) p. 160601.
- [59] EVANS, M. R. and MAJUMDAR, S. N. Diffusion with resetting in arbitrary spatial dimension. *Journal of Physics A: Mathematical and Theoretical* **47** (2014) p. 285001.
- [60] EVANS, M. R., MAJUMDAR, S. N., and ZIA, R. K. P. Factorized steady states in mass transport models. *Journal of Physics A: Mathematical and General* **37** (2004) p. L275.
- [61] EVANS, M. R., MAJUMDAR, S. N., and ZIA, R. K. P. Canonical Analysis of Condensation in Factorised Steady States. *Journal of Statistical Physics* **123** (2006) pp. 357.
- [62] EVANS, M. R. and WACLAW, B. Condensation in stochastic mass transport models: beyond the zero-range process. *Journal of Physics A: Mathematical and Theoretical* **47** (2014) p. 095001.
- [63] FAMILY, F. and MEAKIN, P. Kinetics of droplet growth processes: Simulations, theory, and experiments. *Phys. Rev. A* **40** (1989) pp. 3836.
- [64] FAMILY, F. and VICSEK, T. Scaling of the active zone in the Eden process on percolation networks and the ballistic deposition model. *Journal of Physics A: Mathematical and General* **18** (1985) p. L75.
- [65] FINN, C. B. *Thermal physics*, volume 5. CRC Press, 1993.
- [66] FISHER, M. E. Walks, walls, wetting, and melting. *Journal of Statistical Physics* **34** (1984) pp. 667.
- [67] FISHER, M. E. and BERKER, A. N. Scaling for first-order phase transitions in thermodynamic and finite systems. *Phys. Rev. B* **26** (1982) pp. 2507.
- [68] FLAMM, D. History and outlook of statistical physics, 1998. [arXiv:physics/9803005](https://arxiv.org/abs/physics/9803005).
- [69] GARDINER, C. *Stochastic Methods: A Handbook for the Natural and Physical Sciences*. Springer, 2010.

BIBLIOGRAPHY

- [70] DE GIER, J. and ESSLER, F. H. L. Bethe Ansatz Solution of the Asymmetric Exclusion Process with Open Boundaries. *Phys. Rev. Lett.* **95** (2005) p. 240601.
- [71] DE GIER, J. and ESSLER, F. H. L. Exact spectral gaps of the asymmetric exclusion process with open boundaries. *Journal of Statistical Mechanics: Theory and Experiment* **2006** (2006) p. P12011.
- [72] GINELLI, F., AHLERS, V., LIVI, R., MUKAMEL, D., PIKOVSKY, A., POLITI, A., and TORCINI, A. From multiplicative noise to directed percolation in wetting transitions. *Phys. Rev. E* **68** (2003) p. 065102.
- [73] GINELLI, F. and HINRICHSEN, H. Mean field theory for skewed height profiles in KPZ growth processes. *Journal of Physics A: Mathematical and General* **37** (2004) p. 11085.
- [74] GINELLI, F., HINRICHSEN, H., LIVI, R., MUKAMEL, D., and POLITI, A. Directed percolation with long-range interactions: Modeling nonequilibrium wetting. *Phys. Rev. E* **71** (2005) p. 026121.
- [75] GODRÈCHE, C. Dynamics of condensation in zero-range processes. *Journal of Physics A: Mathematical and General* **36** (2003) p. 6313.
- [76] GROSSKINSKY, S., SCHÜTZ, G. M., and SPOHN, H. Condensation in the Zero Range Process: Stationary and Dynamical Properties. *Journal of Statistical Physics* **113** (2003) pp. 389.
- [77] GUNAWARDENA, J. Models in biology: ‘accurate descriptions of our pathetic thinking’. *BMC biology* **12** (2014) p. 29.
- [78] GUPTA, S., MAJUMDAR, S. N., and SCHEHR, G. Fluctuating Interfaces Subject to Stochastic Resetting. *Phys. Rev. Lett.* **112** (2014) p. 220601.
- [79] HALPIN-HEALY, T. and ZHANG, Y.-C. Kinetic roughening phenomena, stochastic growth, directed polymers and all that. Aspects of multidisciplinary statistical mechanics. *Physics Reports* **254** (1995) pp. 215 .
- [80] HINRICHSEN, H. Non-equilibrium critical phenomena and phase transitions into absorbing states. *Advances in Physics* **49** (2000) pp. 815.
- [81] HINRICHSEN, H. On possible experimental realizations of directed percolation. *Brazilian Journal of Physics* **30** (2000) pp. 69 .
- [82] HINRICHSEN, H., LIVI, R., MUKAMEL, D., and POLITI, A. Model for Nonequilibrium Wetting Transitions in Two Dimensions. *Phys. Rev. Lett.* **79** (1997) pp. 2710.
- [83] HINRICHSEN, H., LIVI, R., MUKAMEL, D., and POLITI, A. First-order phase transition in a (1 + 1)-dimensional nonequilibrium wetting process. *Phys. Rev. E* **61** (2000) pp. R1032.

- [84] HINRICHSEN, H., LIVI, R., MUKAMEL, D., and POLITI, A. Wetting under nonequilibrium conditions. *Phys. Rev. E* **68** (2003) p. 041606.
- [85] HIRSCHBERG, O., MUKAMEL, D., and SCHÜTZ, G. M. Condensation in Temporally Correlated Zero-Range Dynamics. *Phys. Rev. Lett.* **103** (2009) p. 090602.
- [86] HIRSCHBERG, O., MUKAMEL, D., and SCHÜTZ, G. M. Motion of condensates in non-Markovian zero-range dynamics. *Journal of Statistical Mechanics: Theory and Experiment* **2012** (2012) p. P08014.
- [87] HIRSCHBERG, O., MUKAMEL, D., and SCHÜTZ, G. M. Emergent motion of condensates in mass-transport models. *Phys. Rev. E* **87** (2013) p. 052116.
- [88] HOHLFELD, E. and GEISSLER, P. L. Communication: Dominance of extreme statistics in a prototype many-body Brownian ratchet. *The Journal of Chemical Physics* **141** (2014) 161101.
- [89] HORVAI, P., NAZARENKO, S., and STEIN, T. Coalescence of Particles by Differential Sedimentation. *Journal of Statistical Physics* **130** (2008) pp. 1177.
- [90] HOUDAYER, J. and HARTMANN, A. K. Low-temperature behavior of two-dimensional Gaussian Ising spin glasses. *Phys. Rev. B* **70** (2004) p. 014418.
- [91] IMRY, Y. Finite-size rounding of a first-order phase transition. *Phys. Rev. B* **21** (1980) pp. 2042.
- [92] IMRY, Y. and BERGMAN, D. Critical Points and Scaling Laws for Finite Systems. *Phys. Rev. A* **3** (1971) pp. 1416.
- [93] ITÔ, K. and MCKEAN, H. P. Diffusion Processes and Their Sample Paths. *Grundlehren der Mathematischen Wissenschaften* **125** (1965).
- [94] JAFARPOUR, F. H. Exact solution of an exclusion model in the presence of a moving impurity on a ring. *Journal of Physics A: Mathematical and General* **33** (2000) p. 8673.
- [95] JAFARPOUR, F. H. Partially asymmetric simple exclusion model in the presence of an impurity on a ring. *Journal of Physics A: Mathematical and General* **33** (2000) p. 1797.
- [96] JENSEN, I. Low-density series expansions for directed percolation: I. A new efficient algorithm with applications to the square lattice. *Journal of Physics A: Mathematical and General* **32** (1999) p. 5233.
- [97] JEON, I. Phase transition for perfect condensation and instability under the perturbations on jump rates of the zero-range process. *Journal of Physics A: Mathematical and Theoretical* **43** (2010) p. 235002.
- [98] JEON, I., MARCH, P., and PITTEL, B. Size of the Largest Cluster under Zero-Range Invariant Measures. *The Annals of Probability* **28** (2000) pp. pp. 1162.

BIBLIOGRAPHY

- [99] JULLIEN, R. and MEAKIN, P. Simple Three-Dimensional Models for Ballistic Deposition with Restructuring. *EPL (Europhysics Letters)* **4** (1987) p. 1385.
- [100] KAFRI, Y., LEVINE, E., MUKAMEL, D., SCHÜTZ, G. M., and TÖRÖK, J. Criterion for Phase Separation in One-Dimensional Driven Systems. *Phys. Rev. Lett.* **89** (2002) p. 035702.
- [101] KARDAR, M., PARISI, G., and ZHANG, Y.-C. Dynamic Scaling of Growing Interfaces. *Phys. Rev. Lett.* **56** (1986) pp. 889.
- [102] KAUPUŽS, J., MAHNKE, R., and HARRIS, R. J. Zero-range model of traffic flow. *Phys. Rev. E* **72** (2005) p. 056125.
- [103] KIM, J. M. and KOSTERLITZ, J. M. Growth in a restricted solid-on-solid model. *Phys. Rev. Lett.* **62** (1989) pp. 2289.
- [104] KRAPIVSKY, P. L., REDNER, S., and LEYVRAZ, F. Connectivity of Growing Random Networks. *Phys. Rev. Lett.* **85** (2000) pp. 4629.
- [105] KRUG, J. Origins of scale invariance in growth processes. *Advances in Physics* **46** (1997) pp. 139.
- [106] KURCHAN, J. Non-equilibrium work relations. *Journal of Statistical Mechanics: Theory and Experiment* **2007** (2007) p. P07005.
- [107] LANDAU, L. The theory of phase transitions. *Nature* **138** (1936) pp. 840.
- [108] LEE, S. B., KIM, I. C., MILLER, C. A., and TORQUATO, S. Random-walk simulation of diffusion-controlled processes among static traps. *Phys. Rev. B* **39** (1989) pp. 11833.
- [109] VAN LEEUWEN, J. and HILHORST, H. Pinning of a rough interface by an external potential. *Physica A: Statistical Mechanics and its Applications* **107** (1981) pp. 319 .
- [110] LEVINE, E., MUKAMEL, D., and ZIV, G. The condensation transition in zero-range processes with diffusion. *Journal of Statistical Mechanics: Theory and Experiment* **2004** (2004) p. P05001.
- [111] LEVINE, E., ZIV, G., GRAY, L., and MUKAMEL, D. Phase Transitions in Traffic Models. *Journal of Statistical Physics* **117** (2004) pp. 819.
- [112] LIGHTHILL, M. J. and WHITHAM, G. B. On Kinematic Waves. II. A Theory of Traffic Flow on Long Crowded Roads. *Proceedings of the Royal Society of London. Series A. Mathematical and Physical Sciences* **229** (1955) pp. 317.
- [113] MACDONALD, C. T., GIBBS, J. H., and PIPKIN, A. C. Kinetics of biopolymerization on nucleic acid templates. *Biopolymers* **6** (1968) pp. 1.
- [114] MACHLUP, S. and ONSAGER, L. Fluctuations and Irreversible Process. II. Systems with Kinetic Energy. *Phys. Rev.* **91** (1953) pp. 1512.

- [115] MAJUMDAR, S. N., EVANS, M. R., and ZIA, R. K. P. Nature of the Condensate in Mass Transport Models. *Phys. Rev. Lett.* **94** (2005) p. 180601.
- [116] MAJUMDAR, S. N., KRISHNAMURTHY, S., and BARMA, M. Nonequilibrium Phase Transitions in Models of Aggregation, Adsorption, and Dissociation. *Phys. Rev. Lett.* **81** (1998) pp. 3691.
- [117] MAJUMDAR, S. N., KRISHNAMURTHY, S., and BARMA, M. Nonequilibrium Phase Transition in a Model of Diffusion, Aggregation, and Fragmentation. *Journal of Statistical Physics* **99** (2000) pp. 1.
- [118] MALY, I. V. and BORISY, G. G. Self-organization of a propulsive actin network as an evolutionary process. *Proceedings of the National Academy of Sciences* **98** (2001) pp. 11324.
- [119] MANRUBIA, S. C. and ZANETTE, D. H. Stochastic multiplicative processes with reset events. *Phys. Rev. E* **59** (1999) pp. 4945.
- [120] MEAKIN, P., RAMANLAL, P., SANDER, L. M., and BALL, R. C. Ballistic deposition on surfaces. *Phys. Rev. A* **34** (1986) pp. 5091.
- [121] MELCHERT, O. autoScale.py - A program for automatic finite-size scaling analyses: A user's guide, 2009. [arXiv:0910.5403](https://arxiv.org/abs/0910.5403).
- [122] MOGILNER, A. and OSTER, G. Cell motility driven by actin polymerization. *Biophysical Journal* **71** (1996) pp. 3030 .
- [123] MOGILNER, A. and OSTER, G. Force Generation by Actin Polymerization II: The Elastic Ratchet and Tethered Filaments. *Biophysical Journal* **84** (2003) pp. 1591 .
- [124] MONTANARI, A. and ZECCHINA, R. Optimizing Searches via Rare Events. *Phys. Rev. Lett.* **88** (2002) p. 178701.
- [125] MONTERO, M. and VILLARROEL, J. Monotonic continuous-time random walks with drift and stochastic reset events. *Phys. Rev. E* **87** (2013) p. 012116.
- [126] MONTROLL, E. W. Random walks in multidimensional spaces, especially on periodic lattices. *Journal of the Society for Industrial and Applied Mathematics* (1956) pp. 241.
- [127] MONTROLL, E. W. and WEISS, G. H. Random Walks on Lattices. II. *Journal of Mathematical Physics* **6** (1965) pp. 167.
- [128] MUELLER, M., JANKE, W., and JOHNSTON, D. A. Nonstandard Finite-Size Scaling at First-Order Phase Transitions. *Phys. Rev. Lett.* **112** (2014) p. 200601.
- [129] MUELLER, M., JANKE, W., and JOHNSTON, D. A. Transmuted Finite-size Scaling at First-order Phase Transitions. *Physics Procedia* **57** (2014) pp. 68 . Proceedings of the 27th Workshop on Computer Simulation Studies in Condensed Matter Physics (CSP2014).

BIBLIOGRAPHY

- [130] MULLINS, R. D., HEUSER, J. A., and POLLARD, T. D. The interaction of Arp2/3 complex with actin: Nucleation, high affinity pointed end capping, and formation of branching networks of filaments. *Proceedings of the National Academy of Sciences* **95** (1998) pp. 6181.
- [131] NATTERMANN, T. and TANG, L.-H. Kinetic surface roughening. I. The Kardar-Parisi-Zhang equation in the weak-coupling regime. *Phys. Rev. A* **45** (1992) pp. 7156.
- [132] NEWMAN, M. and BARKEMA, G. Monte Carlo methods in statistical physics. 1999. *New York: Oxford* **475** (1999).
- [133] O'LOAN, O. J., EVANS, M. R., and CATES, M. E. Jamming transition in a homogeneous one-dimensional system: The bus route model. *Phys. Rev. E* **58** (1998) pp. 1404.
- [134] ONSAGER, L. and MACHLUP, S. Fluctuations and Irreversible Processes. *Phys. Rev.* **91** (1953) pp. 1505.
- [135] OSHANIN, G., LINDENBERG, K., WIO, H. S., and BURLATSKY, S. Efficient search by optimized intermittent random walks. *J. Phys. A: Math. Theor.* **42** (2009) p. 434008.
- [136] PESKIN, C. S., ODELL, G. M., and OSTER, G. F. Cellular motions and thermal fluctuations: the Brownian ratchet. *Biophysical Journal* **65** (1993) pp. 316.
- [137] PLISCHKE, M. and BERGERSEN, B. *Equilibrium statistical physics*. World Scientific, 2006.
- [138] POLLARD, T. D. Rate constants for the reactions of ATP- and ADP-actin with the ends of actin filaments. *The Journal of Cell Biology* **103** (1986) pp. 2747.
- [139] POLLARD, T. D. and BORISY, G. G. Cellular Motility Driven by Assembly and Disassembly of Actin Filaments. *Cell* **112** (2003) pp. 453 .
- [140] RAJESH, R. and KRISHNAMURTHY, S. Effect of spatial bias on the nonequilibrium phase transition in a system of coagulating and fragmenting particles. *Phys. Rev. E* **66** (2002) p. 046132.
- [141] RAJESH, R. and MAJUMDAR, S. N. Exact phase diagram of a model with aggregation and chipping. *Phys. Rev. E* **63** (2001) p. 036114.
- [142] RAUCHER, D. and SHEETZ, M. P. Cell Spreading and Lamellipodial Extension Rate is Regulated by Membrane Tension. *The Journal of Cell Biology* **148** (2000) pp. 127.
- [143] REDNER, S. Random multiplicative processes: An elementary tutorial. *Am J Phys* **58** (1990) pp. 267.
- [144] REDNER, S. *A guide to first-passage processes*. Cambridge University Press, 2001.

- [145] REIF, F. *Fundamentals of statistical and thermal physics*. Waveland Press, 2009.
- [146] ROBERTS, G. E. and KAUFMAN, H. *Table of Laplace Transforms*. W.B. Saunders Company, 1966.
- [147] SANO, H. and TACHIYA, M. Partially diffusion-controlled recombination. *J. Chem. Phys.* **71** (1979) p. 1276.
- [148] SASAMOTO, T. One-dimensional partially asymmetric simple exclusion process with open boundaries: orthogonal polynomials approach. *Journal of Physics A: Mathematical and General* **32** (1999) p. 7109.
- [149] SASAMOTO, T. Density Profile of the One-Dimensional Partially Asymmetric Simple Exclusion Process with Open Boundaries. *Journal of the Physical Society of Japan* **69** (2000) pp. 1055.
- [150] SASAMOTO, T. One-dimensional partially asymmetric simple exclusion process on a ring with a defect particle. *Phys. Rev. E* **61** (2000) pp. 4980.
- [151] SCHADSCHNEIDER, A. Traffic flow: a statistical physics point of view. *Physica A: Statistical Mechanics and its Applications* **313** (2002) pp. 153 . Fundamental Problems in Statistical Physics.
- [152] SCHAFER, D. A., JENNINGS, P. B., and COOPER, J. A. Dynamics of capping protein and actin assembly in vitro: uncapping barbed ends by polyphosphoinositides. *The Journal of Cell Biology* **135** (1996) pp. 169.
- [153] SCHRÖDINGER, E. *What is life?: With mind and matter and autobiographical sketches*. Cambridge University Press, 1992.
- [154] SCHWARTZ, M. and EDWARDS, S. F. Nonlinear Deposition: a New Approach. *EPL (Europhysics Letters)* **20** (1992) p. 301.
- [155] SCHWARZKOPF, Y., EVANS, M. R., and MUKAMEL, D. Zero-range processes with multiple condensates: statics and dynamics. *Journal of Physics A: Mathematical and Theoretical* **41** (2008) p. 205001.
- [156] SHEINMAN, M., BÉNICHOU, O., KAFRI, Y., and VOITURIEZ, R. Classes of fast and specific search mechanisms for proteins on DNA. *Reports on Progress in Physics* **75** (2012) p. 026601.
- [157] SILK, J. and WHITE, S. The development of structure in the expanding universe. *The Astrophysical Journal* **223** (1978) pp. L59.
- [158] SMALL, J. V., ISENBERG, G., and CELIS, J. E. Polarity of actin at the leading edge of cultured cells. *Nature* **272** (1978) pp. 638.
- [159] SUGDEN, K. E. P. and EVANS, M. R. A dynamically extending exclusion process. *Journal of Statistical Mechanics: Theory and Experiment* **2007** (2007) p. P11013.

BIBLIOGRAPHY

- [160] SUGDEN, K. E. P., EVANS, M. R., POON, W. C. K., and READ, N. D. Model of hyphal tip growth involving microtubule-based transport. *Phys. Rev. E* **75** (2007) p. 031909.
- [161] SVITKINA, T. M. and BORISY, G. G. Arp2/3 Complex and Actin Depolymerizing Factor/Cofilin in Dendritic Organization and Treadmilling of Actin Filament Array in Lamellipodia. *The Journal of Cell Biology* **145** (1999) pp. pp. 1009.
- [162] SVITKINA, T. M., VERKHOVSKY, A. B., MCQUADE, K. M., and BORISY, G. G. Analysis of the Actin-Myosin II System in Fish Epidermal Keratocytes: Mechanism of Cell Body Translocation. *The Journal of Cell Biology* **139** (1997) pp. 397.
- [163] SZABO, A., LAMM, G., and WEISS, G. Localized partial traps in diffusion processes and random walks. *J. Stat. Phys.* **34** (1984) pp. 225.
- [164] SZABO, A., ZWANZIG, R., and AGMON, N. Diffusion-Controlled Reactions with Mobile Traps. *Phys. Rev. Lett.* **61** (1988) pp. 2496.
- [165] TAKEUCHI, K. A., KURODA, M., CHATÉ, H., and SANO, M. Directed Percolation Criticality in Turbulent Liquid Crystals. *Phys. Rev. Lett.* **99** (2007) p. 234503.
- [166] TAKEUCHI, K. A., KURODA, M., CHATÉ, H., and SANO, M. Experimental realization of directed percolation criticality in turbulent liquid crystals. *Phys. Rev. E* **80** (2009) p. 051116.
- [167] THOMPSON, A. G., TAILLEUR, J., CATES, M. E., and BLYTHE, R. A. Zero-range processes with saturated condensation: the steady state and dynamics. *Journal of Statistical Mechanics: Theory and Experiment* **2010** (2010) p. P02013.
- [168] TONER, J., TU, Y., and RAMASWAMY, S. Hydrodynamics and phases of flocks. *Annals of Physics* **318** (2005) pp. 170 . Special Issue.
- [169] TOUSSAINT, D. and WILCZEK, F. Particle-antiparticle annihilation in diffusive motion. *The Journal of Chemical Physics* **78** (1983) pp. 2642.
- [170] VERKHOVSKY, A. B., SVITKINA, T. M., and BORISY, G. G. Self-polarization and directional motility of cytoplasm. *Current Biology* **9** (1999) pp. 11 .
- [171] VOLD, M. J. A numerical approach to the problem of sediment volume. *J. Coll. Sci.* **14** (1959) pp. 168.
- [172] WACLAW, B. and EVANS, M. R. Explosive Condensation in a Mass Transport Model. *Phys. Rev. Lett.* **108** (2012) p. 070601.
- [173] WEISS, G. *Aspects and Applications of the Random Walk (Random Materials & Processes S.)*. North-Holland, 2005.

- [174] WHITEHOUSE, J., COSTA, A., BLYTHE, R. A., and EVANS, M. R. Maintenance of order in a moving strong condensate. *Journal of Statistical Mechanics: Theory and Experiment* **2014** (2014) p. P11029.
- [175] WHITEHOUSE, J., EVANS, M. R., and MAJUMDAR, S. N. Effect of partial absorption on diffusion with resetting. *Phys. Rev. E* **87** (2013) p. 022118.
- [176] WILEMSKI, G. and FIXMAN, M. General theory of diffusion-controlled reactions. *J. Chem. Phys.* **58** (1973) p. 4009.
- [177] WOLFF, K., BARRETT-FREEMAN, C., EVANS, M. R., GORYACHEV, A. B., and MARENDOZZO, D. Modelling the effect of myosin X motors on filopodia growth. *Physical Biology* **11** (2014) p. 016005.
- [178] YEOMANS, J. M. *Statistical mechanics of phase transitions*. Oxford University Press, 1992.
- [179] ZHU, J. and CARLSSON, A. Growth of attached actin filaments. *The European Physical Journal E* **21** (2006) pp. 209.

BIBLIOGRAPHY

Publications

Whitehouse, J., Evans, M. R. and Majumdar, S. N. Effect of partial absorption on diffusion with resetting. In *Phys. Rev. E*, 2013

Whitehouse, J., Costa, A., Blythe, R. A. and Evans, M. R. Maintenance of order in a moving strong condensate. In *J. Stat. Mech.*, 2014